Title
Structure-Function Relationships in Biomineralized Composites: Analysis of the Architectural Complexities of Sponge Skeletal Systems

Author
Weaver, James C.

Publication Date
2006

Peer reviewed

UNIVERSITY OF CALIFORNIA

Santa Barbara

Structure-Function Relationships in Biomineralized Composites: Analysis of the Architectural Complexities of Sponge Skeletal Systems

A Dissertation submitted in partial satisfaction of the
requirements for the degree Doctor of Philosophy
in Marine Science

by

James Christopher Weaver

Committee in charge:

Professor Daniel E. Morse, Chair

Professor J. Herbert Waite

Professor Galen D. Stucky

December 2006

UMI Number: 3257389

ProQuest Information and Learning Company
300 North Zeeb Road
P.O. Box 1346
Ann Arbor, MI 48106-1346

The dissertation of James Christopher Weaver is approved.

_____
J. Herbert Waite

_____
Galen D. Stucky

_____
Daniel E. Morse, Committee Chair

June 2006

Structure-Function Relationships in Biomineralized Composites:
Analysis of the Architectural Complexities of Sponge Skeletal Systems

ACKNOWLEDGEMENTS

It is my pleasure to thank the many people who helped make this thesis possible:

First and foremost, I'd like to thank my advisor Daniel Morse, for introducing me to the field of biomineralization, and with his enthusiasm, support, and sound advice, has been a pleasure to work with for the past several years.

Thanks also to the other members of my committee, Herb Waite and Galen Stucky, who have continually guided me in new and exciting directions of research.

To Joanna Aizenberg, Peter Fratzl, Steve Weiner, and Lia Addadi, for continually being a source of inspiration during my graduate career.

To Peter Allen and Dottie McLaren, for all of the graphical expertise you've both provided.

I would like to thank the many people who provided technical assistance, insight, and guidance during my graduate work:

Professors Paul Hansma, Frank Zok, Brad Chmelka, Everett Lipman, Jim Kennett, Yannicke Dauphin, Kathy Foltz, Mark Brzezinski, Armand Kuris, Genny Anderson, and Larry Jon Friesen;

Postdocs David Kisailus, Michi Izumi, Philipp Thurner, Martina Michenfelder, Ali Miserez, Henrik Birkedal, Lía Pietrasanta, Niklas Heden, Alexander Woesz, Birgit Schwenzer, John Gomm, Ralph Imondi, Markus Merget, Giuseppe Falini, Jennifer Cha, Katsuhiko Shimizu, Jixiang Cao, and Yan Zhou;

Graduate Students Georg Fantner, Johannes Kindt, Ralf Jungmann, Mark Demarest, Clarissa Anderson, Charlie Boch, and Camille Lawrence;

Staff Scientists Mark Cornish, Jan Löfvander, Shane Anderson, Dave Farrar, Tom Mates, John Gaul, Brian Matsumoto, Amy Butros, Neal Hooker, and Bonnie Bosma.

I am also indebted to the talented undergraduate students who I've had the pleasure of working with, especially Garrett Milliron, Michael Porter, Pablo Cabrera, and Mark Najarian.

To my many student colleagues for providing a stimulating and supporting environment, both on and off campus to live and work: I am especially grateful to Mark Zegler, Dijanna Figueroa, Nadia Talhouk, Marla Ranelletti, Michelle Roux, Elizabeth Becker, Stephanie Oakes, and Craig Nelson for their friendship.

Lastly, I'd like to thank Richard A. Armstrong - mentor, colleague, and dear friend - who has provided encouragement and support throughout my educational career. He, probably more than anyone else, was instrumental in stimulating my interest in the biological sciences and for this I am eternally grateful. Working with him for the past ten years has been a truly memorable and rewarding experience in all ways measurable. He will be greatly missed, and to him, I dedicate this thesis.

Curriculum Vita of
James Christopher Weaver
June 2006

EDUCATION

Undergraduate Education
Santa Barbara City College
Santa Barbara, CA

B.S. Aquatic Biology (Spring, 1999)
University of California, Santa Barbara
Santa Barbara, CA

Ph.D. Interdepartmental Marine Science Program (Spring, 2006)
University of California, Santa Barbara
Santa Barbara, CA

PROFESSIONAL EMPLOYMENT

- Undergraduate course in Zoology (Bio 102, Santa Barbara City College)
  Spring, 1994 to Spring, 2005

- Undergraduate course in Invertebrate Zoology (EEMB 112, UCSB)
  Fall, 2003: Laboratory teaching assistant
  Fall, 2005: Guest lecturer

PUBLICATIONS

High-speed photography of compressed human trabecular bone correlates whitening to microscopic damage
Thurner PJ, Erickson B, Jungmann R, Schriock Z, Weaver JC, Fantner GE, Schitter G, Morse DE, Hansma PK
Engineering Fracture Mechanics
2006 (in press)

Mechanical consequences of biomolecular gradients in byssal threads
Waite JH, Weaver JC, Vaccaro E
In: Bionanotechnology, Kluwer Publications.
2006 (in press)

Kinetically controlled catalytic formation of zinc oxide thin films at low temperature
Kisailus D, Schwenzer B, Gomm J, Weaver JC, Morse DE
Journal of the American Chemical Society
128(31): 10276-10280 **2006**

Micromechanical properties of biological silica in skeletons of deep sea sponges
Woesz A, Weaver JC, Kazanci M, Dauphin Y, Aizenberg J, Morse DE, Fratzl P
Journal of Materials Research
21 (8): 2068-2078 **2006**

Self-assembled bifunctional surface mimics an enzymatic and templating protein for the synthesis of a metal oxide semiconductor
Kisailus D, Truong Q, Amemiya Y, Weaver JC, Morse DE
Proceedings of the National Academy of Sciences (USA)
103 (15): 5652-5657 **2006**

Hierarchical interconnections in the nano-composite material bone: fibrillar cross-links resist fracture on several length scales
Fantner GE, Rabinovych O, Schitter G, Thurner P, Kindt JH, Finch MM, Weaver JC, Golde LS, Morse DE, Lipman EA, Rangelow IW, Hansma PK
Composites Science and Technology
66: 1202-1208 **2006**

High-speed photography of the development of microdamage in trabecular bone during compression
Thurner PJ, Erickson B, Schriock Z, Langan J, Scott J, Zhao M, Weaver JC, Fantner GE, Turner P, Kindt JH, Schitter G, Morse DE, Hansma PK
Journal of Materials Research
21 (5): 1093-1100 **2006**

Sacrificial bonds and hidden length dissipate energy as mineralized fibrils separate during bone fracture *
Fantner GE, Hassenkam T , Kindt JH, Weaver JC, Birkedal H, Pechenik L, Cutroni JA, Cidade GAG, Stucky GD, Morse DE, Hansma PK
Nature Materials
4 (8): 612-616 **2005**

Skeleton of *Euplectella sp.*: structural hierarchy from the nanoscale to the macroscale *
Aizenberg J, Weaver JC, Thanawala MS, Sundar VC, Morse DE, Fratzl P
Science
309 (5732): 275-278 **2005**

Developing macroporous bicontinuous materials as scaffolds for tissue engineering
Martina M, Subramanyam G, Weaver JC, Hutmacher DW, Morse DE, Valiyaveettil S
Biomaterials
26 (28): 5609-5616 **2005**

Functionalized gold nanoparticles mimic catalytic activity of a polysiloxane-synthesizing enzyme *
Kisailus D, Najarian M, Weaver JC, Morse DE
Advanced Materials
17 (10): 1234-1239 **2005**

Enzymatic synthesis and nanostructural control of gallium oxide at low temperature
Kisailus D, Choi JH, Weaver JC, Yang WJ, Morse DE
Advanced Materials
17 (3): 314-318 **2005**

The tube cement of *Phragmatopoma californica*: a solid foam
Stewart RJ, Weaver JC, Morse DE, Waite JH
Journal of Experimental Biology
207 (26): 4727-4734 **2004**

Influence of the degradation of the organic matrix on the microscopic fracture behavior of trabecular bone *
Fantner GE, Birkedal H, Kindt JH, Hassenkam T, Weaver JC, Cutroni JA, Bosma BL, Bawazer L, Finch MM, Cidade GAG, Morse DE, Stucky GD, Hansma PK
BONE
35 (5): 1013-1022 **2004**

High-resolution AFM imaging of intact and fractured trabecular bone *
Hassenkam T, Fantner GE, Cutroni JA, Weaver JC, Morse DE, Hansma PK
BONE
35 (1): 4-10 **2004**

Macroporous monoliths of functional perovskite materials through assisted metathesis
Toberer ES, Weaver JC, Ramesha K, Seshadri R
Chemistry of Materials
16 (11): 2194-2200 **2004**

Biological glass fibers: correlation between optical and structural properties
Aizenberg J, Sundar VC, Yablon AD, Weaver JC, Chen G
Proceedings of the National Academy of Sciences (USA)
101 (10): 3358-3363 **2004**

Structure-function studies of the Lustrin A polyelectrolyte domains, RKSY and D4.
Wustman BA, Weaver JC, Morse DE, Evans JS
Connective Tissue Research
44: 10-15 **2003**

Characterization of two molluscan crystal-modulating biomineralization proteins and identification of putative mineral binding domains.
Michenfelder M, Fu G, Lawrence C, Weaver JC, Wustman BA, Taranto L, Evans JS, Morse DE
Biopolymers
70: 522-533 **2003**

Molecular biology of demosponge axial filaments and their roles in biosilicification
Weaver JC, Morse DE
Microscopy Research and Technique
62 (4): 356-367 **2003**

Biocatalytically templated synthesis of titanium dioxide
Sumerel JL, Yang WJ, Kisailus D, Weaver JC, Choi JH, Morse DE
Chemistry of Materials
15 (25): 4804-4809 **2003**

Nanostructural features of demosponge biosilica
Weaver JC, Pietrasanta LI, Hedin N, Chmelka BF, Hansma PK, Morse DE
Journal of Structural Biology
144 (3): 271-281 **2003**

Characterixation of a Ca (II)-, mineral-interactive polyelectrolye domain from the adhesive elastomeric biomineralization protein, Lustrin A
Wustman BA, Weaver JC, Morse DE, Evans JS
Langmuir
19: 9373-9381 **2003**

* Journal Covers:

CONFERENCE TALKS AND POSTER PRESENTATIONS

Hierarchical Assembly in Siliceous Skeletal Networks: A Survey of Biomineral Structural Diversity in the Hexactinellid Sponges
Biomineralization Gordon Conference (Colby-Sawyer College: New London, New Hampshire)
August, 2006

Sophisticated, Hierarchically Ordered, Fracture Resistant Composites: Lessons from Nature
NASA-BIMat Annual Review (UCSB: Santa Barbara, California)
May, 2006

Engineering Lessons Learned from the Study of Sponge Skeletal Systems
Guest Lecture, Department of Biological Sciences (Santa Barbara City College: Santa Barbara, California)
March, 2006

Biotechnology and Biomimetics Opens New Routes to the Nanofabrication of Silica and Metal Oxide Semiconductors
ICB Army-Industry Collaboration Conference (UCSB: Santa Barbara, California)
May, 2006

A Survey of Biomineral Structural Diversity in the Hexactinellid Sponges
Composites Gordon Research Conference (Ventura, California)
January, 2006

Hierarchical Assembly in Siliceous Skeletal Networks
Pacifichem 2005 Conference (Honolulu, Hawaii)
December, 2005

Biologically Inspired Materials Design and Synthesis Strategies
Marine Science Colloquium (UCSB: Santa Barbara, California)
March, 2005

Structure-Function Relationships in Biological Glass Fibers
Spring 2005 MRS Meeting (San Francisco, California)
March, 2005

Structure-Function Relationships in Sponge Skeletal Systems
Biomineralization Gordon Conference (Colby-Sawyer College: New London, New Hampshire)
August, 2004

Sponge Biomineralization and Optics
Batsheva Workshop on Biomineralization (Eilat, Israel)
February, 2004

Red Sea Biodiversity
Batsheva Workshop on Biomineralization (Eilat, Israel)
February, 2004

Novel Approaches for Investigating Spicule Biosynthesis in Living Demosponges
NATO Advanced Study Institute
Learning from Nature How to Design New Implantable Biomaterials: From Biomineralization Fundamentals to Biomimetic Materials and Processing Routes (Alvor, Portugal)
October, 2003

Catalysis of Synthesis and Structure-Directed Growth of Nanocrystalline Metal Oxides Using Proteins Derived From *Tethya aurantia*
Materials Research Outreach Symposium (UCSB: Santa Barbara, California)
January, 2003

Novel Approaches for Investigating Spicule Biosynthesis in Living Demosponges.
Biomineralization Gordon Conference (Colby-Sawyer College: New London, New Hampshire)
August, 2002

Highly Ordered Substrate-Directed Silica Deposition in Three Dimensional Space
Materials Research Outreach Symposium (UCSB: Santa Barbara, California)
January, 2002

Biomolecular Polymers and Mechanisms Yield New Methods for Shape-Controlled Synthesis of Patterned Silicon-Based Materials
Materials Research Outreach Symposium (UCSB: Santa Barbara, California)
January, 2001

ABSTRACT

Structure-Function Relationships in Biomineralized Composites:

Analysis of the Architectural Complexities of Sponge Skeletal Systems

by

James Christopher Weaver

The Porifera represent an ancient metazoan lineage with a fossil record that dates back more than half a billion years, and during their evolution since the mid to late Proterozoic, have presumably changed very little, maintaining their characteristically simple body plans. Although they lack the physiological complexities of many of the higher metazoa, sponges are well known for their ability to synthesize a wide range of intricately architectured siliceous skeletal elements, the formation of which in many instances far exceeds modern engineering capabilities. Because of their high precision fabrication, species-specific nanoscale structural attributes, fracture-resistant mechanical properties, and rapid rates of biosynthesis, siliceous sponge spicules have attracted a great deal of attention in recent years as model systems for the analysis of biosilicate nanofabrication.

Contained within the core of each siliceous skeletal element is a proteinaceous axial scaffold that is critically responsible for establishing spicule symmetry.

Silicateins, the most abundant proteins comprising the axial filaments of demosponges, prove to be members of a well-known superfamily of proteolytic and hydrolytic enzymes and can be easily collected after silica dissolution with hydrofluoric acid. Consistent with these findings, the intact filaments are more than simple, passive templates; *in vitro*, they actively catalyze and spatially direct the hydrolysis and polycondensation of silicon alkoxides to yield silica at neutral pH and low temperature. TEM and XRD analyses of these catalytic organic scaffolds from both demosponges and hexactinellids reveal that their constituent proteins exhibit highly regular ordering, and biochemical and structural analyses have provided new insight into the factors regulating their observed packing geometries and resulting spicule symmetry.

Because of their unusually large size and remarkable flexibility, spicules from the predominantly deep-sea hexactinellid sponges have provided a great deal of insight into new design strategies for more fracture resistant composite materials. In addition to their remarkable mechanical properties, the hexactinellids are also well known for the ability to form extremely complex hierarchically ordered robust skeletal networks from their constituent spicules. The design principles learned from these analyses as well as new techniques for investigating the synthesis mechanisms of sponge spicules *in vivo* are discussed in detail.

TABLE OF CONTENTS

LIST OF FIGURES

Chapter 1

Chapter 2

Chapter 3

Chapter 4

Chapter 5

Chapter 6

Chapter 1

Introduction:

Molecular Biology of Demosponge Axial Filaments and their Roles in Biosilicification

This Chapter is adapted from:
Molecular biology of demosponge axial filaments and their roles in biosilicification
Weaver JC, Morse DE
Microscopy Research and Technique
62 (4): 356-367 **2003**

Contributing researchers: James C. Weaver, Jennifer N. Cha, Katsuhiko Shimizu, Yan Zhou, Jixiang Cao, Camille Lawrence, Lía I. Pietrasanta, Jan L. Sumerel, Pablo F. Cabrera, Mark A. Brzezinski, Galen D. Stucky, Paul K. Hansma, Brad F. Chmelka, and Daniel E. Morse

1.1 Introduction

Nature produces a remarkable diversity of intricately architectured biomineralized materials, the formation of which in many instances far exceeds modern human engineering capabilities (Figure 1.1). In stark contrast to the harsh processing conditions currently used in the synthesis of their anthropogenic counterparts, biological systems are able to create extremely complex and often multifunctional organic-inorganic composite materials at near neutral pH using benign molecular precursors and processes with no caustic byproducts. The resulting mineralized structures frequently exhibit extremely complex three-dimensional organizations that are ordered over multiple length scales.

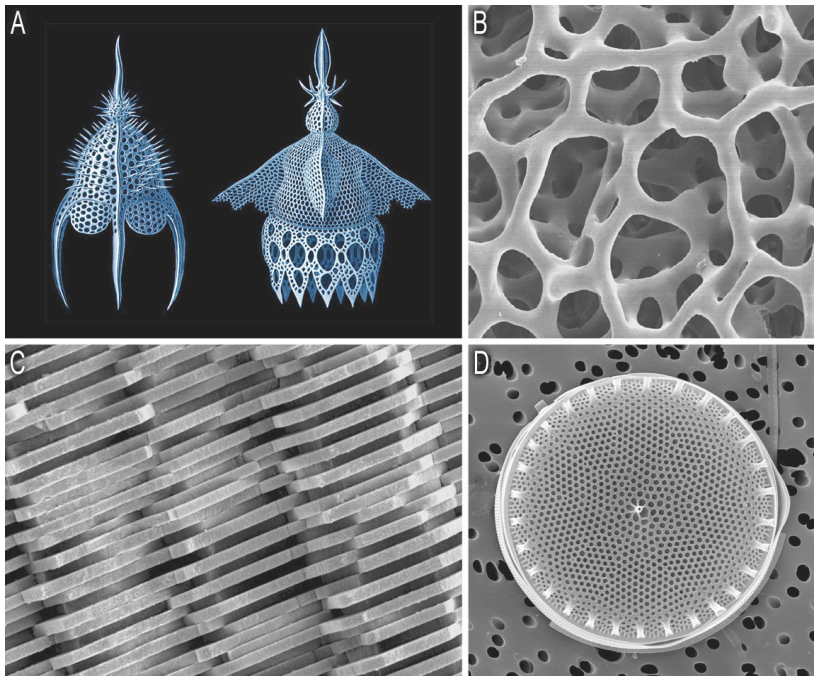

Figure 1.1: Structural diversity in invertebrate biominerals. (A) Polycystine radiolaria (adapted from Haeckel, 1904), (B) asteroid ossicle, (C) gastropod nacre, and (D) diatom frustule.

While all biominerals exhibit various degrees of compositional complexity, in terms of micro- and nanoscale structural diversity, the siliceous skeletons of diatoms and radiolarians reign supreme (Figure 1.1). Interest in the remarkable structural complexity and the benign conditions for synthesis of these and other biosilicas and the potential to harness these strategies for the synthesis of advanced materials and devices prompted our investigations into the mechanisms of biosilicification in a much simpler biological system, the marine sponges.

The sponges (phylum Porifera) represent an ancient metazoan lineage with a fossil record that dates back more than half a billion years. Among the earliest forms of multicellular life on the planet, they have apparently changed very little during their evolution since the mid to late Proterozoic (Gehling and Rigby, 1996; Brasier, et al., 1997), maintaining their characteristically simple body plans (Müller and Müller, 2003). Sponges are thought not to form tissues in the traditional sense, consisting predominantly of loose aggregations of cooperatively interacting cell types (Müller, et al., 1999). Their cells lack a basal lamina, and intercellular junctions are few and far between. Although they lack the physiological complexities of many of the higher metazoa, sponges are well known for their ability to synthesize a wide range of intricately architectured skeletal elements (spicules) of either silica or calcium carbonate (Hartman, 1981; Simpson, 1984). These spicules are generally classified as either megascleres or microscleres based on their relative dimensions. Because of their high-precision hierarchical fabrication (Aizenberg, et al., 2005), species-specific nanoscale structural intricacies, fracture-resistant mechanical properties, and

relatively rapid rates of biosynthesis, siliceous sponge spicules have attracted a great deal of attention in recent years as model systems for the analysis of biosilica nanofabrication and translation of the underlying mechanisms to the synthesis of new nanostructured materials and devices for advanced applications (Cha, et al., 1999, 2000; Zhou, et al., 1999; Shimizu and Morse, 2000; Shimizu, et al., 1998; Morse, 1999, 2000, 2001; Sumerel, et al., 2003; Kisailus et al., 2005a,b, 2006; Roth, et al., 2005; Schwenzer, et al., 2006).

These features coupled with their overall organizational simplicity also make sponges useful research candidates for understanding the fundamental mechanisms of cellular recognition, differentiation, and specialization (Müller, et al., 1999). Although major breakthroughs in recent years have yielded much insight into the biology of sponges, the specific requirements for long-term maintenance of sustainable sponge cell cultures for many species has remained enigmatic. In addition, the mechanisms underlying the formation of their supporting skeletal frameworks, until only recently, have to a large extent remained a mystery (Shimizu, et al., 1998; Cha, et al., 1999; Krasko, et al., 2000, 2002).

1.2 Axial filaments and spicule morphology

For many years, the intracellular versus extracellular locus of megasclere synthesis in demosponges had been unresolved (Simpson, 1984), although recent work with *Crambe crambe* (Uriz, et al., 2000) would seem (at least for this species) to support the latter hypothesis. In this proposed process, the central proteinaceous axial

filament (Shore, 1972) is synthesized in its entirety, exocytosed to the mesohyl, and in a microenvironment created between a sclerocyte's pseudopodial plasma membrane and the axial filament, silica deposition takes place (Uriz, et al., 2000).

It has long been known that most, if not all siliceous sponge spicules (including those from both demosponges and hexactinellids) contain organic axial filaments. Although the most frequently observed cross-sectional shape of demosponge axial filaments is hexagonal (Rützler and Smith, 1993), we have observed that it can vary considerably from spicule to spicule, even within the same species, from regular and irregular hexagonal to triangular to nearly circular and is reflected in morphological variations of the surrounding axial channel (Figure 1.2).

Because of this apparent high degree of intraspecific phenotypic plasticity characteristic of demosponge axial filaments, their cross-sectional morphological characteristics should not be used as a basis for taxonomic characterization or for inferring degrees of evolutionary relatedness between species. Although this may be the case, there are marked differences in axial filament cross-sectional morphologies between hexactinellids and demosponges. Hexactinellid axial filaments are distinctively square in cross-section (Reiswig, 1971), while, as discussed above, those from demosponges are hexagonal or some derivative thereof. As we will see in Chapters 4 and 6, differences in axial filament cross-sectional geometry between members of these two sponge classes have dramatic effects on both spicule symmetry and the way in which they are used in skeletal structuring.

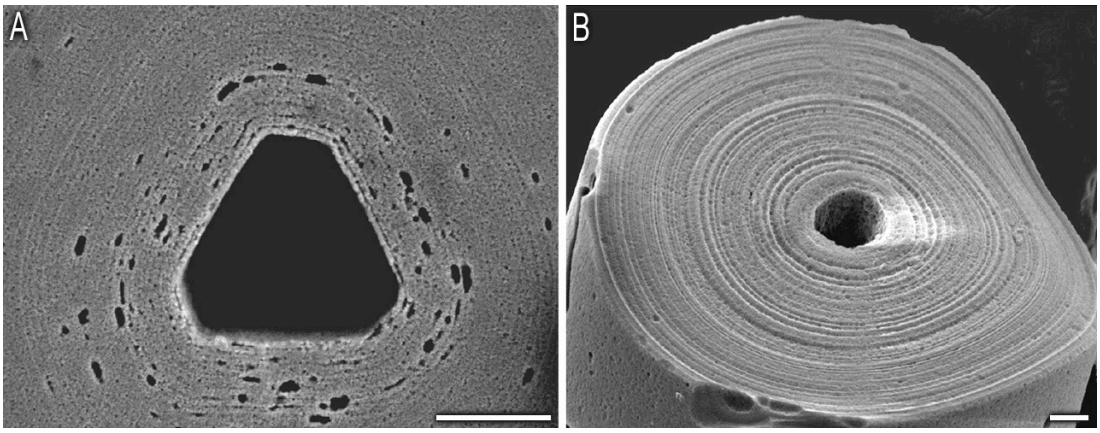

Figure 1.2: Scanning electron micrographs of cross-sections through strongyloxea from the temperate Eastern Pacific demosponge, *Tethya aurantia*, revealing the diversity in axial channel morphologies. See also Figure 1.4. Cross-sections include regular and irregular hexagonal (A), triangular and nearly circular (B). The annular siliceous deposits surrounding the preexisting axial filaments are clearly visible. Scale bars: A: 1μm; B: 1μm.

These axial filaments have been proposed to play an essential role in dictating the gross morphological attributes of the spicules that contain them. While previous studies investigating these relationships have predominantly concentrated on analyses of monaxonal megascleres (Garrone, 1969; Simpson and Vaccaro, 1974; Weissenfels and Landschoff, 1977; Wilkinson and Garrone, 1980), there are several specific examples of tetraxons that beautifully illustrate the roles of these axial filaments in the determination of spicule morphology (Simpson, et al., 1985). The dichotriaenes from the temperate Eastern Pacific astrophorid demosponge *Penares saccharis* clearly illustrate that the genetically predetermined synthesis of the silica precisely follows the contours of the bifurcated axial filaments (Figure 1.3).

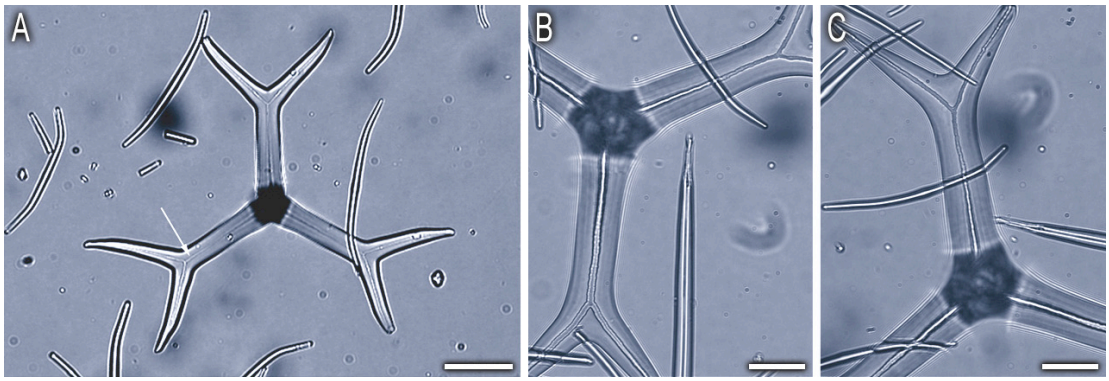

Figure 1.3: Optical micrographs revealing locations of axial filaments in dichotriaenes from the temperate Eastern Pacific demosponge, *Penares saccharis*. (A) illustrates an unaltered spicule, the arrow indicating the axial filament. Similar spicules, (B) and (C), have been treated with an alkaline etchant (NaOH), dissolving the distal portions of the megascleres and solubilizing the axial filaments. The remaining axial channel clearly illustrates the previous location of the axial filament. Scale bars: A: 50μm; B: 20μm; C: 20μm.

A second dramatic illustration of this can be observed in the rare anomalies of spicule biosynthesis such as dichotomous defects in strongyloxea from the hadromerid demosponge *Tethya aurantia*. Where the axial filament bifurcates, it precisely guides the deposition of annular siliceous deposits around this three dimensional organic template (Figure 1.4). It should be noted that not all spicule features can be explained based on axial filament morphology. In megascleres for example, the smallest superficial elaborations in the submicron range (Figure 1.5) typically do not contain axial filament branches guiding their location on the spicule surface (Garrone, et al., 1981). Therefore, the synthesis of these features may be determined by the silicalemma that surrounds and deposits the silica during spicule formation. Until recently, however, the detailed composition of the axial filaments

and their actual role in spicule biosynthesis was largely unknown (Cha, et al., 1999; Shimizu, et al., 1998).

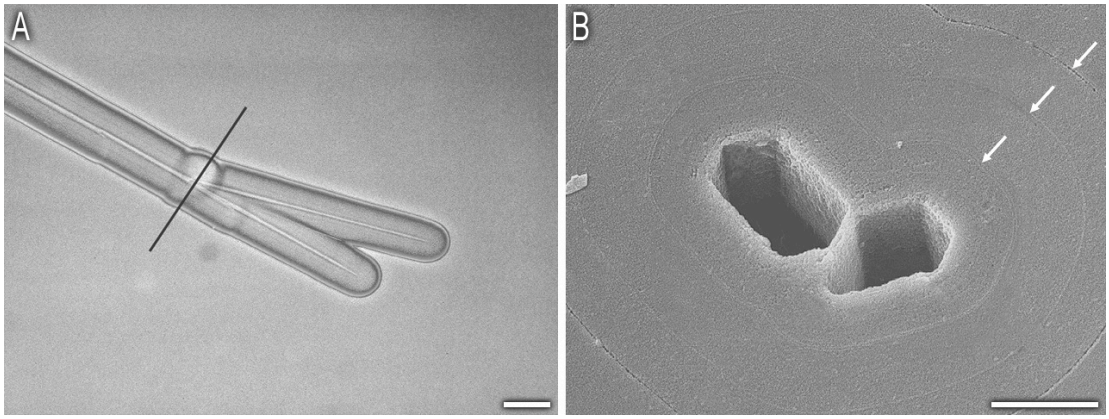

Figure 1.4: Microscopic analyses of dichotomous defects in *Tethya aurantia* strongyloxea. (A) illustrates the dramatic effect that axial filament anomalies can manifest in a mature megasclere. The black line indicates the location of sectioning for the scanning electron micrograph through a similar spicule (B).

The scanning electron micrograph shown in (B) not only illustrates a rare instance of filament bifurcation (reflected in the morphology of the axial channel), but also clearly illustrates the essential role of the axial filaments in dictating the microscale arrangement of the deposited silica; the arrows indicate the successive annular deposits. Scale bars: A: 20μm; B: 1μm.

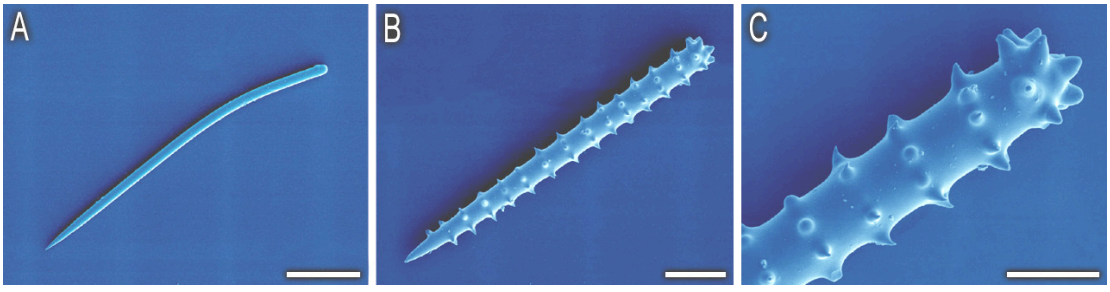

Figure 1.5: Scanning electron micrographs of demosponge megasclere surface modifications. The formation of rounded ends (A) or surface spines (B and C) occur during the final stages of spicule biosynthesis. Scale bars: A: 50μm; B: 20μm; C: 10μm.

Although there exists a remarkable diversity in demosponge megasclere morphology, the most intricate of the siliceous sponge skeletal elements are indeed the microscleres (Hartman, 1981) (Figure 1.6). In contrast to the possible extracellular locus of megasclere formation recently observed in *Crambe crambe* (Uriz, et al, 2000), microsclere biosynthesis appears to be an intracellular process and seems, at least in some species, to occur in dense aggregations of microsclerocytes, frequently restricted to specific regions of the sponge (Figure 1.7). Currently, many of the reported observations of microsclere biosynthesis in demosponges seem to indicate that this is a dynamic, highly variable, and species- and/or spicule-specific process (Garrone, et al., 1981; Simpson, 1984). Because of these discrepancies, additional research is required in this area before any generalities regarding microsclere biosynthetic mechanisms can be made with confidence.

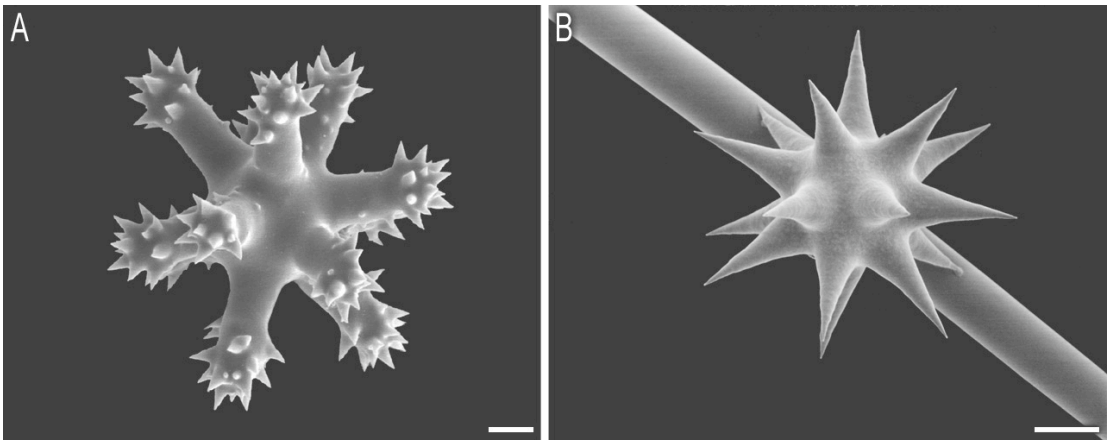

Figure 1.6: Scanning electron micrographs of *Tethya aurantia* cortical microscleres. (A) illustrates an acanthaster isolated form the cortex of *Tethya aurantia*. These are the smallest and most numerous microscleres present in this species. (B) illustrates a typical spheraster from *Tethya aurantia* (foreground) and an unusually small strongyloxea (background). Scale bars: A: 1μm; B: 10μm.

Due to the structural complexity of many microscleres, they seem to be ideal candidates for investigating the mechanisms governing nanoscale silica deposition in three-dimensional space, and like the megascleres, they also exhibit a central organic scaffold that is critically responsible for establishing symmetry in these unique skeletal elements (Figure 1.8). While microsclere abundance in many species can be quite high, their contribution to the total skeletal mass is often negligible. In *T. aurantia* for example, the microscleres typically comprise less than $1/1000^{th}$ of one percent of the total spicule mass in this species.

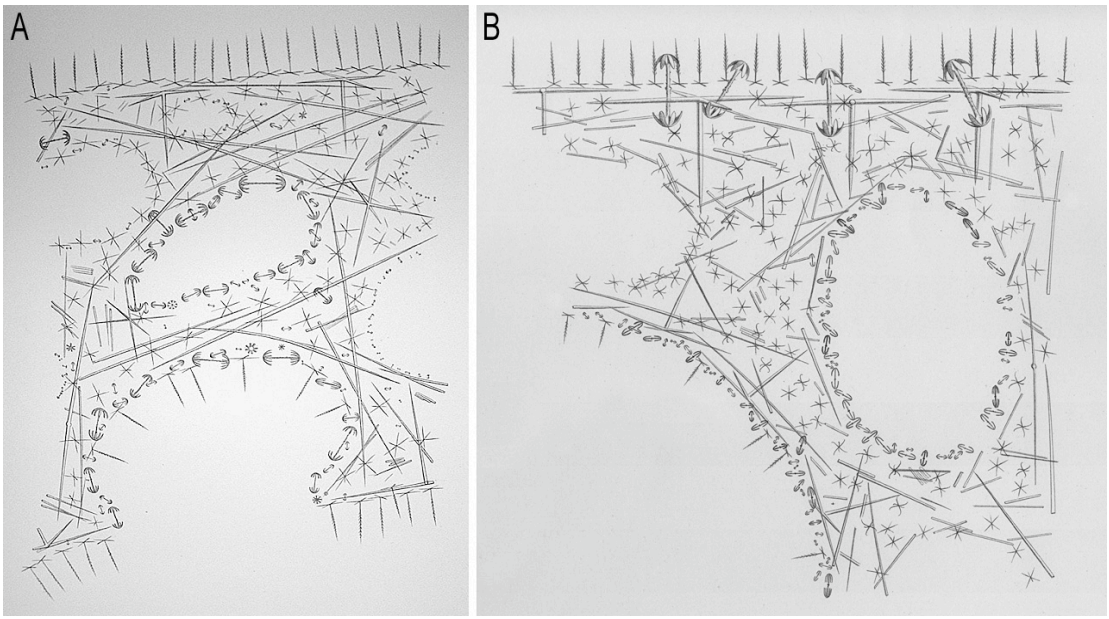

Figure 1.7: Regiospecific microsclere distribution in two species of hexactinellid sponges (A, B) (adapted from Iijima, 1926).

Although there has been some work in recent years investigating the role that environmental and micronutrient variability can exert on the synthesis of microscleres

(Maldonado, et al., 1999), for the most part, because of the complication associated with their manipulation, they have primarily remained items of curiosity, principally of taxonomic significance.

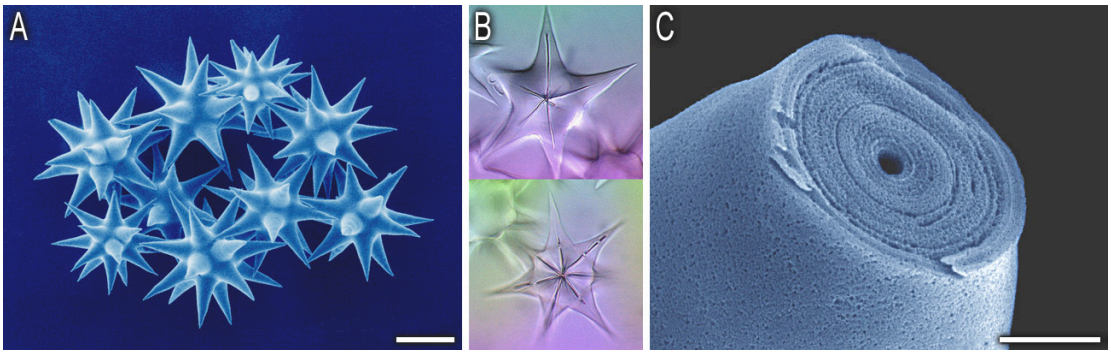

Figure 1.8: Architectural details of spheraster microscleres isolated from the cortex of *Tethya aurantia* (A). Polarized light micrographs of the same spicules, revealing the location of the structure-directing organic scaffold (B). Fracture studies indicate that the silica is deposited as concentric lamellae around this preformed organic template (C). Scale bars: A: 20μm; C: 1μm.

Even more obscure than the mechanisms governing the biosynthesis of the microscleres is their functional significance. It is possible that these silicified structures might provide either small scale or transient skeletal support, their small size perhaps making them ideal for either or both of these roles (Bergquist, 1978; Hartman, 1981; Simpson, 1984). In *T. aurantia* (as is common for many sponge species), microsclere synthesis, while occurring sparsely in the choanosome, is predominantly restricted to the sponge cortex. Because of their small size, these skeletal elements may be more easily mobilized than the megascleres during the reorganization of this region of the sponge during normal sponge growth. During cellular reorganization, they may also provide small-scale support, affording localized

microscale structuring before the consolidation of ordered cellular aggregates takes place.

While most siliceous sponge spicules exhibit well-defined and species-specific geometries, there is one major exception. The lithistid demosponges such as *Discodermia dissoluta*, are well known for their synthesis of unusual asymmetrical antler-like spicules called desmas (Figure 1.9A). The non-uniform morphologies of theses spicules raise intriguing questions as to the location of the organic scaffold within the cores of these spicules and their role in determining spicule geometry. When examined by optical microscopy, it becomes clear that the desma axial filaments are only responsible for controlling the core geometries of these spicules and any further silica deposition at the spicule extremities occurs independently of this organic template (Levi, 1991). For this reason, desmas from a given species or individual are extremely variable in morphology at their termini. The morphological plasticity of these spicules is critical, however, in how they are used in skeletal structuring. Once the central portion of each spicule (the crepis) is synthesized, it is maneuvered in close proximity to neighboring desmas and additional mineralization events take place, intertwining the spicule extremities, resulting in the formation of an interdigitated, consolidated skeletal lattice (Figure 1.9B, C).

The lithistids were abundant in neritic environments of the Jurassic seas but virtually disappeared from these habitats by the Cretaceous and early Tertiary. Extinction of these sponges may have been related to diatom population explosions around the Cretaceous- Tertiary boundary and the subsequent dramatic reduction in

the availability of silicic acid presumably required for the construction of their elaborate skeletal networks (Maldonado, et al., 1999). Modern lithistid diversity represents only a fraction of its Jurassic abundances, with most extant species restricted to deeper water (Carbonnelli, et al., 1999; Qureshi, et al., 2000; Schmidt, et al., 2000; Zampella, et al., 1997; Maldonado, et al., 1996).

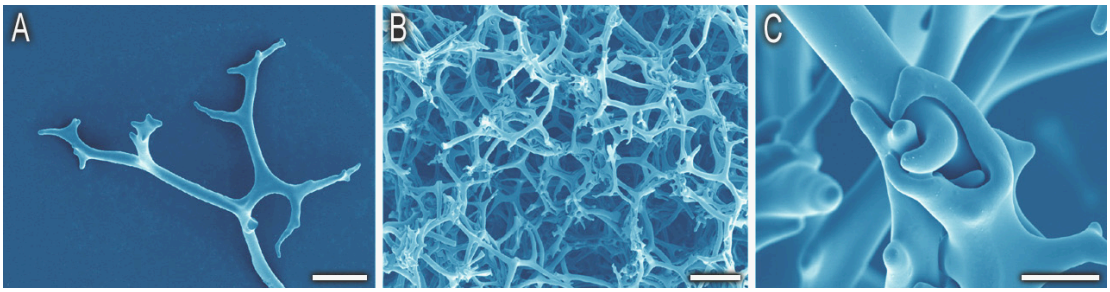

Figure 1.9: Isolated (A) and interdigitated (B and C) desmas from the lithistid demosponge, *Discodermia dissoluta*. Scale bars: A: 100μm; B: 200μm; C: 20μm.

Two known centers of modern lithistid species diversity are the Caribbean and the tropical Western Pacific. The bathymetric distributions of these species within these specific regions are not random, however, with peak species abundances frequently occurring between 500 and 700m in the Caribbean and 100-300m in the tropical Western Pacific (Carbonnelli, et al., 1999; Qureshi, et al., 2000; Schmidt, et al., 2000; Zampella, et al., 1997; Maldonado, et al., 1996). By using *in situ* vertical silicic acid profiles through these two geographic areas, we can estimate that the depth of highest lithistid populations corresponds to a silicic acid concentration of between 20 and 40μM (Figure 1.10).

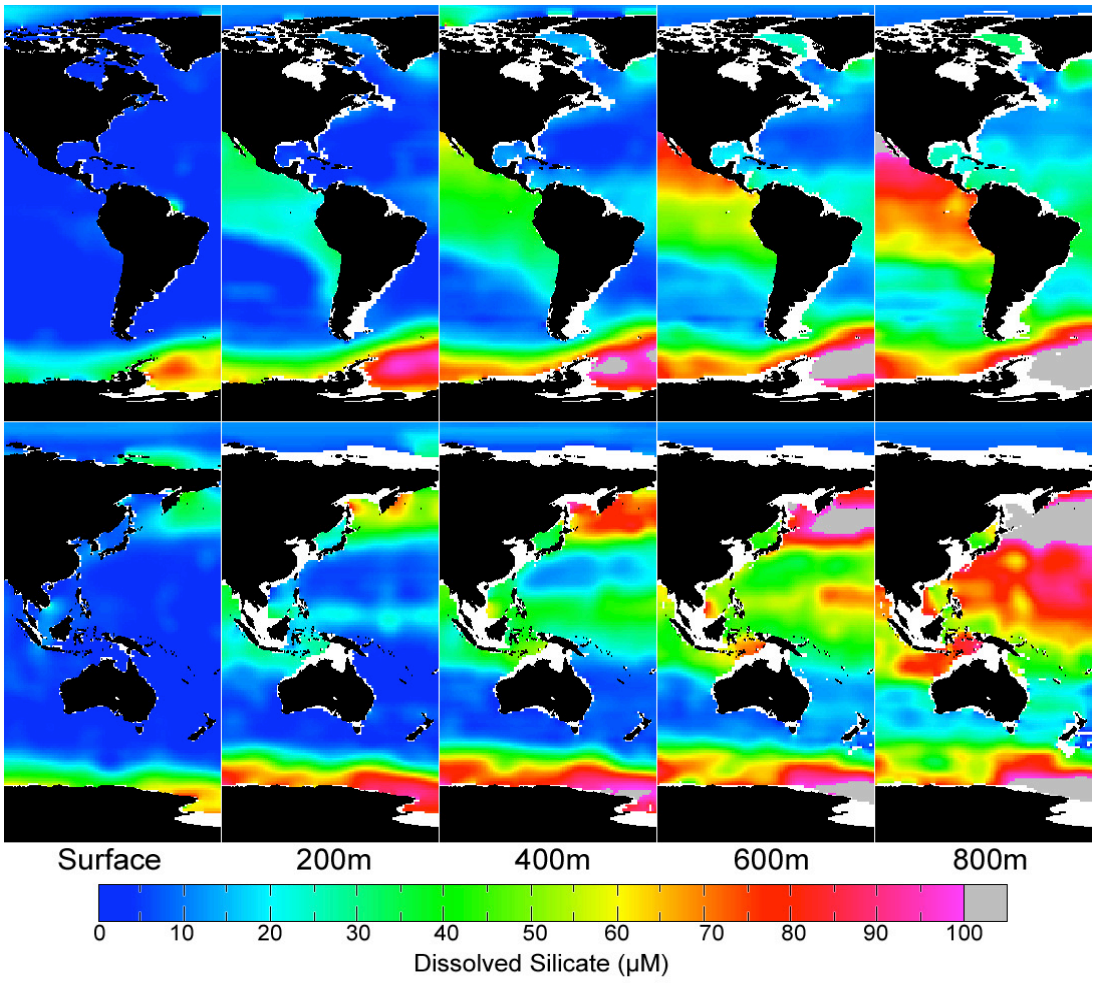

Figure 1.10: Silicic acid concentrations as a function of depth in the tropical Western Atlantic and Pacific oceans, two known centers of lithistid demosponge species diversity. Peak species abundances within these two habitats frequently occur between 400 and 700m in the Atlantic and 100-300m in the Pacific, corresponding to an *in situ* silicic acid concentration of between 20 and 40µM (data from LEVITUS94).

It is important to note that many extant and fossil lithistids have characteristics in common with other sponge orders including the Spirophorida, Astrophorida, Hadromerida, Poecilosclerida, and the Halichondrida with respect to either physiology or spicule composition, raising intriguing questions regarding the

monophyletic nature of this lineage (Kelly, 2000). Additional evidence for the polyphyletic nature of the lithistida has been provided by molecular phylogenetic data obtained from specific members of the various demosponge taxa described above (Kelly-Borges and Pomponi, 1994; Mclnerney, et al., 1999). The shared commonality in characteristics between the lithistids and many extant sponges raises additional questions regarding the evolutionary pressures guiding the synthesis of these desma-containing basal skeletons.

Recent sponge cell culture experiments performed with the Mediterranean poecilosclerid demosponge *Crambe crambe* have provided some insight in to the potential regulatory mechanisms controlling the synthesis of these skeletal elements (Maldonado, et al., 1999). The specimen utilized in these studies originated from a population of *Crambe crambe* that had been studied for almost 15 years. During this time, the only spicule type observed in specimens obtained from wild populations and those cultured under ambient concentrations of silicic acid was the style (a monactinal megasclere, Figure 1.11A). As the concentration of silicic acid under which these sponges were grown was increased, there was a dramatic shift in the morphology and diversity of the skeletal elements synthesized. At 30μM silicic acid, in addition to the styles described above, *C. crambe* also synthesized isocheles and isolated (non-interdigitated) desmas (Figure 1.11B).

At l00μM silicic acid, the synthesized desmas become interconnected, resulting in the formation of a consolidated skeletal network, morphologically

consistent with those observed in the lithistids (cf. Figure 1.9) (Maldonado, et al., 1999).

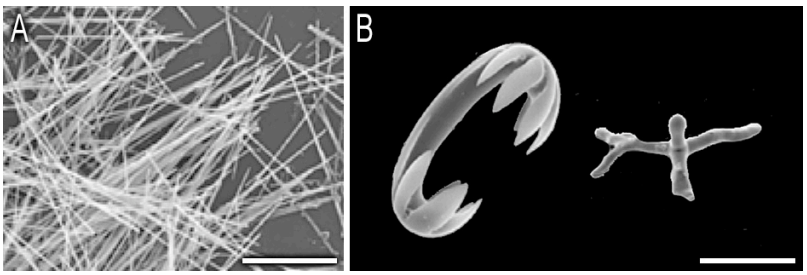

Figure 1.11: Spicule diversity from the Mediterranean demosponge, *Crambe crambe*. (A) Styles, (B) isocheles, and isolated (non-interdigitated) desmas (adapted with permission from Maldonado, et al., 1999). Scale bars: A: 100μm; B: 10μm.

These experiments are significant in that this is the first time that sponges, not traditionally classified as lithistids, could be induced to synthesize desmas by simply altering the environmental conditions under which the sponges were grown. These results also raise additional questions regarding the polyphyletic nature of the lithistida and suggest that *in situ* silicic acid concentration may be a major determining factor in controlling desma biosynthesis, which may have evolved independently in a diverse array of demosponge lineages.

This suggestion is also supported by recent discoveries made while investigating demosponge biodiversity in the tropical Eastern Pacific. At depths between 20 and 40m off the West coast of Panama, a new species of the genus *Crambe* was discovered. Based on the known bathymetric distributions of silicic acid in the tropical Eastern Pacific, it is possible to estimate that its concentrations in the sponge's natural habitat may have been between 10 and 20μM (Figure 1.12).

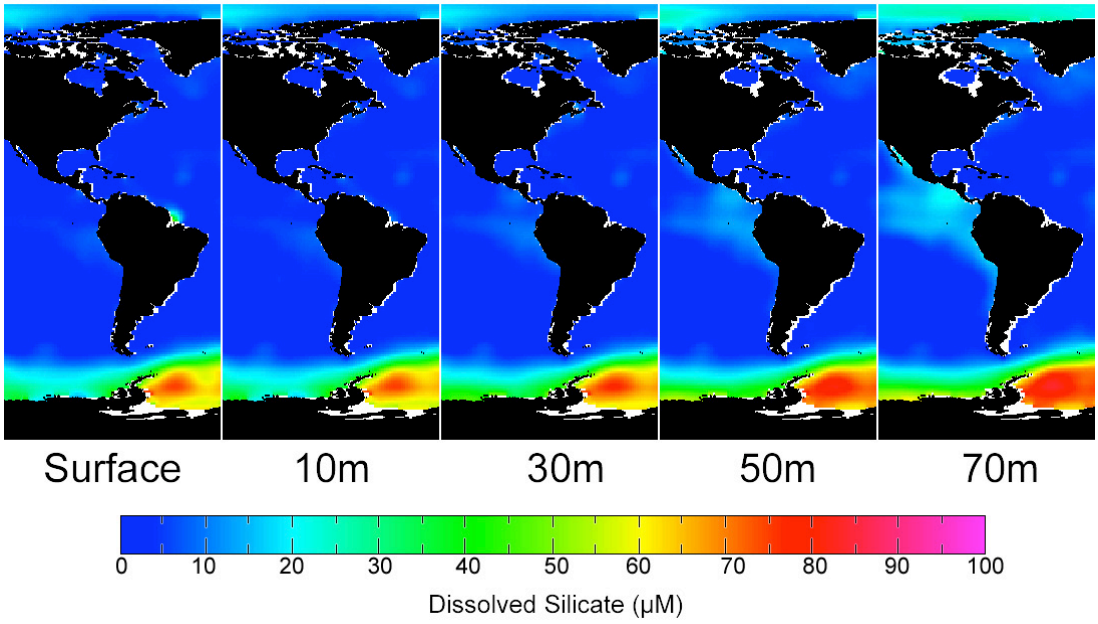

Figure 1.12: Silicic acid concentration as a function of depth in the Tropical Eastern Pacific for the upper 70m (data from LEVITUS94).

As predicted from the previous experiments investigating spicule biosynthesis as a function of silicic acid availability in the Mediterranean *C. crambe* described above, this poecilosclerid contained styles, isocheles, and desmas (Maldonado, et al., 2001).

Although it is now clear that spicule biosynthesis can, at least in some species, be influenced by environmental parameters, the exact mechanism by which this occurs is unfortunately not well understood. Müller and his colleagues recently demonstrated that expression of silicatein genes (the proteins that form the organic template onto which silica is deposited; see additional information in the following section) is regulated by the concentration of silicic acid (Krasko, et al., 2000). Increasing concentrations of available silicic acid strongly upregulates silicatein gene

expression in the sclerocytes, and indirectly the synthesis of spongin collagen in the exopinacocytes. The synthesis of these two components; the silicatein of the axial filament (Cha, et al., 1999; Shimizu, et al., 1998), the precursor to spicule biosynthesis, and the formation of the collagenous organic matrix, are required for the formation of a functional supporting skeleton. It is therefore possible that the threshold of activation for silicatein synthesis and other sponge skeletal components might be coordinately regulated in desma-synthesizing megasclerocytes, and might therefore explain their apparent dependence on high levels of silicic acid (the threshold of synthesis is estimated to be between 20 and 40μM), and thus their modern restriction to deeper water. Once these detailed mechanisms of activation involved in morphologically-distinct spicule biosynthesis have been discovered for a number of species, it may then be possible to utilize them as bioindicators for detecting environmental variability in silicic acid concentration.

1.3 Silicatein biochemistry and silicon biotechnology

The temperate Eastern Pacific demosponge *T. aurantia* provides an excellent model system for studying the detailed molecular mechanisms of biosilicification. The supporting skeleton of this species is dominated by siliceous spicules (strongyloxea) measuring ca. 2mm in length and 30μm in diameter (Figure 1.13), which comprise ca. 75% of the dry weight of this organism (Cha, et al., 1999; Shimizu, et al., 1998). The large quantities of biosilica available make this species a uniquely tractable model system for investigating spicule formation. An additional

advantage of this species is that unlike many other demosponges, *T. aurantia* lacks extensive intraspecific morphological variability, making *in situ* species identification nonproblematic. These attributes, coupled with its ease of culture under laboratory conditions, make *T. aurantia* a useful research subject.

The axial filaments occluded within the strongyloxea can easily be collected after demineralization of the surrounding silica with hydrofluoric acid. The isolated filaments (Figure 1.14) measure ca. 2μm in diameter and 2mm in length and comprise ca. 0.5% of the spicule weight (Cha, et al., 1999; Shimizu, et al., 1998). These filaments consist primarily of three closely related protein subunits, named silicateins (for ***silica*** pro***teins***) α, β, and γ (Shimizu, et al., 1998).

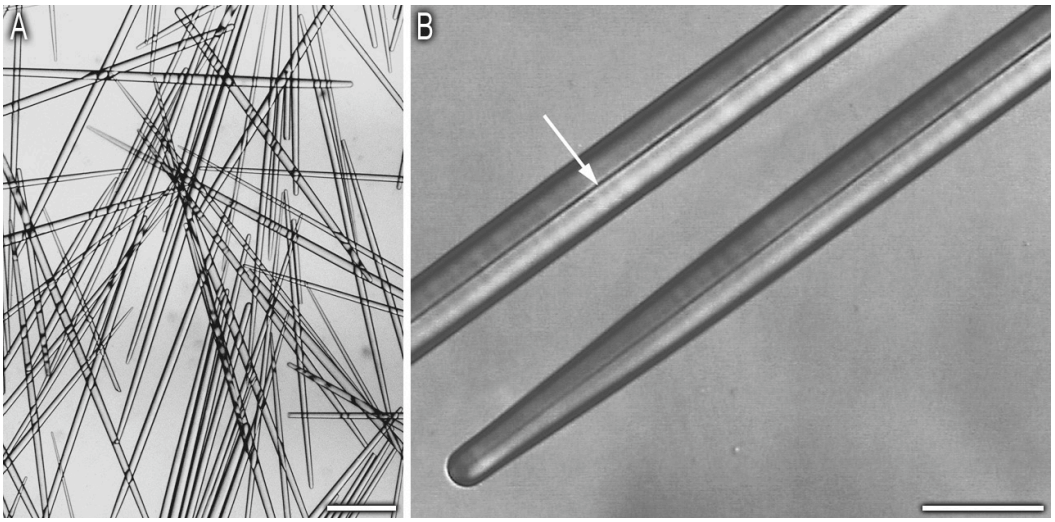

Figure 1.13: Optical micrographs of strongyloxea from *Tethya aurantia* measuring ca. 30μm in diameter and 2mm in length (A). (B) reveals the axial filaments (indicated by the arrow). Scale bars: A: 200μm; B; 50μm.

These axial filaments appear to have a previously unanticipated role in spicule formation. In addition to their role as templates or guides for silica deposition, a

catalytic role is suggested by the discovery that the filaments can catalyze the hydrolysis and polycondensation of various silicon alkoxides such as tetraethoxy-silane (TEOS) and the methyl- and phenyl-triethoxysilanes to yield silica and the corresponding silsesquioxanes (silicones) *in vitro* (Cha, et al., 1999; Shimizu, et al., 1998). In marked contrast to industrial conditions, this protein-catalyzed siloxane polycondensation occurs at ambient temperature and pressure and neutral pH.

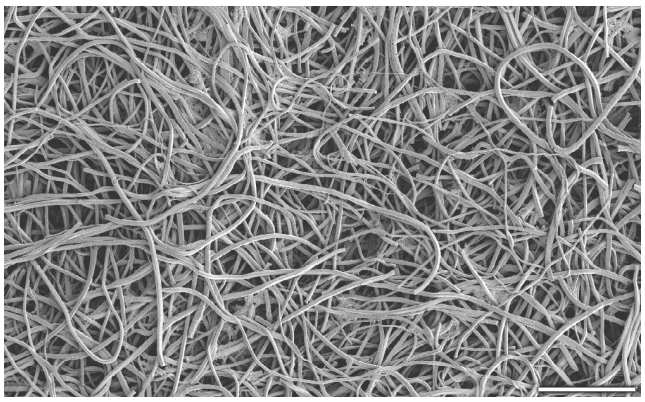

Figure 1.14: Scanning electron micrograph of axial filaments collected from *Tethya aurantia* strongyloxea after demineralization with HF. Each filament measures ca. 2μm in diameter and 2mm in length. Scale bar: 30μm.

While it is unlikely that simple silicon alkoxides are the *in vivo* precursors of biogenic silica polymerization, they may be related to conjugates of silicic acid through the association with intracellular ionophores, or the formation of covalent complexes via condensation with alcohols, polyols, sugars, or catechols (Bhattacharyya, et al., 1983; Evans, et al, 1990; Harrison, 1996; Harrison and Loton, 1995; Kinrade, et al., 1999a,b; Perry and Yun, 1992) that may be formed prior to silica deposition and recently suggested to be involved in diatom biosilicification

(Kinrade, et al., 2002). In diatoms, silicic acid is accumulated in intracellular pools at much higher concentrations than that at which it would otherwise normally spontaneously precipitate, suggesting some form of sequestration or chemical conjugation (Chisholm, et al., 1978; Sullivan, 1986). If silicic acid is conjugated with organic moieties after transport and concentration in the sclerocytes during spicule formation in demosponges, the catalytic mechanism observed *in vitro* may be essential for the *in vivo* induction of silica condensation. Although there is currently no evidence to support the silicatein-mediated silicon alkoxide hydrolysis mechanism *in vivo*, further analyses of the early stages of spicule formation in demosponges can be expected to shed new insight into the biological role these proteins play in the mineralization process.

A second activity of the axial filaments is templating; *in vitro*, they guide the deposition of the polycondensed product along the entire filament length (Cha, et al., 1999). The silica produced *in vitro* by this process is nanoparticulate (particle size: 74 ± 13nm; cf. Chapter 2), deposited on the filament in a coating several particles thick. This silica is morphologically consistent the product obtained from the synthesis catalyzed by the silicatein monomers made from recombinant DNA templates cloned in bacteria (Figure 1.15A). Neither silk fibroin nor cellulose fibers, both of which possess high densities of surface hydroxyls (as does the axial filament), promote the hydrolysis and polycondensation of silicon alkoxides at neutral pH, demonstrating that more than the simple presence of hydroxyl rich domains are responsible for the observed activity (Cha, et al., 1999).

One remaining paradox in understanding demosponge spicule biosynthesis is the mechanism by which silica deposition continues once the proteinaceous axial filament has become completely covered during the early stages of spicule formation.

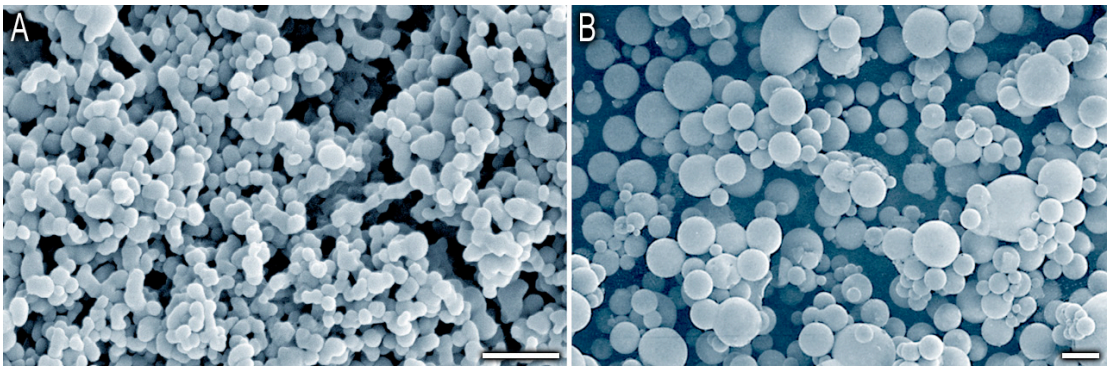

Figure 1.15: Scanning electron micrographs of silica products synthesized from tetraethoxysilane (TEOS) at ca. 20ºC, neutral pH and atmospheric pressure. (A) Silica nanoparticles grown in the presence of recombinantly derived silicatein β, the second most abundant of the *Tethya aurantia* silicateins. (B) Glassy microspheres grown in the presence of the reduced form of the biomimetic Cys_{30}-Lys_{200} block copolypeptide (adapted from Cha, et al., 2000).

The polymerization activity reported previously for the silicateins revealed that its mechanism is catalytic and not stoichiometric. Based on our observations, and previous reports that this catalytic activity is retained by the individual subunits liberated after axial filament solubilization (Cha, et al., 1999), it is possible that the controlled punctuated secretion of monomeric silicateins, pulses in the transitory flux of silica-precursor molecules, oscillations in the pH, ionic or other conditions of the condensation environment, or a combination of these factors may be responsible for the continued deposition of silica during spicule biosynthesis *in vivo* once the axial filament has become completely covered during the early stages of mineralization

around this proteinaceous core (cf. Chapter 2). In addition, recent observations by Schröder, et al., have raised the possibility that there may be extra-filamentous silicateins that provide additional catalytic sites for the controlled hydrolysis of silica precursor molecules during spicule growth (Schröder, et al., 2006).

Small angle x-ray diffraction analysis of the protein filaments reveals a distinct ultrastructural periodicity, suggesting that the macroscopic filaments are constructed from a highly regular, repeating subassembly of its protein subunits (Cha, et al., 1999) (cf. Chapter 6). These results are consistent with previous transmission electron microscopy studies that first revealed the apparent paracrystallinity of demosponge axial filaments (Garrone, 1969; Garrone and Pottu-Boumendil, 1981). While the templating activity of the silicateins is lost upon filament disaggregation and solubilization, the catalytic activity is retained by the constituent monomers. Heat denaturation of both the intact axial filaments and their constituent subunits abolishes their catalytic activity, suggesting that the native conformation of the proteins is required for their catalysis of silica polymerization (Cha, et al., 1999; Zhou, et al., 1999).

These subunits are present in the approximate ratio of $\alpha:\beta:\gamma$ = 12:6:1 (Shimizu, et al., 1998), although the detailed distribution of the different proteins within individual filaments is not yet known. Electrophoretic characterization of silicateins α, β, and γ reveals that they are very similar in terms of both molecular weight and isoelectric point. The amino acid sequences of both silicatein α and β have been determined from the sequences of the cloned cDNAs, in conjunction with

partial sequence analyses of the purified proteins initially isolated from the strongyloxea (Shimizu, et al., 1998; Zhou, Cao, and Morse, unpublished). Native silicatein α and β purified from the axial filaments, and the proteins produced from recombinant DNA templates cloned in bacteria, yield functional, catalytically active proteins, indicating that the silicateins are in fact the constituents of the axial filaments responsible for their observed activity (Cha, et al., 1999; Zhou, et al., 1999).

Sequence analysis of silicateins α and β revealed the surprising fact that they are homologous to members of the papain superfamily of cysteine proteases. Computer-assisted alignment reveals that silicatein α, the most abundant of the axial filament protein constituents, contains nearly 50% amino acid identity to a well-known human digestive enzyme, cathepsin L (Figure 1.16).

Not only are all of the cysteine residues involved in the formation of intra-molecular disulfide crosslinks conserved between these two molecules, but also are the locations of the active site residues (cysteine, histidine, and asparagine in cathepsin L and serine, histidine, and asparagine in silicatein α), suggesting that the three-dimensional conformations of these two proteins are highly similar (Cha, et al., 1999; Shimizu, et al., 1998).

Amino acid sequence analysis of the n-terminal flanking regions of the proteins involved in directing cellular trafficking during protein maturation reveal an additional degree of relatedness between the biosilica associated silicatein α and the cathepsin L protease.

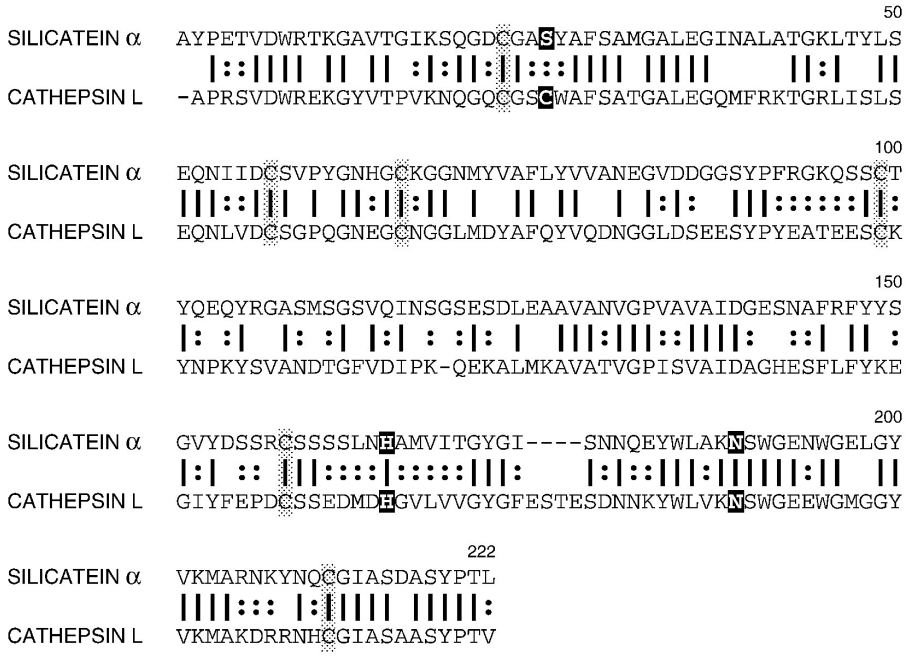

Figure 1.16: Comparison of the amino acid sequence of *Tethya aurantia* silicatein α and human cathepsin L. The vertical bars (|) indicate identical residues shared between the two proteins and the colons (:) indicate those residues with biochemical or codon similarity. The locations of the conserved active site residues are indicated by black boxes and the cysteine residues (C), responsible for the formation of intramolecular disulfide crosslinks, are dotted (adapted from Shimizu, et al., 1998).

Both hydrolases are successively modified by sequence-specific proteases involved in peptide cleavage during incorporation into membrane-bound vesicles and subsequent three-dimensional conformational folding. These findings, the hydrolytic functionalities and their vesicular packaging all strongly suggest that the demosponge silicateins and the papain family of lysosomal proteases have evolved from a common molecular ancestor (Cha, et al., 1999; Shimizu, et al., 1998; Krasko, et al., 2000).

Based on these observations, we have suggested that the silicateins' putative active-site serine-histidine sidechain couple functions as a general acid-base catalyst of the rate-limiting hydrolysis of the silicon alkoxides, in a manner parallel to the

catalysis of peptide bond hydrolysis by the homologous cysteine-histidine pair in the proteolytic enzymes (Figure 1.17).

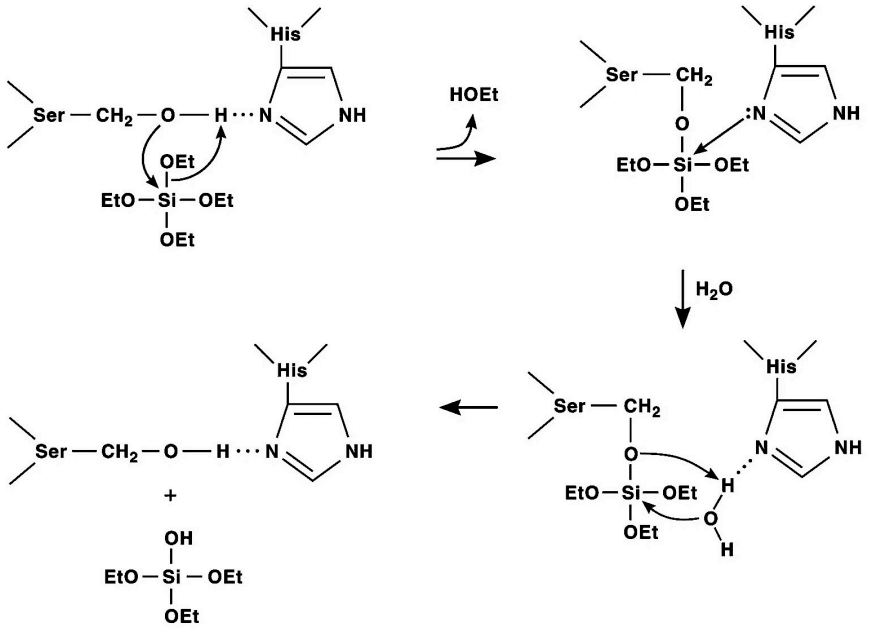

Figure 1.17: Proposed mechanism of silicatein-mediated silicon alkoxide hydrolysis modeled after the known catalysis of the related proteases. This reaction illustrates the generation of the reactive silanol, the rate limiting step in the polymerization and condensation of silica at neutral pH (adapted from Cha, et al., 1999).

In the proposed silicatein α-mediated reaction, hydrogen bonding between the imidazole nitrogen of the conserved histidine 165 (at position 165 in the protein chain) and the hydroxyl of the active site serine (at position 26) is postulated to increase the nucleophilicity of the serine oxygen, facilitating its attack on the silicon atom. Nucleophilic attack on the silicon atom would then displace ethanol, with the formation of a transitory covalent protein-O-Si intermediate that is structurally

analogous to the enzyme-substrate intermediate formed by the protease and other hydrolases. This intermediate might be further stabilized as a pentavalent silicon species via a donor bond from the imidazole nitrogen. Addition of water would then complete the hydrolysis of the first alkoxide bond (the rate limiting step at neutral pH), with condensation then initiated by nucleophilic attack of the released Si-OH on a second molecule of substrate (Cha, et al., 1999; Shimizu, et al., 1998).

Site-directed mutagenesis experiments performed with recombinant silicatein DNA templates expressed in bacteria confirmed the suggested roles of the putative active site residues in silicatein α (Zhou, et al., 1999). Replacement of the active site serine (with a hydroxyl sidechain) and/or histidine (with its H-bonding imidazole sidechain) with amino acids of significantly different structural motifs (e.g. alanine with a methyl sidechain), dramatically lowered the catalysis of silica formation from the alkoxide substrate. The requirement for histidine was further substantiated by the partial rescue of activity of the histidine-replaced mutant protein by supplementation with exogenous imidazole (Merget, et al., unpublished). Similar results also were obtained by site-directed mutagenesis studies of the β subunit (Cao, et al., unpublished).

Kinetic analyses confirm that silicatein α reacts with the silicon alkoxides in a typical enzyme-like manner, displaying substrate saturation with true Michaelis-Menten kinetics, although the rate of reaction is quite slow compared to that of the related proteases (Zhou, et al., unpublished). In site-directed mutagenesis studies with proteolytic enzymes, replacement of either of the two residues required for

activity typically results in a reduction in catalytic activity by several orders of magnitude (Carter and Wells, 1988), while in mutagenized silicatein α, the loss of activity is only on the order of ca. 90%. This might suggest that by sacrificing speed in the hydrolysis of the silica precursor, the protein may be able to exert a greater degree of structural control over the polymerization process. Relatively low rates of silica formation also may facilitate the precise fabrication of the superficial elaborations often observed on sponge skeletal elements (Hartman, 1981) (cf. Figure 1.5). This activity might be further regulated, either at the level of the protein or the delivery of substrate to produce pauses and reinitiation of silica deposition, resulting in the annular deposits of differentially condensed silica described by Schwab and Shore, (1971a,b) (cf. Figure 2.2).

Based on the identification of the catalytic residues in the silicatein molecule confirmed by the mutagenesis experiments described above, we have synthesized di-block copolypeptides that mimic both the catalytic and structure-directing activities of the protein (Cha, et al., 2000). The block copolypeptides were synthesized using lysine and cysteine amino acid N-carboxyanhydride monomers (Deming, 1997) with a final stoichiometry of L-cysteine$_{30}$-L-lysine$_{200}$. In these synthetic peptides, the cysteine residues provide the nucleophilic sidechains and the lysine residues provide the required hydrogen-bonding amine functionalities. When in their reduced form, these polymers self assemble into 600nm-diameter aggregates and when combined with TEOS in a biphasic emulsion, catalyze the formation of silica microspheres measuring ca. 100μm in diameter (Figure 1.15). Interestingly, when the sulfhydryl

sidechains of the cysteins are partially oxidized, causing the peptides to form multi-chain concatenates, reaction with the silicon alkoxide yields ordered bundles of fibrillar silica. These experiments suggest that the three-dimensional architecture of these self assembled block-copolypeptides is an important determinant of the structure of the final product. Based on these results and further mutagenesis studies, we are examining additional domains of the silicatein molecules that may prove important in controlling the order and orientation of the polymerized siloxane product (Cha, et al., 2000).

Recent investigations have also explored the use of the intact filaments to promote the hydrolysis and condensation of other metal oxides including, but not limited to, TiO_2 (Sumerel, et al., 2003), Ga_2O_3 (Kisailus, et al., 2005a), and ZnO (Kisailus, et al., in preparation). These oxides are industrially useful in a wide range of applications such as gas and biological sensors, photovoltaic cells and light emitting diodes.

Recent results indicate that the axial filaments can catalyze the structure-directed synthesis of gallium oxide (Figure 1.18A) from simple alkoxide-like precursors at room temperature (Kisailus, et al., 2005a). Thermal denaturation of the filaments abolishes this observed catalytic activity (Figure 1.18B), again suggesting that the native geometries of the active site residues on the filament surface play a critical role in the hydrolysis and condensation of the parent oxide. Silk fibers do not promote the hydrolysis and polycondensation of the metal oxide precursor to yield Ga_2O_3 (Figure 1.18C), demonstrating that, as in the case with the silicon alkoxide

precursors, more than the simple presence of hydroxyl-rich domains are responsible for the observed activity.

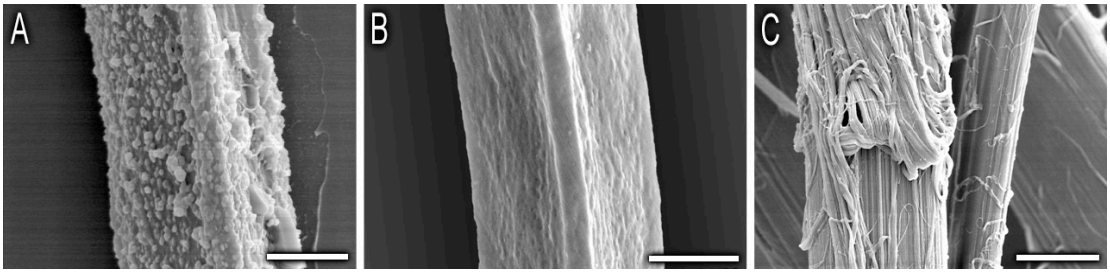

Figure 1.18: Enzymatic catalysis and structure-directed synthesis of Ga_2O_3 at room temperature. (A) Ga_2O_3 product formed on the surface of the native filaments. (B) Thermal denaturation of the filaments abolishes this observed catalytic activity. (C) Silk fibers do not promote the hydrolysis and polycondensation of the metal oxide precursor and thus yield no product (adapted from Kisailus, et al., 2005a). Scale bars: A: 1μm; B: 1μm; C: 10μm.

Under kinetically constrained conditions (reduced precursor concentrations and extended reaction times) a thermodynamically metastable phase is formed on the filament surface. High-resolution TEM and selected area electron diffraction (Figure 1.19) at the interface of the filament and the Ga_2O_3 coating indicate that the oxide is the nanocrystalline spinel (normally formed only at elevated temperatures above 400ºC). These results suggest the potential that a pseudo-lattice match between the crystalline product and the catalytic filament surface may be responsible for lowering the thermodynamic barrier to the formation of a normally high-temperature metastable phase.

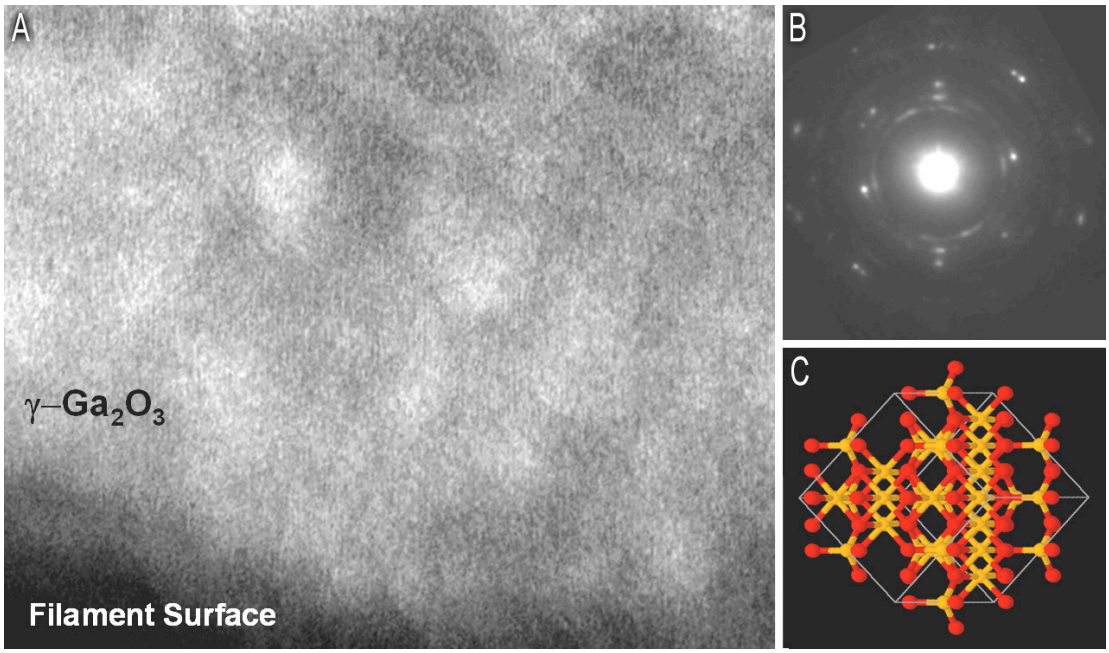

Figure 1.19: Ga_2O_3 characterization by HRTEM and SADP. (A) High resolution TEM of Ga_2O_3 nanoparticles on the filament surface. SADP (B) confirms the γ-Ga_2O_3 polymorph (C) (adapted from Kisailus, et al., 2005a).

Recently, techniques have also been developed for creating ordered arrays via self-assembled monolayers (SAMs, Figure 1.20A) that mimic both the hydrolytic activities and templating abilities of the native filaments (Cha, et al., 1999). These methods are based on the use of microcontact printing to prepare bifunctionalized surfaces of imidazole and hydroxyl-terminated SAMs on gold wafers, thus positioning the interfacial catalytic functionalities at positions that would optimize the potential for hydrogen-bonding interactions to occur (Kisailus, et al., 2006). When placed in semiconducting metal oxide precursor solutions and analyzed by electron microscopy, these bifunctional wafers catalyze the hydrolysis of these precursor

molecules and spatially direct the freshly hydrolyzed condensate on prefabricated nucleation sites.

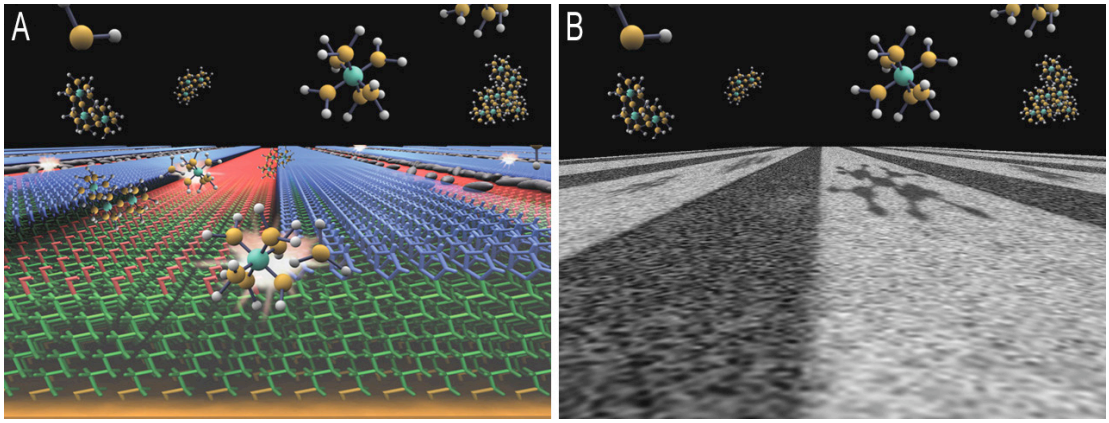

Figure 1.20: Synthesis of catalytic and structure-directing bifunctional self-assembled monolayers. Schematic (A) of the synthesized catalytic substrate and a superimposed SEM image (B) showing the site-specific deposition of Ga_2O_3 nanoparticles on the OH-terminated SAMs (adapted from Kisailus, et al., 2006) (cf. Figure 1.21).

Low magnification scanning electron microscopy (Figure 1.20B and 1.21A) reveals that the product formed under these reaction conditions precisely reflects the topology of the underlying organically functionalized surface, thus demonstrating the ability to synthetically adapt the remarkable complexity of biological systems for the controlled 2-dimensional synthesis of metal oxide semiconductors under environmentally benign reaction conditions. SEM analyses reveal a much higher nucleation density of gallium oxide on hydroxyl-terminated surfaces than those functionalized with imidazole, while non-catalytic substrates (Figure 1.21B) yield

insignificant quantities of oxide product and exhibited little to no preferential nucleation.

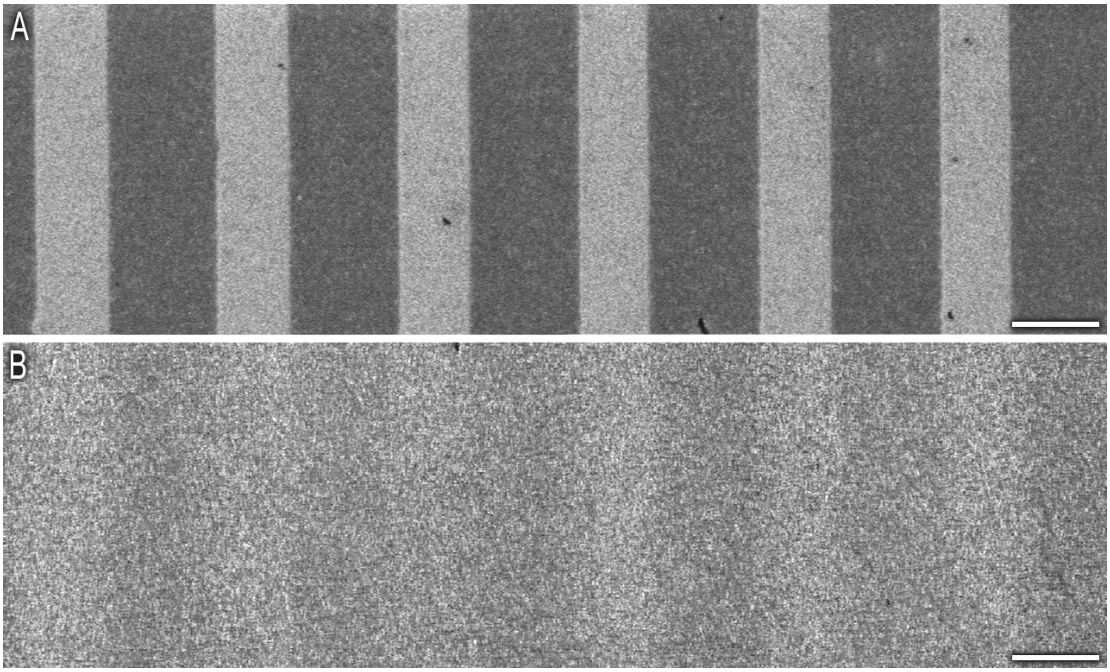

Figure 1.21: Catalytic and non-catalytic SAMs. (A) Imidazole / OH terminated SAMs yield large quantities of product, while non-catalytic substrates (methyl / OH) yield insignificant quantities of oxide product and exhibited little to no preferential nucleation (B) (adapted from Kisailus, et al., 2006). Scale bars: 10μm.

In an alternative strategy developed to expand the catalytic functionality discovered in the SAM studies from two dimensional surfaces to bulk solution metal oxide synthesis, 5–10nm gold nanoparticles (GNPs, Figure 1.22) have been synthesized with specific chemical functionalities (imidazole and hydroxyl) (Kisailus, et al., 2005b) that mimic the active site chemistry of silicatein α (Shimizu, et al., 1999; Zhou, et al., 2000).

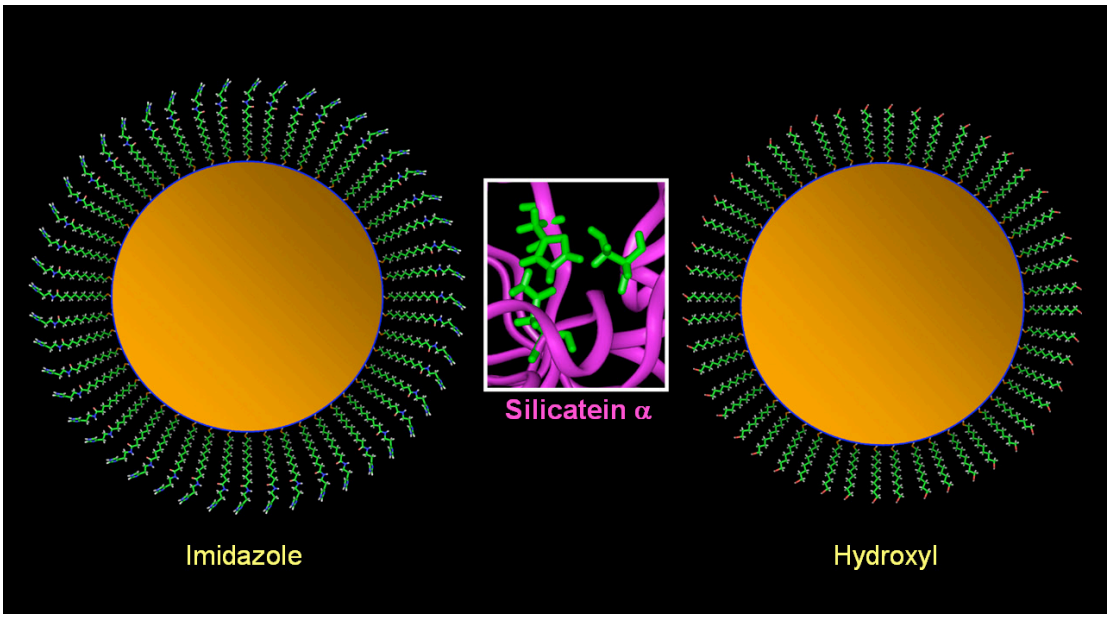

Figure 1.22: Biomimetic catalytic gold nanoparticles. Two distinct populations of imidazole- and hydroxyl-terminated gold nanoparticles were synthesized that mimic the active site stereochemistry of the silicatein enzyme (adapted from Kisailus, et al., 2005b).

In an initial feasibility study, mixtures of these functionalized GNPs were tested as potential catalysts towards the hydrolysis of TEOS. Quantitative analyses (Figure 1.23) by molybdate assay of the reaction products formed from various functionalized GNP mixtures confirmed the necessity of proximal hydrogen bonding agents (imidazole) and nucleophilic constituents (hydroxyl) for hydrolytic activity. This was demonstrated by a 10-fold increase in product yield over combinations of GNPs lacking either one of these critical catalytic functionalities (Kisailus, et al., 2005b). Current research is aimed at the use of these and other biomimetic approaches for controlling polymorph, orientation, and morphology of a wide range metal oxide and nitride semiconductors for the potential use in device applications.

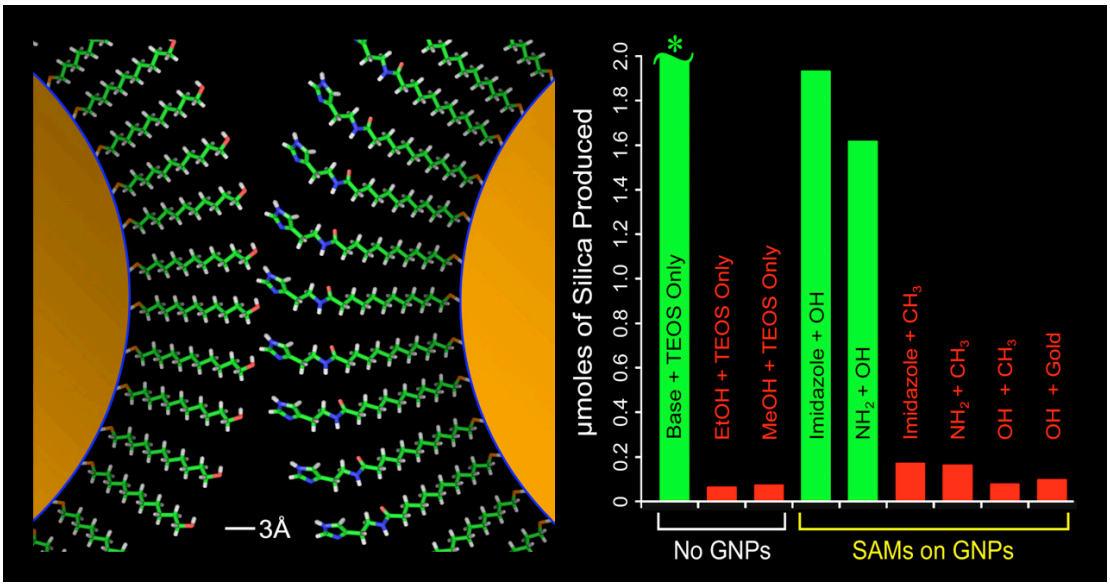

Figure 1.23: Product yield obtained from catalytic and non catalytic mixtures of gold nanoparticles. *Quantity of product formed: 6.1µmol (adapted from Kisailus, et al., 2005b).

In addition to the use of the silicateins and their biologically inspired synthetic analogs for semiconductor synthesis, advances are also currently being made in the understanding of the nano- and microscale organic and inorganic components of the spicules themselves. As we will see in Chapter 2, *T. aurantia* has continued to be a useful model system for silica biomineral ultrastructural investigations.

Chapter 2

Nanostructural Features of Demosponge Biosilica

This Chapter is adapted from:
Nanostructural features of demosponge biosilica
Weaver JC, Pietrasanta LI, Hedin N, Chmelka BF, Hansma PK, Morse DE
Journal of Structural Biology
144 (3): 271-281 **2003**

2.1 Introduction

The emerging field of silicon biotechnology has centered on understanding the mechanisms controlling biosilicification and its applications to the *in vitro* development of low-temperature routes to highly ordered silicon-based materials synthesis (Morse, 1999, 2001; Brott, et al., 2001). Additional interest in the silica structures made by sponges has been stimulated by the recent characterization of the superior mechanical and interesting optical properties of these materials (Levi, et al., 1989; Sarikaya, et al., 2001; Sundar, et al., 2003). Similarly, the remarkably complex structures made by diatoms, a class of unicellular algae (Figure 1.1), have led to suggestions that these also might be used for technological applications (Parkinson and Gordon, 1999; Vrieling, et al., 1999; Sandhage, et al., 2002). Due to the complex nature of biosilicification, development of a tractable model system is essential if one is to understand the fundamentals of the underlying complex and dynamic biological processes. While previous research in this field has focused on structural analyses of diatom frustules (Heckey, et al., 1973; Lobel, et al., 1996; Kröger, 1999, 2000), and plant phytoliths (Theunissen, 1994; Carnelli, et al., 2001), we have concentrated our efforts on biosynthetic skeletogenesis in siliceous demosponges (Porifera) (Simpson and Vaccaro, 1974; Jones, 1979; Garrone, et al., 1981; Simpson, 1984; Simpson, et al., 1985; Uriz, et al., 2000). In demosponges, skeletal support is often provided by highly ordered siliceous structures ranging in morphology from long needle-like strongyles to articulated, interdigitated fused networks of hypersilicified desmas as in the lithistid sponges, *Racodiscula sp*. (Hartman, 1981) and *Discodermia sp*. (Weaver

and Morse, 2003) (cf. Figure 1.9).

Interest in sponge biosilicification is not a new field, but rather dates back to the early 1800s when it was first demonstrated that demosponge spicules are siliceous (Minchin, 1909). From fracture studies, these early investigations concluded that these spicules are composed of concentric lamellae (Bütschli, 1901), with a central axial filament of HF-resistant material that blackens upon heating, suggesting the presence of organic constituents. More recently, it was demonstrated that this axial filament is proteinaceous (Shore, 1972) and has both templating as well as catalytic activity in directing the polymerization of silica and silsesquioxanes *in vitro* (Shimizu, et al., 1998; Cha, et al., 1999; Zhou, et al., 1999; Morse, 1999, 2000, 2001; Shimizu and Morse, 2000; Sumerel and Morse, 2003; Weaver and Morse, 2003) (cf. Chapter 1).

Although the untreated spicules of *Tethya aurantia* appear smooth, transparent, and glassy (Figure 2.1), several observations prompted our more detailed investigation of their substructure: (1) investigations of the spicules of various demosponge taxa have revealed that they are composed of annular lamellae of silica (Bütschli, 1901; Schwab and Shore, 1971b; Simpson, et al., 1985); (2) partial etching of spicules with HF revealed a nanoparticulate substructure (Figure 2.5B) (Cha, 2001); (3) the biosilicas made by diatoms (unicellular algae), revealed both by SEM (Schmid and Shulz, 1979; Volcani, 1981) and AFM (Wetherbee, et al., 2000; Noll, et al., 2002) analyses, exhibit a nanoparticulate substructure; and (4) silica formation *in vitro* mediated by diatom silaffins (Kröger, et al., 1999, 2000) and by sponge spicule

silicateins (Cha, et al., 1999) (cf. Figure 1.15) is nanoparticulate. In fact, chemically synthesized silaffins have been used to guide the synthesis of an array of silica nanoparticles that functioned as a photonic crystal (Brott, et al., 2001).

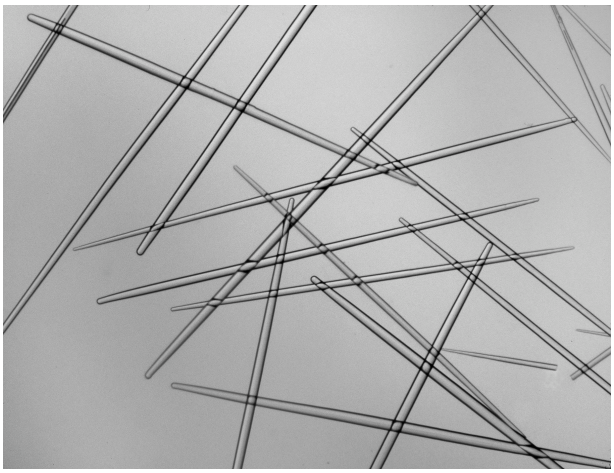

Figure 2.1: Polarized light micrograph of strongyloxea isolated from the temperate demosponge *Tethya aurantia*. Each spicule measures approximately 2mm in length and 30μm in diameter.

Schwab and Shore (1971a,b) observed conspicuous rings and concentric striations upon etching transverse spicule sections with HF. Their observations that prior heating of the biosilica prevented the appearance of etch-rings, in conjunction with their thermogravimetric analyses, led them to conclude that the etch-sensitive rings represented regions of less condensed (and thus, more hydrated) silica.

When observed by scanning electron microscopy, however, the superficial morphology appears highly consistent across the entire fractured spicule (Figure 2.2A), without any indication of the annular deposits (Figure 2.2B) that are revealed by HF etching. This supports the idea that the rings are due to relatively subtle

compositional differences. The presence of zones of secondarily modified, but structurally similar material such as differentially dehydrated (i.e., condensed) silica, is one possible explanation, since variability in the degree of silica condensation could affect rates of etching by HF. Until recently, however, technological limitations have been a major obstacle in further elucidation of the concentric siliceous substructure of demosponge spicules. This current work builds on the pioneering AFM imaging done in 1998 (Egerton-Warburton, et al., 1998) by providing new insights into the nanoscale ultrastructure of the deposited silica.

Recently it was reported that formation of the terminal bulb during tylostyle maturation in the boring demosponges *Cliona tinctoria* and *Pione caesia* results from the secondary deposition of granular silica at one end of these linear spicules (Schonberg, 2001). These results, however, did not reveal the gross silica nanostructuring of the spicule itself, as these observations were principally interpreted as a secondary spicule modification mechanism. Here, we report the use of high resolution SEM in conjunction with AFM techniques to analyze the annular substructure of the siliceous spicules from the temperate demosponge *T. aurantia*. In conjunction with results obtained from NMR analyses of spicule samples heated to different temperatures, these observations relate for the first time the nanoparticulate substructure, the annular organization, and the differential etchant reactivity reported in independent analyses of demosponge biosilica.

2.2 Results

2.2A SEM Analyses of fractured spicules

Investigation of the morphology of freshly cleaved spicule cross-sections by SEM revealed no detectable concentric organization of the deposited silica. In many instances, the axial protein filament was found dislodged, leaving the central hexagonal axial channel empty (Figure 2.2A).

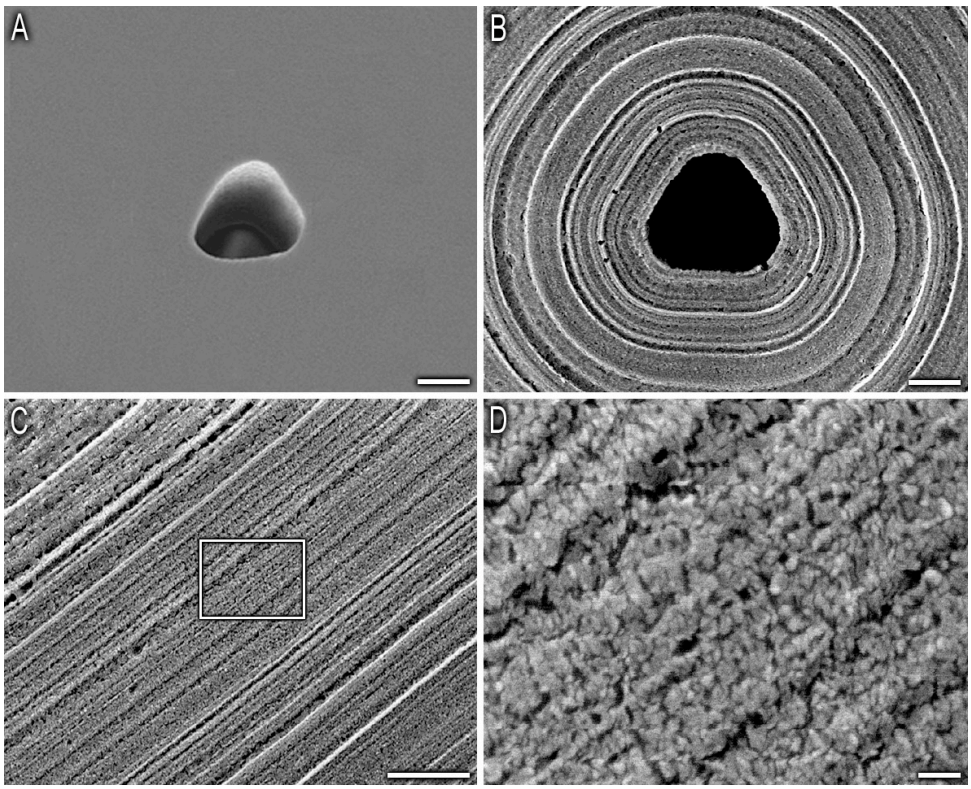

Figure 2.2: Scanning electron micrographs of spicule cross-sections from *Tethya aurantia*. (A) Scanning electron micrograph of an un-etched spicule cross-section. The axial filament has been removed leaving a hollow central hexagonal cavity. Sodium hypochlorite-etched cross-section (B) and longitudinal-section (C) reveal concentric organization of the deposited silica. (D) High magnification (80,000x) scanning electron micrograph of boxed region in panel (C), revealing the nanoparticulate nature of the deposited silica. Scale bars: A: 1μm; B: 1μm; C: 1μm; D: 100nm.

The interior of this channel often exhibited nanoparticulate surface features, while the fractured silica did not. Annular substructure in the spicule cross-sections became apparent only after long-term alkaline or brief HF etching (Figures 2.2B and 2.6). Regions subsequently identified as containing less condensed (more hydrated) siliceous material etched at a faster rate relative to those containing more highly condensed silica (Figures 2.2B and 2.6).

High magnification imaging of sodium hypochlorite-treated longitudinal sections (Figure 2.2C, D) reveals long-range ordering of the deposited silica nanoparticles. Similar results were obtained with other alkaline etchants such as NaOH (data not shown) or brief 1M HF treatments, although, due to the rapid rate of HF-demineralization, nanostructural details of the annular substructure were frequently obscured by extensive surface roughening caused by the HF.

2.2B AFM Analyses of fractured spicules

Although undetectable with high-resolution SEM imaging, AFM analyses revealed the presence of nanoparticulate silica organized around the central axial filament of freshly cleaved (un-etched) spicule cross-sections (Figure 2.3A). The sizes of these particles are consistent with the data obtained from the sodium hypochlorite-treated SEM images (Figure 2.2D), revealing a mean particle diameter of 74 ± 13nm (n=75); the concentric organization of these particles is clearly evident (Figure 2.3A, B). AFM phase imaging also revealed the presence of relatively rare annular regions that exhibit both higher topography and phase contrast (Figure 2.3B,

C). After treatment of fractured spicules with sodium hypochlorite, NaOH, or HF, AFM analyses revealed increased prominence of the annular substructure as the more hydrated regions (cf. below) are etched more quickly. Although the depth of the valleys between successive etch-resistant rings increased with sequential etching (Figure 2.4A, B), there was negligible reduction in mean particle diameter of this more condensed (and thus more etch-resistant) material (standard deviation ≥ magnitude of average difference before and after etching).

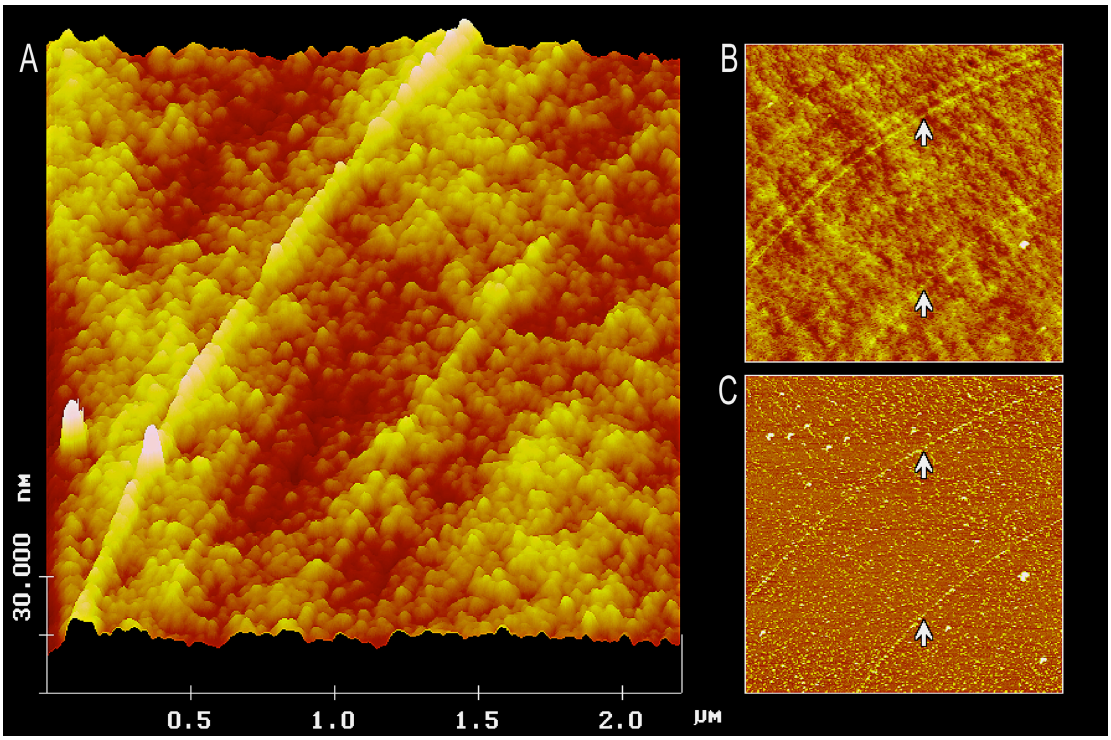

Figure 2.3: AFM images of spicule cross-sections. (A) AFM surface plot of a freshly cleaved (un-etched) spicule cross-section revealing the existence of concentric arrays of nanoparticulate silica. (B) Top view and (C) phase mode image of the same preparation. Note the relatively rare rings of higher phase contrast, as shown by the white arrows (cf. Figure 2.6). Scan sizes: 2.25µm.

High magnification analysis (Figure 2.4C) -with a scan size of 2µm- of longitudinally cleaved sections indicates that each layer is approximately monoparticulate in thickness (Figure 2.5A), revealing an unanticipated level of structural complexity of the deposited silica. While the annular structuring of this material has been known from previous work, these studies reveal for the first time that these annuli are deposited with nanoscale regularity across macroscopic length scales.

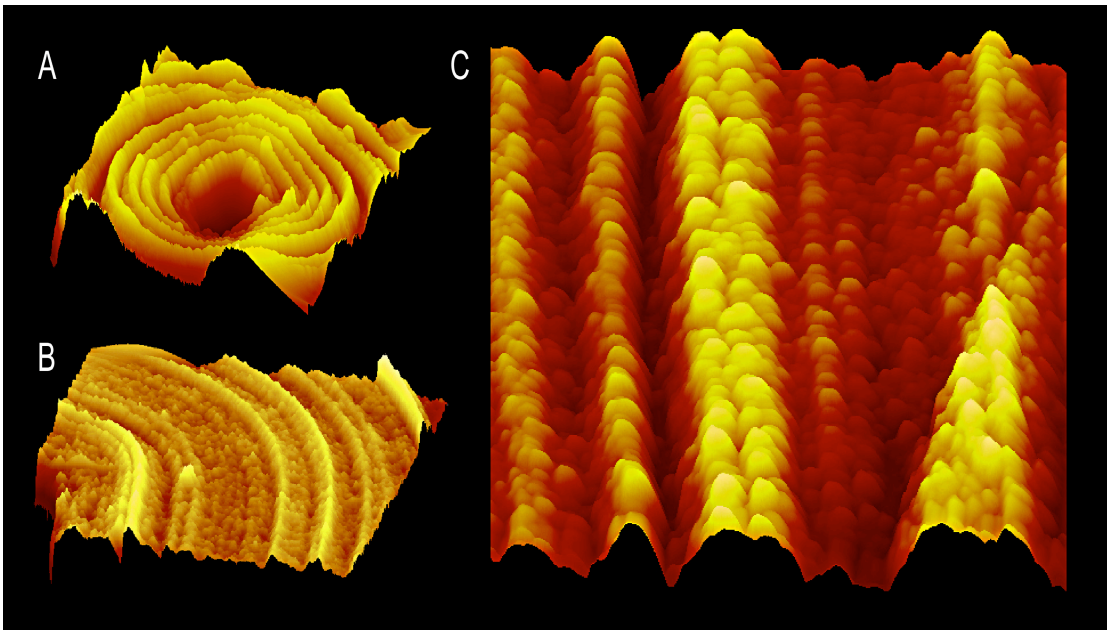

Figure 2.4: AFM surface plots of sodium hypochlorite-treated (etched) spicule cross-sections (A, B) and longitudinal-section (C). (A) illustrates concentric organization of deposited silica, while (B) and (C) reveal the annular nanoparticulate substructure. (A) Scan size 10µm, z data scale 250nm; (B) scan size 3.8µm, z data scale 275nm; (C) scan size 2µm, z data scale 75nm.

2.2C Treatments with HF and heat

Heating spicule cross-sections to 300ºC for one hour appeared to have a negligible effect on both the etchant reactivities and the annular morphologies of samples etched prior to heating. When similar samples were heated to 600ºC for one hour, however, this dramatically altered the subsequent etchant reactivities, as no annular features could be observed upon HF treatment after heating to this temperature. Interestingly, however, there did not appear to be significant morphological alteration to the HF-revealed annular features after heating to 600ºC for previously etched samples (data not shown).

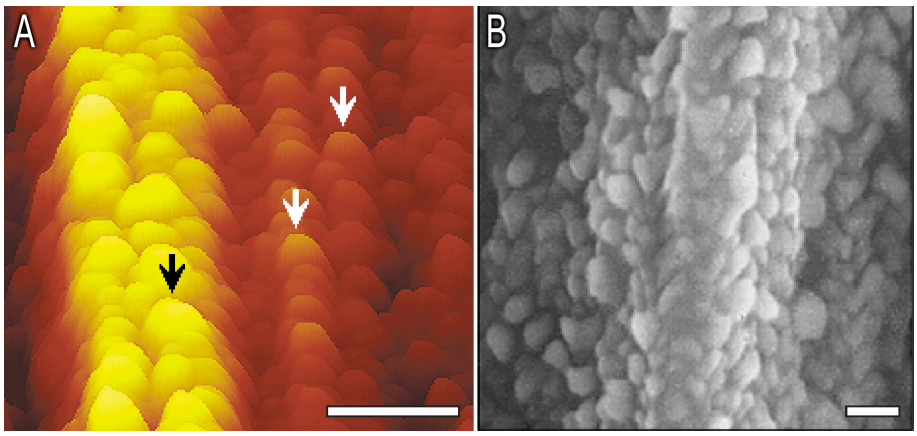

Figure 2.5: Longitudinal organization of silica nanoparticles in *Tethya aurantia* megascleres. (A) AFM surface plot of spicule longitudinal section (enlargement of a portion of Figure 4C) revealing annular organization of the deposited silica. The arrows indicate individual layers that are nearly monoparticulate in thickness. (B) Scanning electron micrograph illustrating nanoparticulate silica visible after brief treatment of intact spicules with HF (adapted from Cha, 2001). Scale bars: A: 250nm; B: 100nm.

In addition to the standard etch rings that appear following exposure to HF, there also were annular regions that exhibited unusually high etch sensitivity. The abundance of these regions varied dramatically from spicule to spicule, from undetectable to several per specimen examined. The spicule cross-section shown in Figure 2.6 exhibits one of these regions (indicated by the arrows).

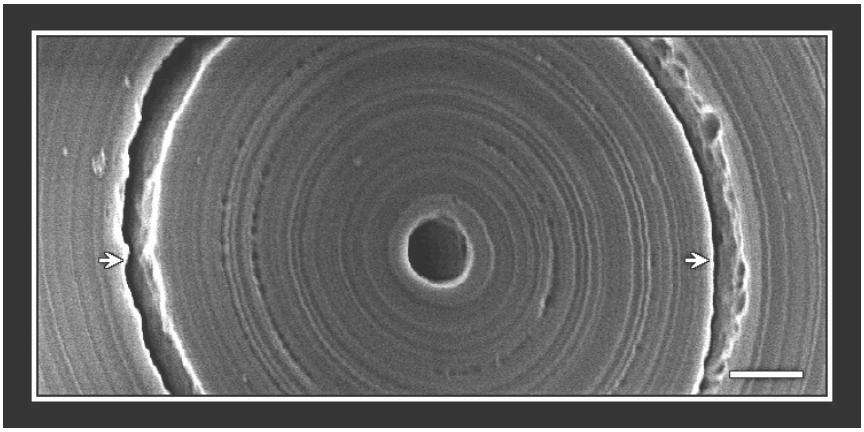

Figure 2.6: Scanning electron micrograph of an HF- treated spicule cross-section revealing regions of differential etchant reactivities. The arrows indicate an uncommon zone that etches at a considerably faster rate compared to that of the surrounding material. This region may correspond to the rings of high AFM phase-contrast shown in Figure 2.3C and could represent a zone of poorly condensed (highly hydrated) silica, which are known to etch at faster rates than more condensed material. Scale bar: 1μm.

2.2D NMR analyses[1]

Single-pulse ^{29}Si MAS NMR spectra of siliceous spicules isolated from *T. aurantia* heated to 300 and 600ºC are shown in Figure 2.7, revealing different degrees of heat-induced silica condensation. The results show that the inorganic silica framework is moderately condensed, even in the non-heat-treated sample. The

chemical shift of the dominant peak at -112ppm in Figure 2.7A corresponds to Q^4 silica units[1], and the less intense peak at -101ppm corresponds to Q^3 moieties (Engelhardt and Michel, 1987). By deconvoluting the spectra in Figure 2.7A, B into two Gaussian spectral lines, the Q^4:Q^3 ratios are estimated to be 3:1 in both the non-heat-treated sample (A) and sample (B) heated to 300°C. The left shoulder and the asymmetry of the peak at -112ppm in Figure 2.7B reveal that Q^3 moieties are still present, while the spectrum obtained from the sample heated to 600°C shows no evidence of Q^3 moieties remaining (Figure 2.7C). These differences correlate with differences in ^{29}Si T_1 relaxation times: the samples with appreciable Q^3 species (A, B) have substantially shorter T_1 values than sample (C), which is comprised almost exclusively of Q^4 moieties; an upper limit of the Q^3:Q^4 ratio < 0.1 was estimated by deconvolving the spectrum in Figure 2.7C into two Gaussian spectral components. Under otherwise identical conditions, the narrower linewidth of the Q^4 peak in Figure 2.7A (approximately 70% of that in Figure 2.7B, C) reflects the more homogeneous environments of the fully polymerized (condensed) silica sites in the non-heat-treated sample (A), compared to those in heat-treated samples (B) and (C). This indicates that the heat-induced transformation of Q^3 into Q^4 groups broadens the distribution of Si-O-Si bond angles and distances.[2]

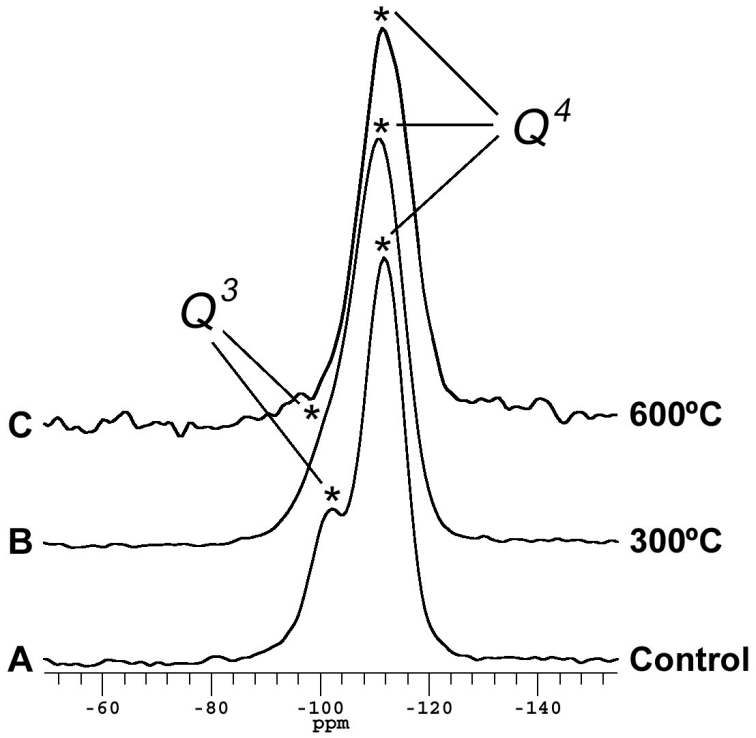

Figure 2.7: Single-pulse magic-angle-spinning ^{29}Si NMR spectra of siliceous spicules isolated from *Tethya aurantia* heated to 300 and 600ºC, revealing the degree of heat-induced silica condensation. Spectrum (A) is from non-heat-treated spicules, (B) from spicules heated to 300°C and (C) from spicules heated to 600°C. The peak at -102ppm in (A) and the shoulder of the peak at -112ppm in (B) correspond to incompletely condensed Q^3 silica moieties (Q^3/ Q^4 is ca. 0.3-0.4 for samples A and B) The larger integral area of the peak at -112ppm shows that fully condensed (Q^4) silica groups are more abundant than Q^3 species. In (C), there is no evidence of a significant fraction of Q^3 moieties remaining (Q^3/ Q^4 < 0.1).

A 2D ^{29}Si{^{1}H} heteronuclear correlation NMR spectrum of non-heat-treated siliceous spicules is shown in Figure 2.8. Two strong intensity correlations are evident between the Q^3 and Q^4 ^{29}Si chemical shifts[3] and one ^{1}H chemical shift. The ^{1}H chemical shift at ca. 5ppm is assigned to Si-OH groups or adsorbed H_2O according to their chemical shift values (Engelhardt and Michel, 1987).

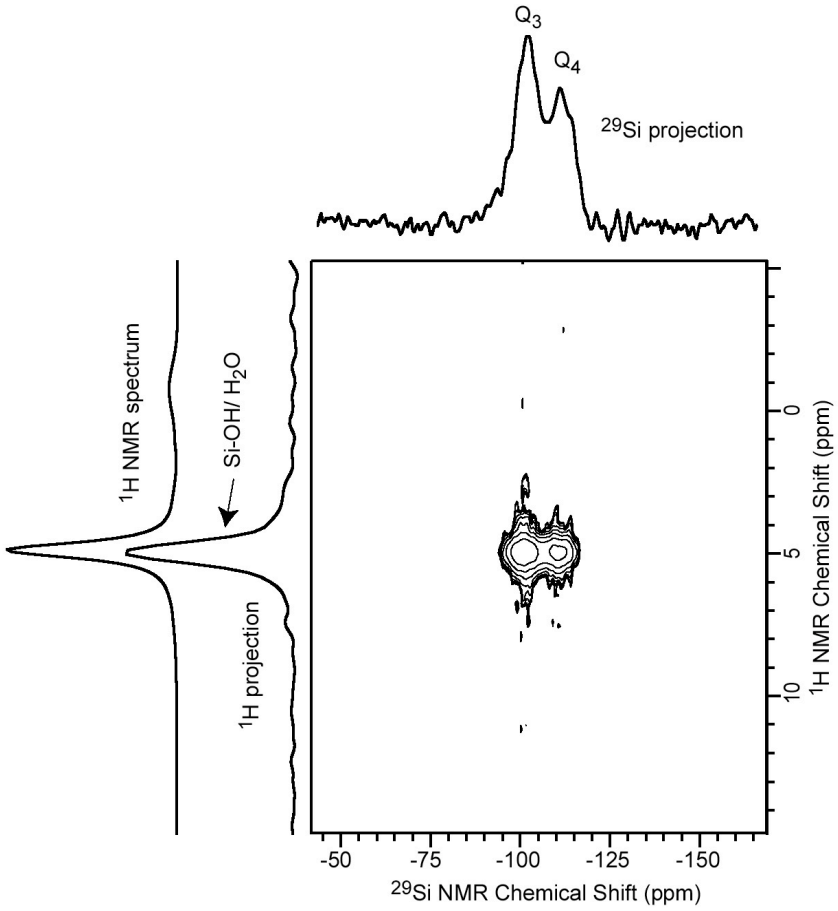

Figure 2.8: A 2D $^{29}Si\{^{1}H\}$ heteronuclear correlation NMR spectrum of the non-heat-treated siliceous spicules, with accompanying projections of the intensities in the contour plot and a single-pulse ^{1}H NMR spectrum. There are strong correlation intensities between the silica Q^3 and Q^4 moieties with Si-OH or adsorbed water at their typical ^{1}H NMR chemical shift value of ca. 5ppm. No evidence for molecular contact between the silica and organic matter was found. The dominant peak at ca. 5ppm in the ^{1}H NMR spectrum corroborates the proposed overall small quantities of organic matter in the silica surrounding the spicule axial filament.

The single-pulse ^{1}H MAS NMR spectrum in Figure 2.8 has two spectral lines, one intense at ca. 5ppm from Si-OH or adsorbed water and one weaker at around -1ppm. These results indicate that the silica moieties are not in molecular proximity to detectable quantities of organic species.

2.3 Discussion

The process of biosilicification has presumably evolved independently in a wide range of phylogenetically diverse taxa with representatives ranging from diatoms and radiolaria to sponges and higher plants (Simpson and Volcani, 1981). The convergent nature of this mineralizational motif is clearly evident from the unique taxa-specific biomolecules that are occluded in the condensed products (Shimizu, et al., 1998; Kröger, et al., 1999, 2000). A common theme that many of these groups employ in the polymerization of silica is that the nature of the polycondensed product is nanoparticulate in nature (Schmid and Schulz, 1979; Volcani, 1981; Cha, et al., 1999; Wetherbee, et al., 2000; Noll, et al., 2002). This is not surprising, since the polycondensation of silica in aqueous media is kinetically driven to form such particles, which then aggregate and condense via their surface hydroxyls (Iler, 1979).

In frustules of the diatom, *Cylindrotheca fusiformis*, for example, the polycationic silaffins (named for their affinity for silica), which are occluded within the frustule silica, are extensively post-translationally modified with polyamine and phosphate functionalities to specific amino acid sidechains (Kröger, et al., 1999, 2002). When added to metastable silicic acid, these peptides induce the rapid polycondensation and synthesis of silica nanospheres with fairly uniform morphologies. In addition to the species-specific silaffins occluded within the frustules of diatoms, high amounts of free (non-peptide linked) long-chain polyamines also are occluded (Kröger, et al., 2000). These polyamines also promote

the precipitation of silica *in vitro*, and the resulting condensed silica spheres exhibit polyamine-specific size dependencies. It is currently thought that the cooperative interactions of these longchain polyamines and the silaffins, in conjunction with phase-separation, may be responsible for mediating the formation of the species-specific nanoscale frustule morphologies observed *in vivo* (Kröger, et al., 2000; Sumper, 2002). Significantly, the sizes of the silica nanoparticles produced by the silaffins and polyamines *in vitro* are similar to those revealed by AFM in native diatom frustules (Wetherbee, et al., 2000; Crawford, et al., 2001; Noll, et al., 2002).

Although it had been previously reported that HF etched demosponge spicules revealed a nanoparticulate substructure (Figure 2.5B), these experiments did not reveal hierarchical, annular ordering of the particles (Cha, 2001). The results reported here reveal the nanostructural architecture of this material and illustrate the precise, hierarchical control that is exhibited over mineral deposition during demosponge spicule formation.

The differential etchant reactivities exhibited by this biosilica in conjunction with our microscopic and NMR analyses before and after high-temperature (600ºC) induced condensation support the suggestion (Schwab and Shore, 1971b) that the annular pattern reflects differences in the extent of silica condensation during deposition, rather than the inclusion of appreciable quantities of organic material. The observation that the SEM-detectable annular substructure of previously HF-etched samples was not significantly altered upon heating to 600ºC indicates that the duration of heating was not sufficient for thermally induced melting of the deposited

silica. Together with the NMR results, this supports the proposal that heating to 600ºC results in almost complete silica condensation (accompanied by a loss in etch sensitivity) and is not an organic degradation or silica mobilization (melting) process. This is confirmed by the disappearance of the Q^3 NMR species and the substantial increase in the T_1 relaxation parameter, corroborating a dramatic decrease in the abundance of free hydroxyls. If large quantities of organic material had been initially incorporated within the deposited silica (e.g., between the annular layers), then at sub-mobilization temperatures, one might expect to see concentric banding or pitting appear after heating-induced destruction of organics, which in these experiments was not observed. The ^{1}H NMR spectrum of the non-heat-treated spicules (Figure 2.8) shows no signals in the range of 1 – 2ppm that are characteristic for aliphatic organic species. The 2D ^{29}Si{^{1}H} NMR spectrum (Figure 2.8) establishes that only signals from Si-OH (or adsorbed water) and the silica framework are strongly correlated and thus in close molecular proximity. The dominance of the Si-OH and water ^{1}H NMR signals is consistent with our proposal that there exist negligible quantities of organic material in intimate association with the silica nanoparticles that surround the spicule axial filament; such organic matter thus could not feasibly contribute appreciably to the observed dramatic difference in etchant reactivity of the silica annuli.

Results from HF- or alkaline-etching experiments reveal the existence of sparsely distributed annular siliceous deposits with unusually high etchant reactivities (Figure 2.6). These localities could represent regions of poorly condensed (highly hydrated) silica and may indicate abnormal variability in silica deposition during

spicule biosynthesis. This suggestion is supported by the relative rarity of these regions within an individual spicule, and by the high degree of spatial variability exhibited from spicule to spicule (in which these low density regions vary in abundance from undetectable to several per specimen examined). Interestingly, the relative rarity of these regions roughly corresponds to the abundance of annuli of high AFM phase-contrast, such as those shown in Figure 2.3C. While at least some of this observed contrast could be explained by topographical differences, there are potentially other contributing factors, such as slight compositional differences in the material being examined, that should be considered. Based on these observations, we cannot rule out the possibility that there may exist a correspondence between these high AFM phase-contrast regions and those of very high etch sensitivity, such as shown in Figure 2.6.

Based on the dramatically different mechanisms of biosilicification in demosponges and diatoms -apparently mediated, at least initially, by insoluble filamentous catalytic protein scaffolds in demosponges and monomeric, stoichiometric polyamines in diatom frustules- it is likely that the similar nanoparticulate structural motifs of the deposited silica are a consequence of the intrinsic colloidal behavior of silica during polycondensation from aqueous media (Iler, 1979). The stoichiometric activity of the diatom silaffins involved in silica polymerization (Kröger, et al., 1999, 2000) is fundamentally similar to the induction of silica polycondensation by synthetic polyamines (Mizutani, et al., 1998), while the silicateins are both catalytic and structure-directing. Although the biomolecular

components directing the condensation and assembly processes may differ, the kinetic drive to form nanoparticulates of silica is evident in these two very different systems.

It should be noted that the paucity of organic material in direct association with the silica annuli surrounding the axial filament in demosponges such as *T. aurantia* differs markedly from the structure of spicules isolated from hexactinellid sponges (Sundar, et al., 2003). This difference also can be expected to result in significant differences in the mechanical and fracture properties of the spicules of these two very different groups of sponges, the Demospongiae and the Hexactinellida (Levi, et al., 1989; Sarikaya, et al., 2001). In Chapter 3, we will explore the architectural details of hexactinellid spicules using the Western Pacific sediment-dwelling *Euplectella aspergillum* as a model system. In addition to the remarkable mechanical properties of the spicules, themselves, this species assembles its constituent spicules into a hierarchically ordered, fracture-resistant three-dimensional skeletal lattice, the mechanical consequences of which will be discussed in detail.

2.4 Footnotes

[1]In this notation, Q^n refers to tetrahedrally coordinated silicon atoms, Q, having n neighboring -O-Si- groups.

[2]Other possible contributions to these differences can effectively be ruled out. The magnitude of the field inhomogeneity is on the order of 20Hz, and homogenous linewidths are expected to be less than 1Hz for ^{29}Si Q^4 moieties in natural abundance in purely siliceous materials (Anderson, 1992).

[3]Note that the ^{29}Si projection of Figure 2.8 is quite different from Figure 2.7A. This is a result of the ^{29}Si{^{1}H} heteronuclear NMR spectrum which was optimized to be more sensitive to Q^3 moieties.

Chapter 3

Hierarchical Assembly of the Siliceous Skeletal Lattice of the Hexactinellid Sponge Euplectella aspergillum

This Chapter is adapted from:
Hierarchical assembly of the siliceous skeletal lattice of the hexactinellid sponge, Euplectella aspergillum
Contributing authors: James C. Weaver, Joanna Aizenberg, Georg E. Fantner, David Kisailus, Alexander Woesz, Peter Allen, Kirk Fields, Michael J. Porter, Frank W. Zok, Paul K. Hansma, Peter Fratzl, and Daniel E. Morse

3.1 Introduction

The hexactinellids are a remarkably diverse and ancient lineage of sponges with a fossil record that dates back more than half a billion years (Gehling and Rigby, 1996; Brasier, et al., 1997). They are important contributors to benthic biomass in predominantly deep-sea environments. The hexactinellids are characterized by the unique three-axis (six-rayed) symmetry of their skeletal elements (spicules) and their syncytial cellular anatomy (Leys and Lauzon, 1998; Beaulieu, 2001a,b; Janussen, 2004). The earliest known descriptions of hexactinellid skeletal systems in the scientific literature date back to 1780, when spicules from *Dactylocalyx sp.* were described in Rozier's Journal de Physique, although at that time, the true biological origin of the examined material was not yet known (Schulze, 1887). Numerous contributions to the fields of hexactinellid anatomy and skeletal morphology were made in the mid 1800s, with studies of specimens from the Challenger expedition of the 1870s being among the most significant (Schulze, 1887). From examination of living specimens (Figure 3.1A), one could hardly predict the presence of such remarkable skeletal systems as are encountered in members of this unique group of sponges. This is exemplified in the descriptions provided by J. E. Gray in 1872, who stated, "It would be difficult to imagine that the thick, somewhat clumsy, brown tube, perforated with irregular openings, contained any arrangement of support so delicate and symmetrical" (cf. Figure 3.1B).

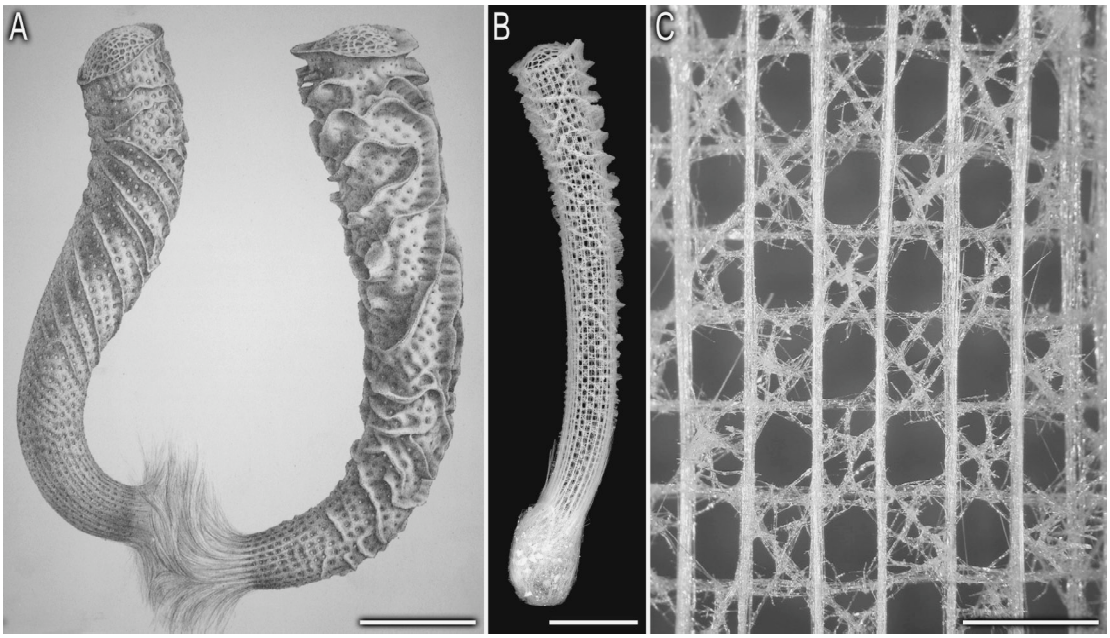

Figure 3.1: Details of the Western Pacific hexactinellid sponge, *Euplectella aspergillum,* and its skeleton. (A) Illustration (from Schulze, 1887) of two preserved specimens, clearly showing the holdfast apparatuses, the external ridge systems, and the terminal sieve plates. (B) Photograph of the underlying siliceous cylindrical skeletal lattice exposed by removal of the organic material. (C) At higher magnification, the square grid architecture and regular ordering of the vertical and horizontal components of the skeletal system are clearly visible. Scale bars: A: 5cm; B: 5cm; C: 5mm.

While the elaborate structural complexity of the hexactinellid skeletal systems made them particularly appealing to these early investigators, current research has been aimed at understanding the detailed biosynthetic mechanisms and unique mechanical and optical properties of these remarkable skeletal materials (CattaneoVietti, et al., 1996; Levi, et al., 1989; Sarikaya, et al., 2001). Recently, for example, it was shown that the anchor spicules (basalia) from the Western Pacific sediment dwelling hexactinellid sponge, *Euplectella aspergillum* were comparable to man-made optical fibers in terms of optical properties and superior in terms of

fracture resistance (Sundar, et al., 2003; Aizenberg, et al., 2004). As remarkable as these spicules are, however, they represent only one level of hierarchy in the extremely complex skeletal system of this species (Schulze, 1887; Aizenberg, et al., 2005). Recent advances in wide angle and high depth of field scanning electron microscopy have now permitted a reexamination of the early descriptive studies of the skeletal architecture of *E. aspergillum*. Combining an electron micrographic study with three-dimensional structural renderings and design theory, we present here an updated detailed analysis of this complex skeletal system.

3.2 Results and Discussion

Using modern advances in electron microscopy and three-dimensional structural rendering, we have combined our observations with Schulze's original descriptions of *E. aspergillum* collected during the Challenger expedition between 1873-1876, in an attempt to update and unify the already impressive coverage of the individual design elements present. The main levels of structural hierarchy, which range in dimensions from 10s of nm to 10s of cm, are summarized in Figure 3.2 and described in detail below. Briefly, in this skeletal system, organic and inorganic components assemble to form a composite spicule structure. Non-planar cruciform spicules are organized to form a three-dimensional cylindrical network. The walls of the resulting structure are cemented and strengthened by spicule bundles, oriented vertically, horizontally and diagonally with respect to the cylindrical lattice. At a coarser scale, spicules are arranged to form a series of diagonal (helical) ridges on the

external wall of the lattice. The entire configuration is cemented by additional silica-rich composite layers. The structural components that exist at each hierarchical level are described below.

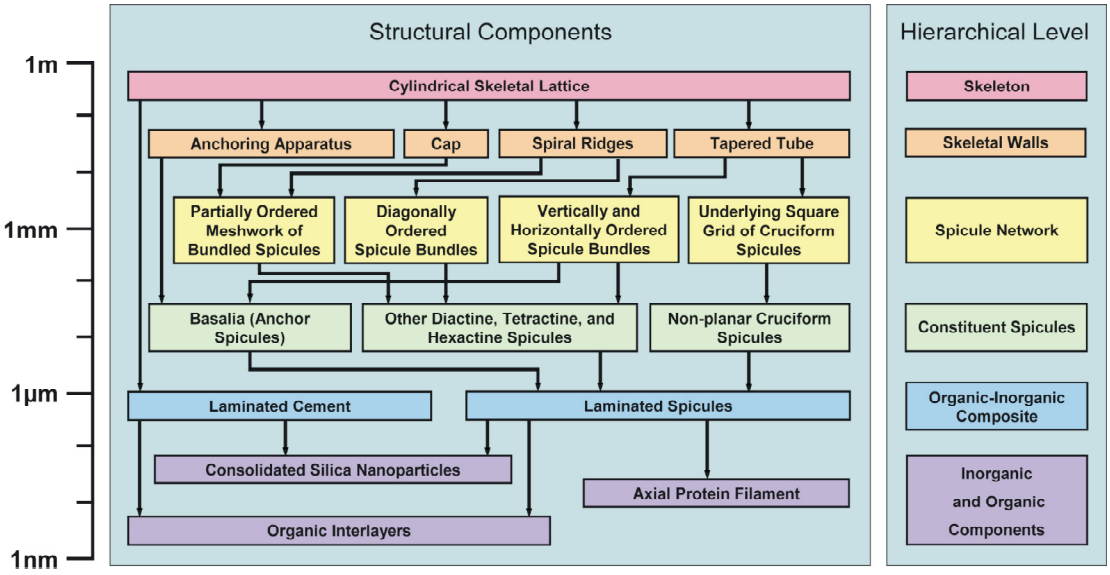

Figure 3.2: Schematic representation of the hierarchical levels (right) of organization in the *Euplectella aspergillum* skeletal lattice and the individual structural components (left). The levels of complexity increase with the length scale. The arrows indicate the component parts of each successively more complex structural level.

3.1A Axial filament

The organic scaffold onto which silica is deposited consists of a central proteinaceous axial filament that exhibits a distinctly square or rectangular cross-section (Figure 3.3A) (Reiswig, et al., 1983). This is in stark contrast to the pseudohexagonal cross-sectional morphology characteristic of demosponge axial filaments (Garrone, 1969), the biochemistry and histology of which have been heavily investigated (Shimizu, et al., 1998; Cha, et al., 1999; Zhou, et al., 1999;

Pozzolini, et al., 2004; Müller, et al., 2005, Murr and Morse, 2005; Schröder, et al, 2006). In demosponges, these axial filaments have been demonstrated *in vitro* to catalyze the hydrolysis and polycondensation of silicon alkoxides and related molecular precursors to form silica at ambient temperature and pressure and near neutral pH, and to serve as templates for the deposition of the silica. These observations suggest that the axial filaments and their constituent globular enzymatic proteins, the silicateins, may play a critical role *in vivo* in the initial induction of silica deposition during spicule formation (Morse, 1999, 2000; Shimizu and Morse, 2000; Sumerel and Morse, 2003). Based on the fact that both demosponge and hexactinellid spicules contain proteinaceous axial filaments, it is expected that both might exhibit similar catalytic and templating activities. It is important to note, however, that preliminary x-ray diffraction studies of demosponge and hexactinellid axial filaments reveal that the packing arrangements of the constituent proteins are fundamentally different (Croce, et al., 2004). These observations suggest the possibility that the proteins themselves may also be structurally distinct from one another. Preliminary SDS-PAGE analyses support this suggestion (Weaver and Morse, 2003).

Moreover, the fundamental mechanisms by which spicule growth occurs are distinctly different in these two sponge classes. In demosponges, recent evidence suggests that the axial filament is synthesized in its entirety prior to silica deposition (Uriz, et al., 2000): the maximum spicule dimensions thus being predetermined by the length of the axial filament. In contrast, during spicule growth in hexactinellids, the axial filament appears to be connected to the surrounding soft parts through an

opening at the end of each ray. After the ray has ceased to grow in length, the terminal opening is closed by an expansion of the silica layers (Schulze, 1887). In addition to these observations in mature specimens, this growth mode also has been suggested from observations of the early stages of spicule biosynthesis in larval stages of the hexactinellid, *Oopsacas minuta* (Leys, 2003). These data help explain how hexactinellids are able to synthesize the unusually long spicules that are so commonly observed in members of this sponge class (Simpson, 1984; Levi, et al., 1989). It is equally important to note that the remarkable size of hexactinellid spicules is also permitted by (and may be the direct result of) their syncytial architecture at the cellular level (Mackie and Singla, 1983). The polynucleate nature of the syncytial sclerocytes (the cells in which mineralization occurs) facilitates their potential extension across the entire length of the living sponge, thus permitting the synthesis of equally long skeletal elements.

3.1B Consolidated silica nanoparticles

The silica deposited around the proteinaceous axial filament consists of consolidated silica nanoparticles measuring between 50 and 200nm in diameter (Aizenberg, et al., 2004, 2005). The nanoparticles are continually deposited in discrete concentric layers during spicule growth (Figure 3.3B, C). It is important to note that these nanoparticles are only visible by SEM following etching with either sodium hypochlorite or HF (cf. Figure 2.2). Recent small-angle x-ray diffraction studies of the spicule silica reveals that these 50-200nm diameter particles are

themselves composed of even smaller 3nm diameter particles. The resulting silica exhibits an initial elastic modulus that is approximately half that of technical quartz glass (Woesz, et al., 2006), the values for which are in close agreement with those reported from other hexactinellids (Levi, et al., 1989).

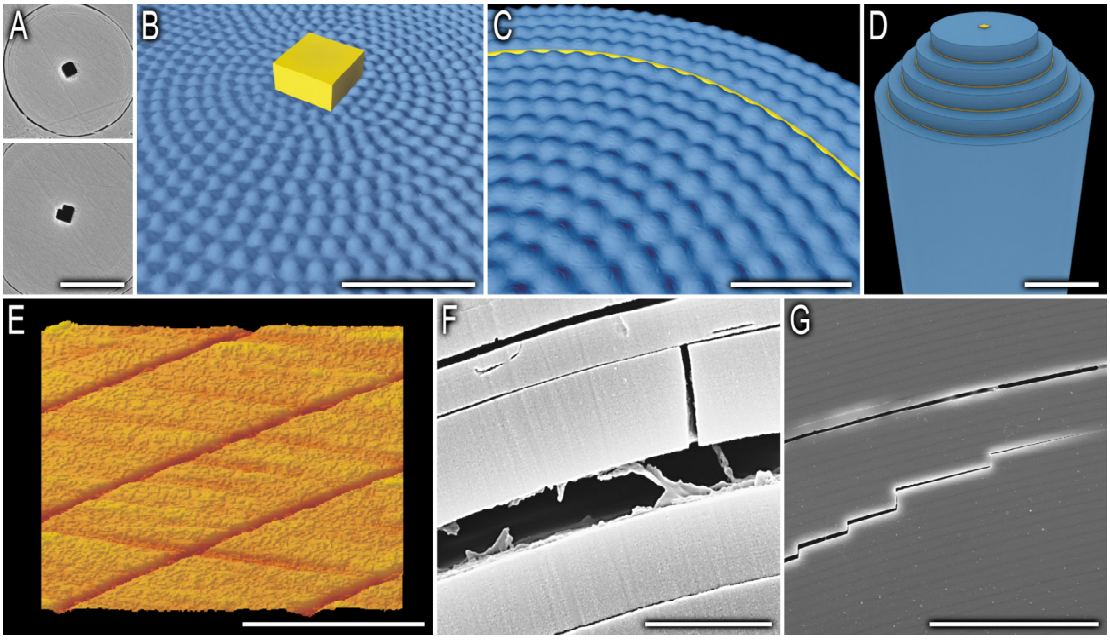

Figure 3.3: Laminated organic/inorganic hybrid structure of the spicules. (A) Scanning electron micrographs of polished spicule specimens reveal the square cross-section of the central proteinaceous axial filament upon which concentric lamellae of consolidated silica nanoparticles are deposited; B-D: Three-dimensional structural renderings of the silica/protein hybrid, depicting the central or axial silica cylinder of the spicule deposited around the axial filament (B), organic interlayers (shown in yellow) deposited throughout the cortex of the spicule (C), and the resulting laminated organic-inorganic composite structure (D). (E) AFM reveals that each of these organic layers measures only 5-10nm in thickness. (F) Scanning electron micrograph showing individual layers revealed during spicule failure. When stressed mechanically, a propagating crack exhibits a distinct stepped architecture as the organic layers induce lateral crack deflection, clearly shown in the scanning electron micrograph from a related species in (G). Scale bars: A: 2.5μm; B: 1μm; C: 500nm; D: 5μm; E: 500nm; F: 500nm; G: 50μm.

From a structural perspective, the silica behaves the same as homogeneous bulk silica; for instance, fracture surfaces are essentially planar and featureless in both. The presence of silica nanoparticles in these spicules, like those from demosponges (Weaver, et al., 2003), is not unexpected, as this is the most kinetically favored form of silica deposited from solution (Iler, 1979). Similar structural motifs have been observed in other silicifying taxa such as diatoms (Crawford, et al., 2001; Noll, et al., 2002), and in the in vitro formation of silica catalyzed and templated by the silicatein filaments from a demosponge (Cha, et al., 1999).

3.1C Laminated spicule structure consisting of alternating layers of silica and organic material

The innermost mineralized portion immediately surrounding the axial filament, the central or axial cylinder, is generally distinguishable from the layered outer cortex by the absence of lamination and appears in fractured spicules as a featureless solid cylinder of hydrated silica (Figure 3.3A, B). Surrounding this central cylinder is the spicule cortex, which exhibits a distinctly laminated architecture (Figure 3.3C, D) (Schulze, 1887). From the behavior of the spicules when heated, and when examined in polarized light, Schultze, in 1860, determined that the individual lamellae are separated from one another by thin organic layers. Despite this significant early discovery, the validity of these observations has been continuously questioned in the scientific literature (Schulze, 1925; Schmidt, 1926; Travis, et al., 1967; Jones, 1979; Simpson, 1984) and has been only recently confirmed by high-resolution secondary and backscattered electron microscopy and Raman

spectroscopic imaging (Aizenberg, et al., 2005; Woesz, et al., 2006). These organic layers (Figure 3.3F) are typically only 5-10nm thick, as measured by AFM of spicule cross-sections (Figure 3.3E). With the intervening silica layers being 0.5-1.0μm thick, the volume fraction of the organic phase is small: typically <1%.

This laminated design is critical for imparting damage tolerance to the individual spicules and the overall skeletal structure (Seshadri, et al., 2002; Chai, et al., 2002). Provided that the organic interlayers are sufficiently weak, cracks propagating through the silica layers are arrested and deflected along the interlayer boundary. Consequently, rather than failing catastrophically, the spicules fracture through a series of successive crack arrest, re-nucleation and discrete propagation events (Figure 3.3G). In contrast, monolithic silica fibers fail by the propagation of a single dominant flaw.

When examined in cross-section, it becomes readily apparent that silica layer thickness does not remain constant within the cortical region of the spicule. Instead, these layers gradually decrease in thickness from the central cylinder to the spicule periphery. During mechanical loading, the thin outer layers fracture first, resulting in the dissipation of large quantities of energy primarily via the spreading of cracks through the delamination of the silica layers at the organic-inorganic interface. These thinner layers also significantly limit the depth of crack penetration into the spicule interior.

At the macroscopic level, the majority of hexactinellid spicules exhibit a unifying design strategy regardless of the number of rays present. This homogeneity

of design is a hallmark of the Hexactinellida, despite the remarkable structural diversity of spicules observed in this group. Recognized by numerous authors in the mid 1800s, the presence of three equal axes intersecting at right angles is the fundamental structure of all hexactinellid skeletal elements, and relates to both those spicules united into a continuous framework, and those which lie isolated in the syncytium.

The deviations from this general design strategy include the following modifications: (l) unequal development of the rays, including the complete suppression of one or more, so that in extreme cases only a single ray attains full development, (2) division of the rays into terminal branches, varying in number, form, and direction, (3) the development of local thickenings or unilateral swellings in the form of knobs, thorns, prickles, knots, and similar ornamental protuberances, and (4) the curvature of the chief rays or their branches (from Schulze, 1887). As seen in the next level of structural hierarchy, this design strategy is critical for the establishment of the basic square lattice symmetry of the skeletal system.

3.1D Formation of the underlying quadrate skeletal lattice from non-planar cruciform spicules

Initial surveys of the skeletal lattice suggest that it is principally composed of a series of overlapping vertical, horizontal and diagonal fibrous struts, forming a basic square lattice reinforced with diagonal braces (Figure 3.1C). A more detailed examination reveals that the vertical and horizontal struts are significantly more ordered than the diagonal ones, suggesting fundamental differences in the origins of

ordering and their dependencies on the underlying constituent spicule geometry. Indeed, the underlying quadrate lattice is principally composed of a network of non-planar cruciform (stauractine) spicules (Figure 3.4A-C), with one of the horizontal rays inclined at approximately 20 degrees to the plane of the other three rays.

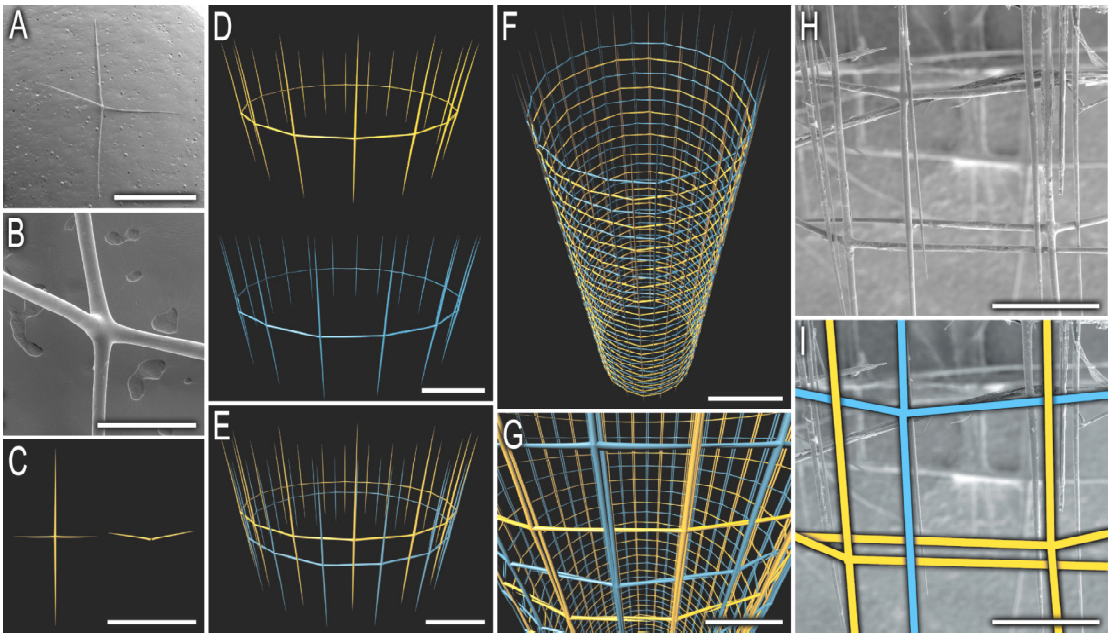

Figure 3.4: Steps in the formation of the underlying quadrate skeletal lattice. Scanning electron micrographs of the stauractine (cruciform) spicules from *Euplectella aspergillum* (A, B), clearly show the nonplanar nature of these skeletal elements. Three-dimensional structural renderings depict how the individual spicules (C) assemble to form the ring-like structures shown in (D) by overlap of the horizontal spicule rays. Two separate lattices (shown in blue and yellow) are juxtaposed to form the basic structural unit shown in (E). Further duplication and vertical growth results in the formation of the quadrate lattice shown in (F). Closer examination reveals that due to the 50% horizontal and vertical offset of the two structures, all of the vertical elements become positioned on the exterior of the lattice and the horizontal components on the interior (G). This design strategy can be seen clearly in scanning electron micrographs of a portion of the native skeletal lattice shown in normal (H) and color-enhanced (I) versions. Scale bars: A: 5mm; B: 500μm; C: 1cm; D: 5mm; E: 5mm; F: 1cm; G: 2.5mm; H: 1mm; I: 1mm.

While their dimensions are somewhat variable, in general the vertical rays are approximately twice the length of the horizontal ones. A generalized spicule schematic is shown in Figure 3.4C with vertical rays measuring ca. 10mm in length and horizontal rays at 5mm. As seen in Figure 3.4B, the base of each spicule ray is between 80 and 100μm in diameter. The horizontal rays of these spicules overlap with those from a neighboring one and assemble to form the ring-like structures shown in Figure 3.4D. Based on this model, the distances between the vertical rays are approximately 5mm, nearly twice the width of the openings in the skeletal structure (Figure 3.1C). Under closer examination, it becomes apparent that the quadrate skeletal lattice is, in reality, composed of two overlapping grid systems: one offset with respect to the other by a distance of half the horizontal ray length. The resulting arrangement, shown in Figure 3.4E, F, has openings approximately 2.5mm wide, consistent with the experimentally measured values. Higher magnification analyses reveal that all of the vertical components of the grid are positioned on the outside of the lattice and all of the horizontal components on the inside, as seen in the three-dimensional structural rendering (Figure 3.4G) and in scanning electron micrographs of the native skeletal lattice (Figure 3.4H, I). This organization was first suggested by Schulze in 1887. In his original descriptions, however, Schulze failed to point out the non-planar nature of the cruciform spicules. With planar cruciforms, the interweaving process could only be accomplished by bending of the horizontal rays. The resulting stresses could not be supported during the early stages of skeletal development (prior to the later cementation processes, described below). Moreover,

such stresses, if present, would significantly reduce the robustness of the skeletal lattice. Using non-planar spicules, the sponge is able to construct the requisite lattice without introducing internal stresses. Construction of the lattice from cruciform spicules also facilitates growth of the skeletal diameter without changing the number of horizontal struts. Most specimens we examined exhibit a noticeable increase in diameter, from about 2.5–3.5cm in the lower portion to 4–5cm in the upper portion: the changes occurring smoothly over a length of 20–30cm (Figure 3.5A, B). This is accomplished by varying the degree of overlap between the horizontal rays of the cruciform spicules (Figure 3.5C): less overlap results in a greater spacing between the vertical rays and hence a larger cylinder diameter. Since the construction of this lattice occurs during the so-called "flexible phase" of sponge growth, these geometric changes can occur without compromising the skeletal symmetry, without inducing large residual stresses, and without the need to synthesize additional skeletal elements. As long as these two distinct lattice systems (shown in blue and yellow in Figure 3.4G) retain their ability to move independently of one another, this design strategy results in the effective division of an applied stress onto two independent strut systems (that are not physically fused to one another). The lack of interconnectivity of this level of design is particularly important in the early stages of synthesis of the skeletal lattice, before secondary reinforcing strategies have yet been implemented.

While fused elements would indeed result in increased stiffness, a consequence of such a rigid design would be decreased strength, as a result of the

inability to dissipate energy during substantial loading events. By maintaining a lack of interconnectivity, the structural elements are able to move independently of one another, resulting in a dramatic increase in toughness.

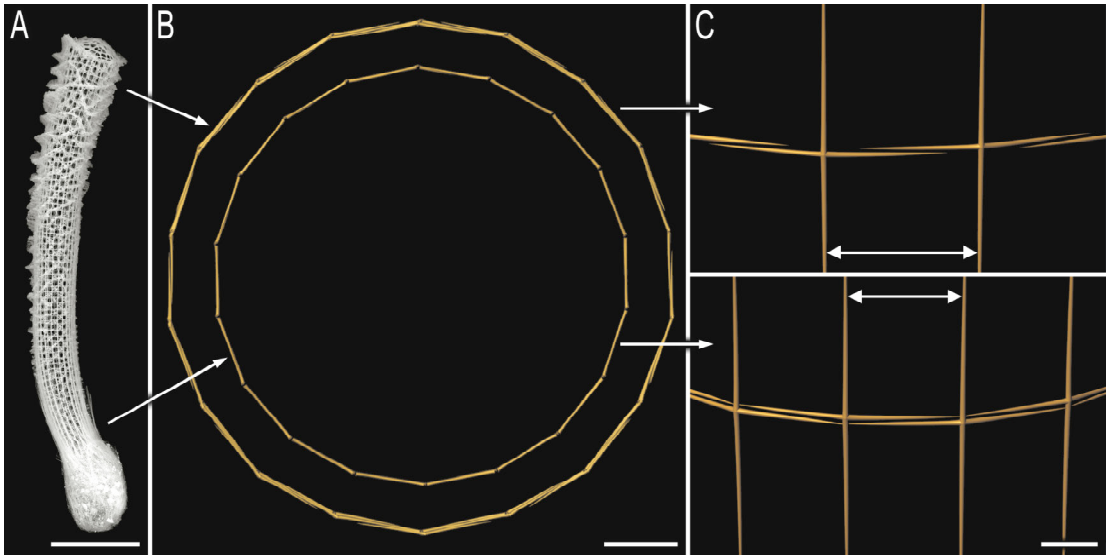

Figure 3.5: Factors regulating cross-sectional area of the skeletal lattice. Three-dimensional structural renderings illustrating cross-sections through the upper and lower regions of the skeletal lattice (A) reveal that the numbers of vertical and horizontal components remain constant in these two areas (B). This is accomplished by varying the percent of lateral ray overlap between neighboring spicules (C). Scale bars: A: 5cm; B: 5mm; C: 2.5mm.

3.1E Vertical and horizontal spicule bundles

Overlaying the quadrate lattice is a series of vertical and horizontal bundled spicular struts between 200 and 400μm in diameter. Each consists of a wide size range of individual spicules, ranging from 5-50μm in diameter and of variable length. These struts help stabilize the lattice and provide additional mechanical support (Clegg, et al., 1990). This design strategy results in the formation of a series of nearly

uniform quadrate meshes averaging 2.5 to 3mm in size. The number of transverse circular spicular struts ranges from sixty to eighty in a full-grown specimen (Schulze, 1887). While the number of vertically oriented struts remains relatively constant along the length of the skeletal lattice, they increase in number by approximately 50% within the upper 2-3cm due to their occasional splitting. The increase in the number of spicular struts in this region of the sponge may be critical for increasing available surface area for attachment of the terminal sieve plate which covers the entire upper opening of the cylindrical lattice (see section 3.1H below). The relative locations of these two supporting strut systems are important for further stabilization of the underlying quadrate lattice. In this arrangement, the vertical spicular struts are predominantly arranged on the exterior lattice surface, while the horizontal ones line the interior, with the cruciform spicule grids sandwiched between the two (Figure 3.6B). This design strategy increases the toughness of the framework by providing uniform support to the underlying structural framework.

The various levels of structural hierarchy discussed thus far are developed during the flexible phase of growth (Saito, et al., 2002). It is during this phase that the basic design of the skeletal lattice is formed and square-grid symmetry is established. Since the lattice is easily deformable, it is capable of lateral expansion: a necessity for permitting the three dimensional growth of the skeletal system. The following structural components are principally designed to reduce flexibility and increase strength as the skeletal lattice matures.

3.1F Diagonal spicule bundles

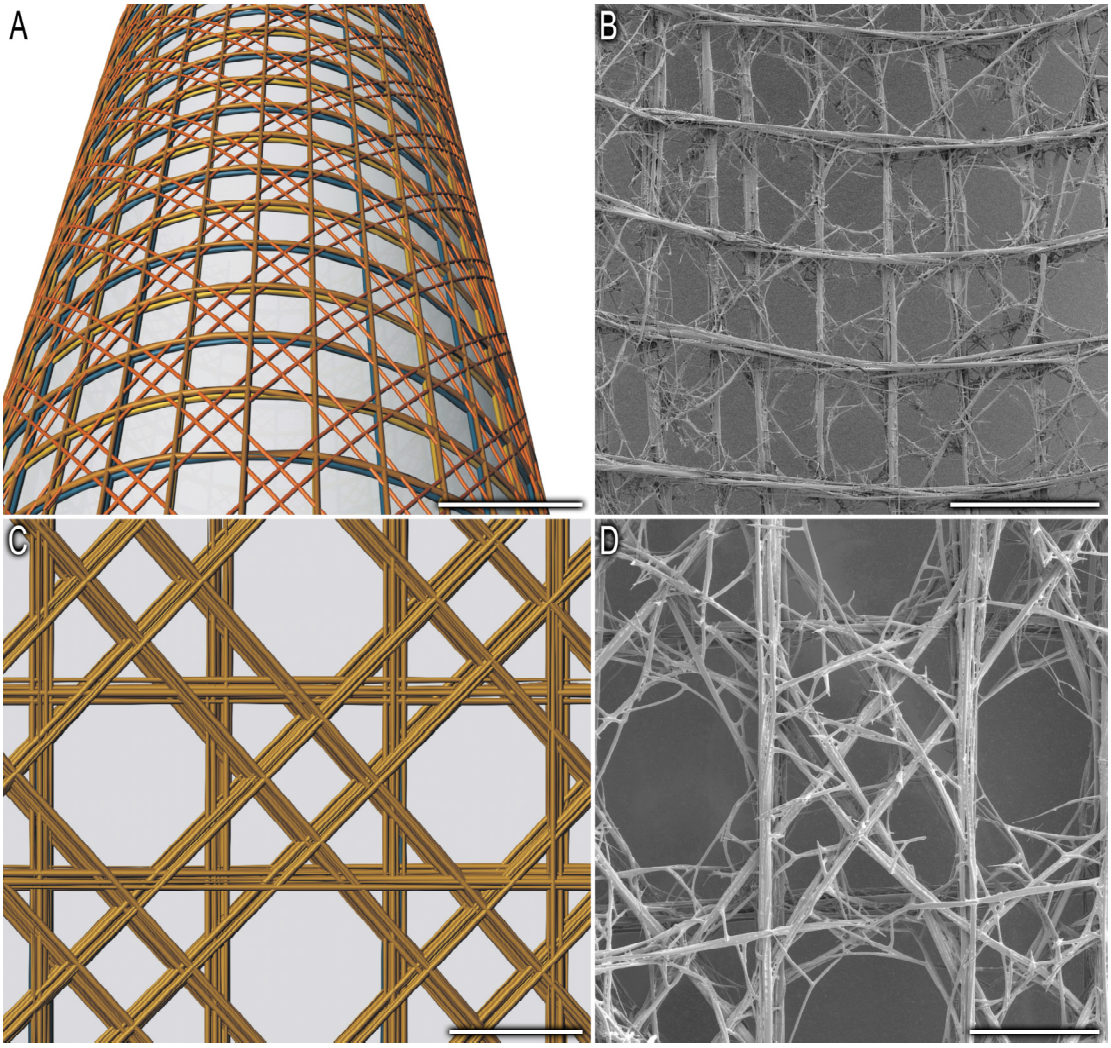

Figure 3.6: Vertical, horizontal, and diagonal reinforcement of the cylindrical skeletal lattice. Three-dimensional structural renderings show that superimposed on the underlying quadrate lattice are a series of vertical, horizontal, and diagonal struts, which form an alternating open and closed cell structure (A). Scanning electron micrograph of the interior lattice wall reveals that the horizontal supporting struts are predominantly positioned on the interior lattice surface and the vertical components are on the exterior (B). Each strut is in turn composed of a series of individual spicules bundled together (C). Scanning electron microscopy provides a comparative view of a similar region of the native skeleton showing the semi-disordered nature of the diagonal components (D). Scale bars: A: 5mm; B: 5mm; C: 2mm; D: 2mm.

Outside of the horizontal and vertical struts is an additional set of orthogonal struts, each consisting of similarly bundled spicules, oriented diagonally (at about 45° to the cylinder axis) and surrounding the tube in oblique spirals (Figure 3.6A). Each of the spiraling strut systems consists of pairs of parallel spicule bundles, intersecting in a manner that creates a series of alternating open and closed cells, reminiscent of a checkerboard pattern (Figure 6C, D) (Schulze, 1887). The center to center distance between two adjoining open cells in the same row is, in the upper portions of fully developed specimens, about 6mm. At the lower end and in young forms, the distance is only 4mm or less.

While the vertical and horizontal struts precisely follow the contours of the underlying quadrate lattice, the diagonal struts on the other hand do not have such a pre-existing roadmap, as is reflected in their semi-disordered nature. It is important to note that in general, the quantity of material forming each of the diagonal strut systems (organized as right or left handed helices) approximately equals that of the vertical or horizontal components. Thus from the perspective of material consumption, the skeletal system does approximately follow the optimum design strategies described by Deshpande, et al. (2001).

The incorporation of diagonal bracings is essential for supporting bending, shear, and torsional loads exerted on the skeletal lattice. The sponge is able to increase strength by reducing the lattice cell area through reinforcement with two sets of partially disordered diagonal strut systems and finite element analysis of equal

volume strut systems reveal the mechanical consequences of this design strategy (Figure 3.7).

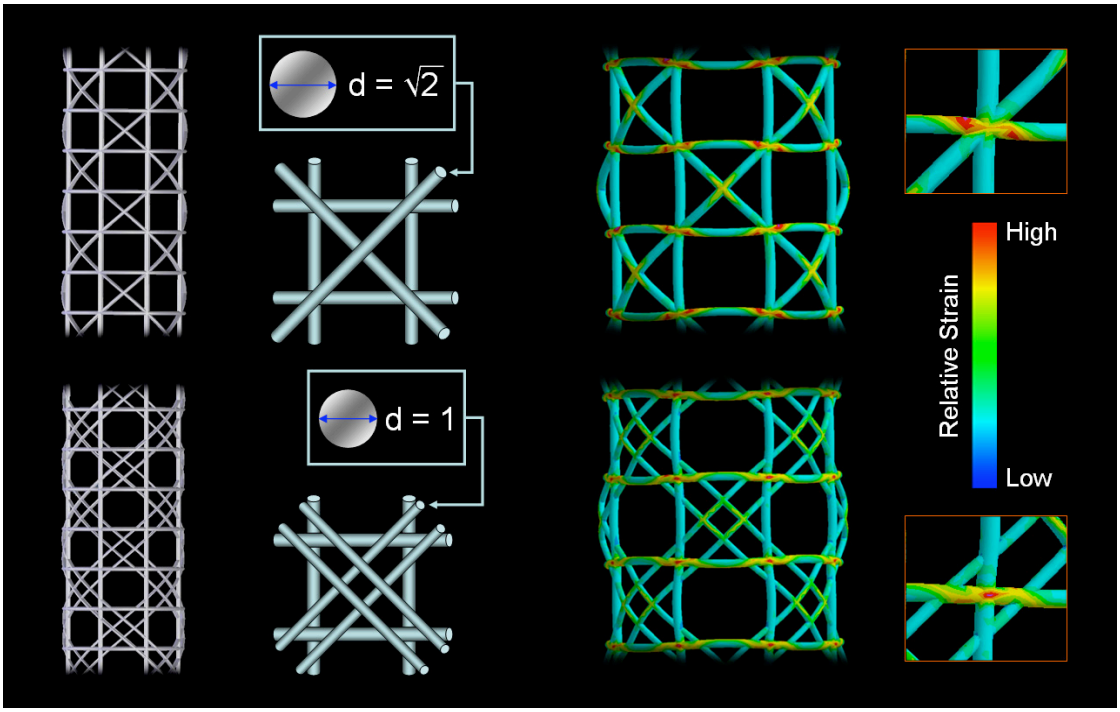

Figure 3.7: Finite element analysis of equal-volume strut systems based on the design principles observed in *Euplectella aspergillum*. By incorporating twice as many diagonal components and subsequently offsetting them from the nodes of the underlying quadrate skeletal lattice results in a significant reduction in node strain accumulation and an overall more diffuse strain field.

This design strategy may also have additional benefits. Since the external ridges are constructed along the diagonal strut systems (as described in the section immediately below), more surface area available for ridge connectivity and support are provided by doubling the number of diagonal structural elements resulting in the formation of a supporting basal grid, without reducing the number of openings available for water filtering. It also is relevant to note that by offsetting the diagonals

from the node (Figure 3.6C, D), roughly octagonal openings are formed, that may help guide the development and provide support for the water-filtering and current-generating structures of the living tissue.

3.1G External diagonally ordered ridge system

In young specimens, and on the lower portions of older forms, a slightly arched protuberance is formed in the middle of every four openings in the quadrate lattice. By the fusion of these elevations which lie between two adjacent spiral rows, raised bands are formed, which, after further development, become prominent ridges (Figure 3.1A). While the arrangement and development of these ridges varies greatly on the walls of the lower portion of the tube, they are always present, albeit only feebly developed (Figure 3.11, left half of image). These ridges gradually increase in height towards the upper end of the skeletal tube. In some specimens they hardly attain a maximum dimension of 2 or 3mm, while in other cases they extend 10mm or more (from Schulze, 1887).

The ridges are supported by a series of steeply set beams which unite at an acute angle corresponding to the sharp edge of the ridges. They are also firmly fused laterally to one another and to the strong latticework of the tube. The beams are crossed both by long spiraling fibers which run parallel to the edge of the ridges and by small short beams which run through the ridges transversely, forming the basic ridge structure shown in Figure 3.8A.

Although they run predominantly parallel to the spiral rows of gaps, the ridges seldom continue in the same direction beyond a semirevolution. They often bend around at right angles, at the end of half a spiral turn, and extend in the opposite direction down the other side of the tube (Figure 3.8B, C). Sometimes they assume an angular or undulating course and occasionally may even form a well-defined grid-like structure (Schulze, 1887).

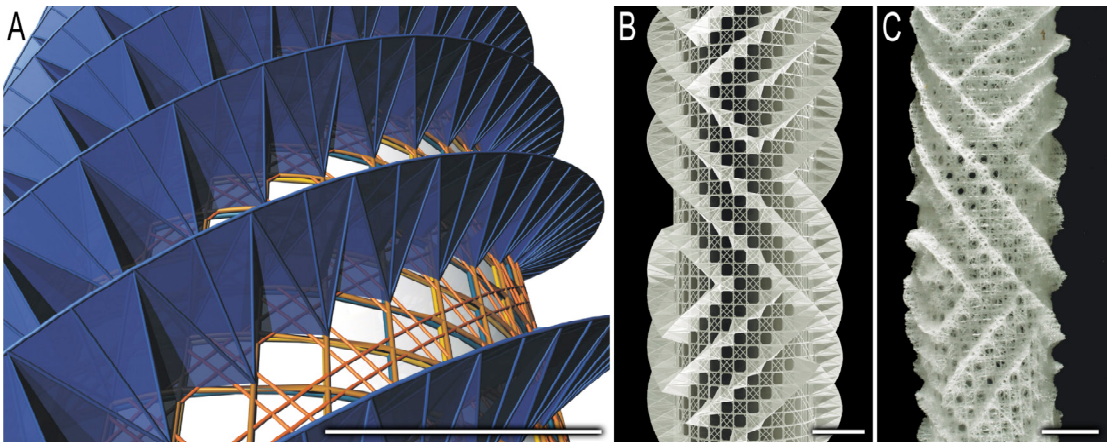

Figure 3.8: Structural details of the external spiraling ridges. (A) Three-dimensional structural renderings of the external design elements of the vertical ridge system that spiral around the skeletal lattice. Additional spicules fill in the gaps between the external design elements. (B) The bidirectional ridges occupy a position on every other diagonal set of paired spicular struts. (C) A photograph of the actual specimen after which (B) was modeled. Scale bars: 1cm.

A typical failure mechanism of a cylindrical tube is ovalization, i.e., deformation of the cross-section from the original circular shape. The presence of a reinforcing ridge or ridges extending perpendicular to the cylinder wall and wrapped circularly around the primary cylinder tends to prevent this failure mechanism, although allowing failure by torsion. By constructing oblique, helical ridges running

in opposite directions, the sponge is able to resist both failure modes (ovalization and torsion).

3.1H Terminal sieve plate

At the apex of the skeletal lattice, the open cylinder is covered with an irregular network-like structure that constitutes the terminal sieve plate (Figure 3.9A). At higher magnification, it is readily apparent that this structure results from the incorporation of a wide range of morphologically distinct spicules (Figure 3.9B).

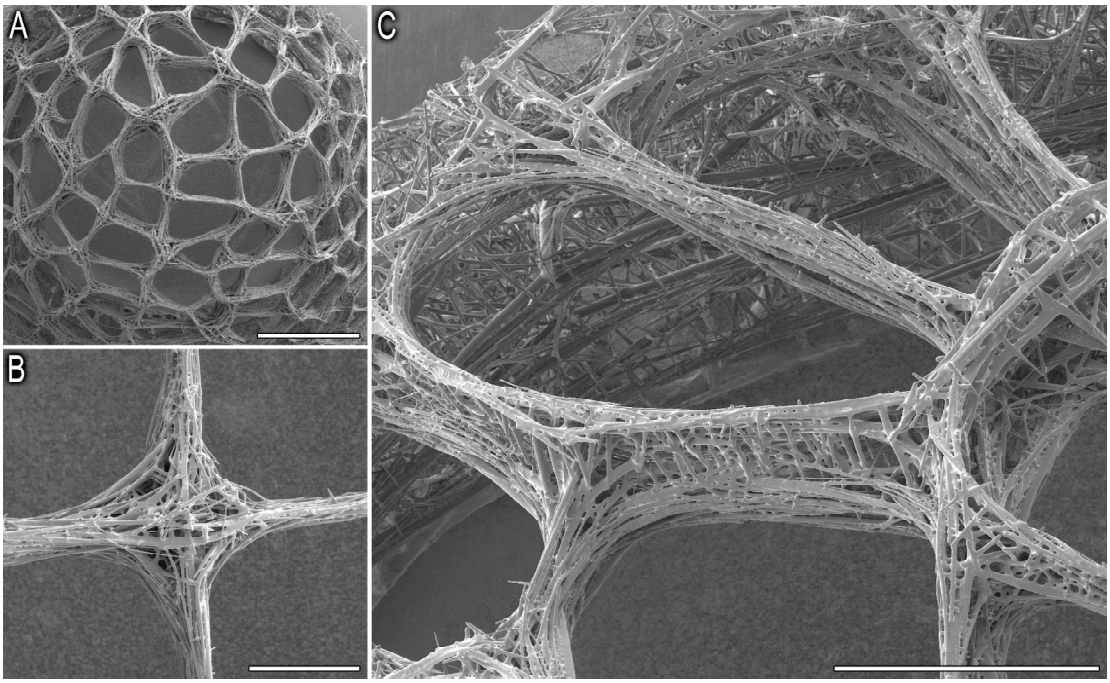

Figure 3.9: Organizational detail of the terminal sieve plate. (A) Scanning electron micrograph illustrating the convex nature of the terminal sieve plate. (B) Higher magnification views of this structure reveal that it is composed of a wide range of morphologically distinct spicules cemented together. (C) Lateral and vertical flaring of the peripheral spicules results in complete interdigitation of the sieve plate with the inner wall of the cylindrical skeletal lattice (C). Scale bars: A: 5mm; B: 1mm; C: 2mm.

These spicules include various diactines (2-rayed), tetractine (4-rayed) and hexactine (6-rayed) forms. Anchoring of the terminal sieve plate to the lateral walls of the skeletal lattice is facilitated by the vertical and lateral flaring of the constituent spicules, significantly increasing the available surface area for subsequent structural integration (Figure 3.9C).

Bordering the terminal sieve plate is a distinctive ring-like lateral ledge (Figure 3.1A). While in many individuals, this structure may be barely visible, it can in others attain a height of 10mm or more. Usually, however, the "cuff" is not in direct connection with the rest of the ridge system, but is separated from it by a concave circular zone ranging from 5 to 10mm in width. It is distinguished from the other ridges by being thinner, and typically possessing sharper edges (from Schulze, 1887).

In addition to the ability to protect the sponge interior, the development of a rigid capping structure has important mechanical consequences as well. By preventing lateral collapse of the top of the skeletal lattice, strength and stiffness are significantly increased. Due to the reduced diameter at the base of the skeletal lattice, this secondary reinforcing mechanism may not be necessary in this region for increasing the strength of the bulk composite. While this is the case in most specimens, occasionally a basal sieve plate also may be present (Figure 3.10A); it is typically located approximately 1-2cm above the region at which the anchor spicules become incorporated into the main skeletal lattice. Morphologically, this structure superficially resembles the terminal sieve plate, although it is significantly less

developed (Figure 3.10B, C). Whether this structure provides additional support in this region of the skeleton is not known. However, its overall rarity, occurring in less than 1% of the specimens we examined, suggests the possibility that it may represent a defect that may develop during skeletogenesis, rather than a functionally significant structure.

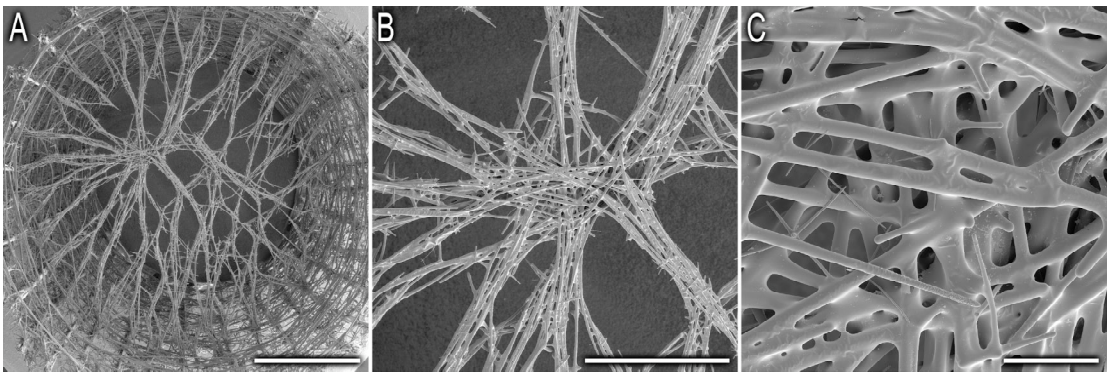

Figure 3.10: Scanning electron micrographs of the rare basal sieve plate structure of *E. aspergillum* (A). Higher magnification views of this structure (B, C) suggest a similar design strategy to that observed in the terminal sieve plate. Scale bars: A: 5mm; B: 2mm; C: 200μm.

3.11 Holdfast apparatus

Superimposed on the reinforced quadrate skeletal lattice in the lower region of the sponge skeleton are bundles of long fibrillar spicules (Figure 3.11A). When viewed in cross-section (Figure 3.11B), these spicules are easily identifiable. It is these nearly 2000 spicules that go on to form the sponge's anchoring holdfast apparatus (Figure 3.11B). The individual spicules (basalia) are shown in the polarized light micrograph in Figure 3.11C. Each has a smooth distal and a barbed proximal region that is terminated by an apical spinous process (Figure 3.11D) (Aizenberg, et

al., 2004). This design strategy forms an effective anchoring apparatus that secures the sponge in the soft sediments of the sea floor. The smooth portions of these spicules become incorporated into the main vertical spicular struts of the skeletal lattice and terminate approximately 1/3 of the way up the cylinder.

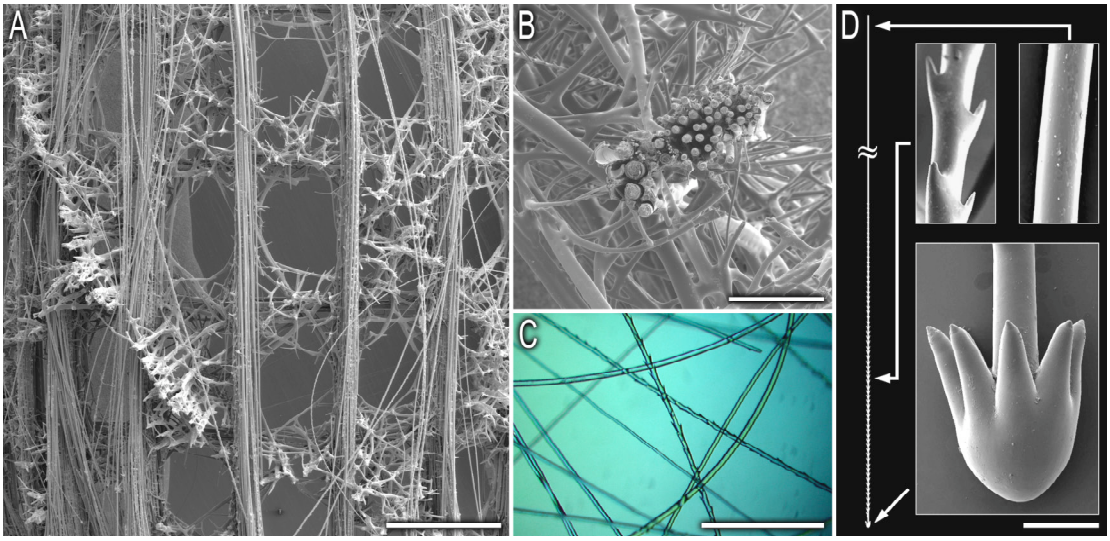

Figure 3.11: Organizational and structural features of the holdfast apparatus. Located on the exterior of the spicular strut system near the base of the sponge are, revealed by scanning electron microscopy, a series of bundled fibrillar spicules (A). The spicules are easily seen in a cross-sectional scanning electron micrograph through the lattice in this region (B) and a polarized light micrograph of individual spicules is shown in (C). Scanning electron microscopy reveals that each spicule has a smooth distal region and a barbed proximal region that is terminated by an apical spinous process (D) that is normally buried deep in the sediments. Scale bars: A: 2.5cm; B: 500μm; C: 500μm; D: 100μm.

As has been discussed in the case of plants (Lichtenegger, et al., 1999), biology has developed several strategies for anchoring an elongated structure that is subjected to lateral forces. One is the use of structures strong enough to withstand typically encountered lateral forces. This is achieved by a considerable over-

strengthening of the anchoring point in order to provide a safety margin sufficient to withstand occasional large forces. A much more economic strategy, also used by young trees (Lichtenegger, et al., 1999), is to make the anchoring and/or the rest of the structure sufficiently flexible to allow for significant bending. The latter strategy appears to have been adopted by the sponge, with a flexible anchoring system at a location, which structurally, is the point of highest stress accumulation in the skeletal lattice during lateral loading.

3.1J Consolidation of the entire skeletal lattice with layered silica matrix

In addition to the larger spicules that go on to form the main struts of the skeletal lattice, there are numerous smaller spicules (Figure 3.12A), which range from 5-15μm in diameter. These spicules are embedded in silica matrix that serves as a cement to consolidate and strengthen the entire skeletal system, as seen in cross-sectional micrographs (Figure 3.12A) and in external views of the main spicular struts (Figure 3.12B). The smaller spicules play a critical role in filling the gaps between the larger spicules, prior to cementation of the skeletal lattice via deposition of multiple layers of silica/organic composite. The use of multiple small spicules cemented as reinforcing filler also can be observed at the junctions of the underlying cruciform spicules (Figure 3.12C, D). Examination of these images makes it possible to clearly see the various stages of hypermineralization of this complex skeletal system by visually reconstructing the temporal sequence of cement layer deposition and its subsequent incorporation of the various individual spicules.

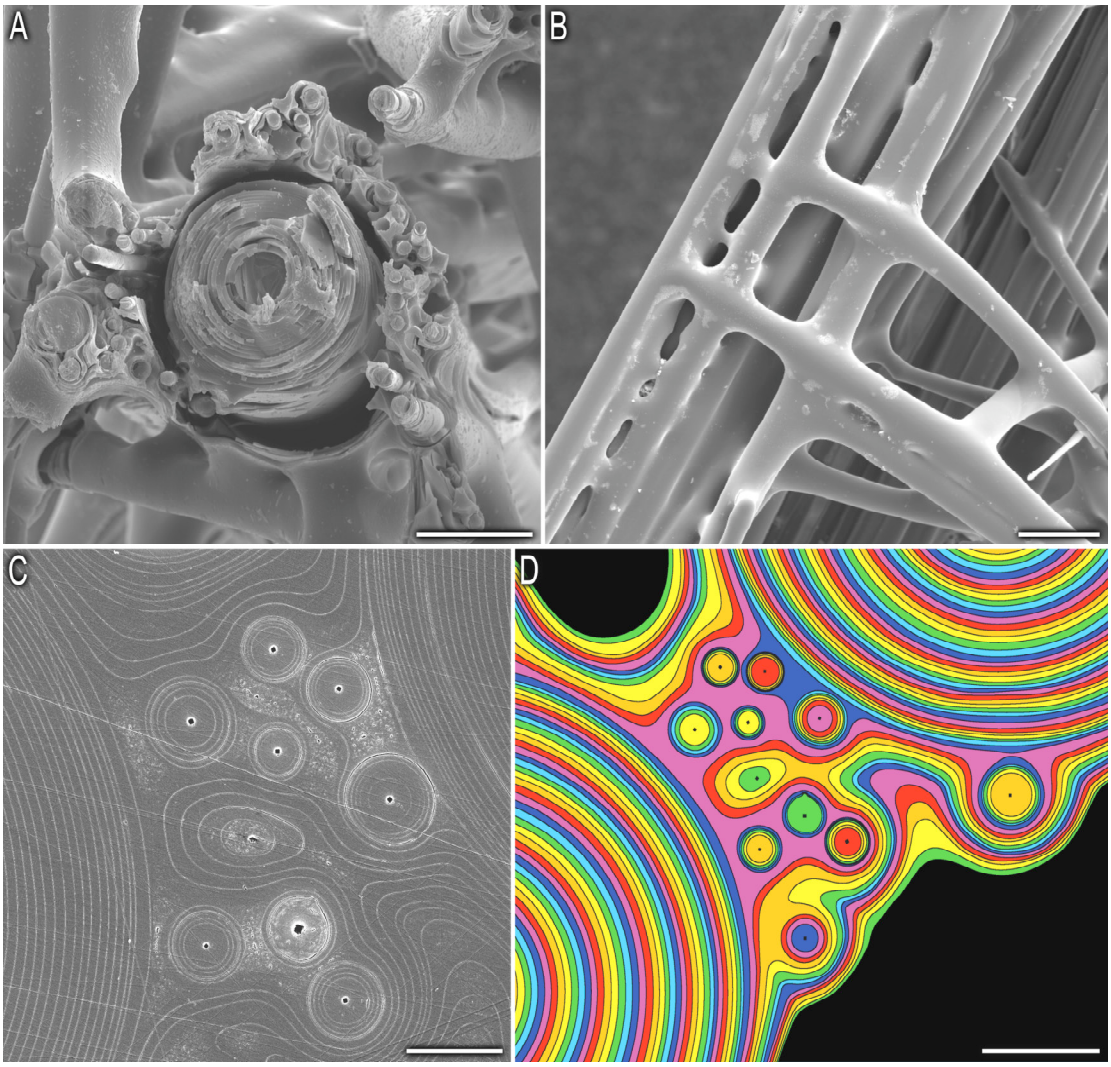

Figure 3.12: Organizational details of the consolidating silica matrix. (A) In cross-section, closer examination reveals that surrounding the larger spicules are a network of smaller spicules. (B) An external view of the skeletal lattice's supporting struts reveals the presence of a secondarily deposited silica matrix that surrounds the constituent spicules. (C-D) Polished cross-sections showing the layers of silica cement. Color enhancement of polished cross-sections through a junction of two stauractines (D) reveals the role of the smaller spicules in filling in the gaps between the main load bearing spicules prior to the deposition of the layered silica cement. False colors are used to indicate the various stages of hypersilicification (red first, followed by orange, then yellow, etc.). A scanning electron micrograph of a region of the actual sample depicted in (D) is shown in (C). Scale bars: A: 50μm; B: 100μm; C: 10μm; D: 20μm.

At higher magnification, it can be seen clearly that the consolidating silica cement precisely follows the contours of the underlying spicules, apparently enhancing the strength of this fiber-reinforced composite, whose structure is similar to armored concrete.

3.2 Conclusions

Despite the characteristically simple cellular organization of members of the phylum Porifera, it would be incorrect to label the group as "primitive". In many respects, the hierarchical organization of their skeletal systems is superior to that of even the most complex anthropogenic structures. As described here for *E. aspergillum*, the assembly of the three-dimensional cylindrical skeletal lattice relies on the organized interplay of various components, each of which appears to provide optimum mechanical performance with minimal material use. This biomineralized structure illustrates the nano-, micro-, and macroscale precision that nature employs to construct a wide range of complex yet resilient three-dimensional structures from inherently brittle constituents. Recent attempts at isolation and characterization of the macromolecules involved in biosilicification (Hecky, et al., 1973; Harrison, 1996; Shimizu, et al., 1998; Cha, et al., 1999; Zhou, et al., 1999; Carnelli, et al., 2001; Kroger, et al., 1999, 2000, 2002) have revealed unique and completely unexpected biosynthetic processes, stimulating the development of novel routes to the room temperature synthesis of silicas, siloxanes and metal oxide semiconductors for potential use in a wide range of industrially relevant applications (Parkinson and

Gordon, 1999; Vrieling, et al., 1999; Morse, 1999, 2001; Cha, et al, 2000; Roth, et al, 2005; Kisailus, et al., 2005a,b, 2006; Schwenzer, et al., 2005). By translating the lessons learned from these species to investigations of skeletal fabrication in hexactinellids such as *E. aspergillum*, we come one step closer to not only potentially understanding the selective pressures that resulted in the formation of these remarkable structures, but also new design and synthesis strategies for the next generation of high performance composites.

3.3 Additional observations

Frequently found growing on the surface of the skeletal lattice of *E. aspergillum* is a highly unusual commensal barnacle species (Figure 3.13A, B). Typically found growing permanently attached to flat surfaces such as rocks, boat hulls, or whale skin, most barnacle species would find the highly irregular fibrillar surface of the *E. aspergillum* skeletal lattice an extremely inhospitable substrate to colonize, due to the characteristically limited availability of continuous flat surfaces.

The commensal barnacle described here, however, has evolved an elegant solution to this problem. Growing out of the external protective plates are a series of cylindrical calcareous structures (Figure 3.13C, D) that eventually become interdigitated with the fibrillar architecture of the host sponge, securing the barnacle in place.

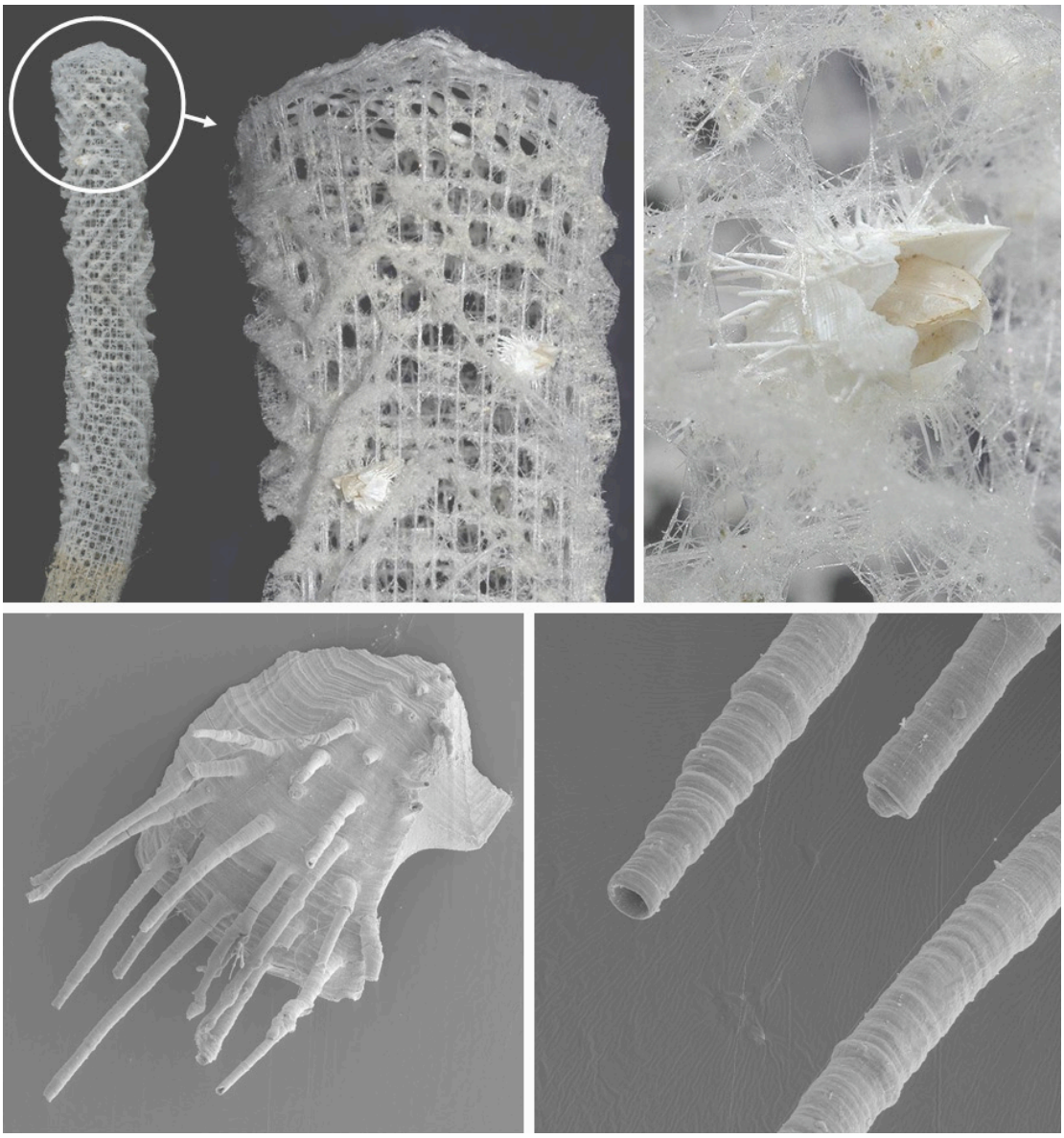

Figure 3.13: Various magnified views of the commensal barnacles encountered on the skeletal lattice of *Euplectella aspergillum* (A, B). Higher magnification imaging of an individual plate (C) reveals the tubular extensions that provide the basis of attachment of the barnacle to the sponge surface. Closer examination of these structures reveals the presence of both open and closed end elements (D). Original photographs (upper) by Larry Jon Friesen.

Chapter 4

Unifying Design Strategies in Demosponge and Hexactinellid Skeletal Systems

This Chapter is adapted from:
Unifying Design Strategies in Demosponge and Hexactinellid Skeletal Systems
Contributing researchers: James C. Weaver, Joanna Aizenberg, Ali Miserez, Georg E. Fantner, David Kisailus, Kirk Fields, Michael J. Porter, Yannicke Dauphin, John Gomm, Birgit Schwenzer, Johannes H. Kindt, Michi Izumi, Frank Zok, Paul K. Hansma, Peter Fratzl, and Daniel E. Morse

4.1 Introduction

The diversity of skeletal systems in the phylum Porifera is truly remarkable and despite the nearly two hundred years of scientific data available on the subject, there is a general lacking of a unified theory that can explain the observed structural complexity both at the ultrastructural level of the individual spicules as well as the mechanisms and design principles by which they assemble to produce hierarchically organized skeletal networks.

The two main silicifying sponge classes, the Demospongiae and the Hexactinellida are significantly different from one another, both in regards to spicule symmetry and structural diversity and their basic histology. While demosponges exist predominantly of loose aggregations of individual cells with specialized functions, the hexactinellids are principally composed of massive multinucleate syncytia. These differences in histology have a dramatic affect on the dimensional limits of the spicules synthesized by members of these two very different sponge classes.

In demosponges, the maximum spicule size encountered is typically on the order of a few millimeters in total length. This limitation is mainly due to the fundamental mechanisms by which these spicules are formed. In demosponges, the most recent evidence suggests that the central axial filament that provides a substrate for early silica deposition is synthesized in its entirety prior to silicification (Uriz, et al., 2000). The consequence of this is that the maximum dimensions of a single

spicule are fundamentally limited by the extensibility of the individual cells involved in axial filament synthesis.

High-resolution structural analyses of demosponge spicules have revealed that the central axial filament is hexagonal or some derivative thereof in cross-section (Figure 4.1) and is surrounded by concentric lamellae of consolidated silica nanoparticles. While the silica surrounding the axial filament is deposited in layers exhibiting variability in the degree of silica condensation, there are no detectable quantities of organic matter present (cf. Chapter 2).

These general design strategies of demosponge spicules differ significantly from those seen in the hexactinellids. In hexactinellids, while the spicules do also possess a proteinaceous axial filament, unlike the hexagonal form found in demosponges, it is distinctly square in cross-section (Figure 4.1).

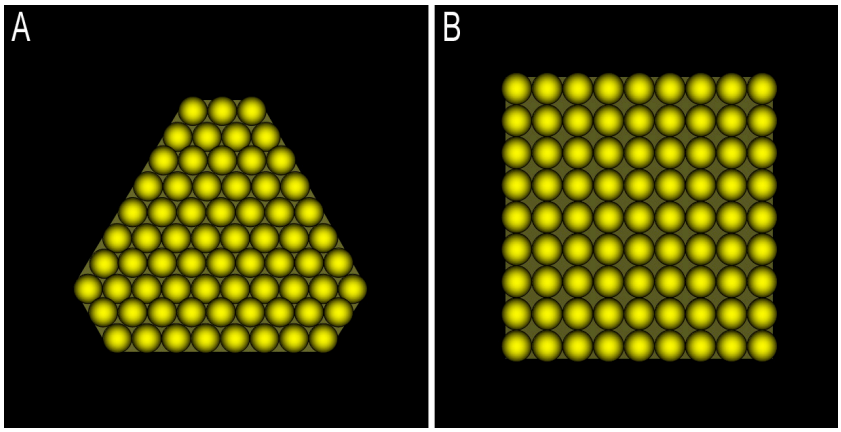

Figure 4.1: Demosponge and hexactinellid axial filament symmetry. Schematic illustrating the characteristic cross-sectional morphologies of demosponge (A) and hexactinellid (B) axial filaments based on TEM (Garrone, 1969) and SAXD. (Constituent protein monomers, illustrated by spheres, are not shown to scale).

This type of axial filament is critical for establishing the unique three-axis (or six rayed) geometry, which is characteristic of hexactinellid spicules. Lateral filament outgrowth from the main central axis results in the formation of three distinct axes that intersect one another at right angles. In addition to the unique axial filament morphology found in the hexactinellids, the mechanism by which it is synthesized appears also to be distinct. Unlike demosponge axial filaments, which are synthesized in their entirety prior to silica deposition, those from hexactinellids appear to grow continuously during spicule biosynthesis (Leys, 2003). This central organic scaffold is reportedly connected to the surrounding syncytia via an opening in the end of each spicule ray and once spicule lateral growth has ceased, the openings are sealed by expansion of the surrounding silica (Schulze, 1887). In addition to the growth potential of the axial filament, because of the syncytial nature of the sclerocytes, there is practically no limitation to the dimensions of the synthesized spicules. The following discussion of sponge spicule architectural diversity is based on the observations obtained from a wide range of different demosponge (cf. Chapters 1 and 2) and hexactinellid species. Based on these observations, we attempt to explain the basic design features from a mechanics perspective in hopes of gaining additional insight into the potential evolutionary pressures that resulted in the observed structural diversity.

4.2 Results and Discussion

4.2A Aphrocallistes vastus

Despite their extraordinary structural diversity (Figure 4.2), the smallest of the hexactinellid spicules exhibit a basic design remarkably similar to those encountered in demosponges and consist of a central axial filament surrounded by concentric lamellae of consolidated silica nanoparticles (cf. Chapter 2).

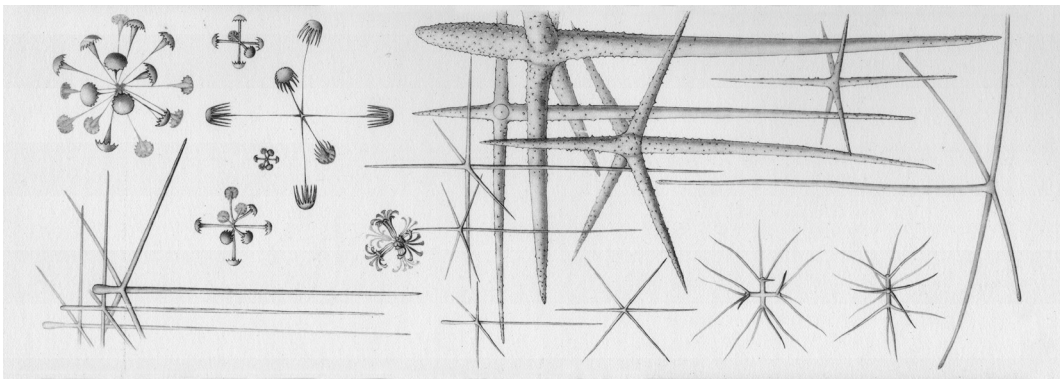

Figure 4.2: Structural diversity of hexactinellid spicules (adapted from Iijima, 1926).

When these spicules are fractured, like those from demosponges, they fail catastrophically without any indication of the presence of structural boundaries (Figure 4.3). In the skeletal system of the lycnossid sponge *Aphrocallistes vastus* (Figure 4.4), for example, the outer surface is almost completely covered with numerous such spicules that are held in place by the syncytium and are positioned perpendicular to the surface (Figure 4.5 A, B). While these spicules do exhibit the unique three-axis symmetry, characteristic of the hexactinellids, the rays are

unequally developed resulting in the formation of the unusual "sword-shaped" or pinnule spicules shown in Figure 4.5C, each of which measures ca. 650μm in length.

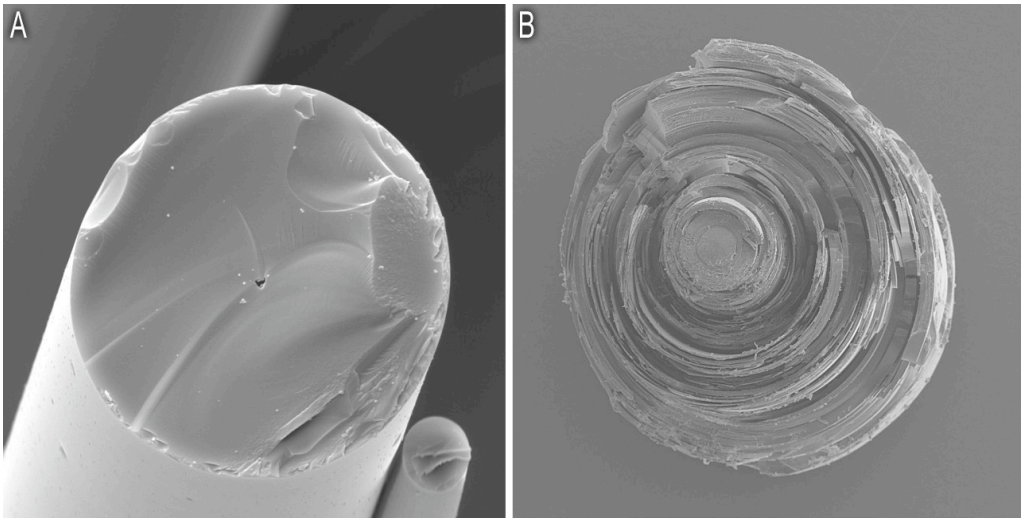

Figure 4.3: Fracture dynamics of nonlaminated (A) and laminated (B) spicules.

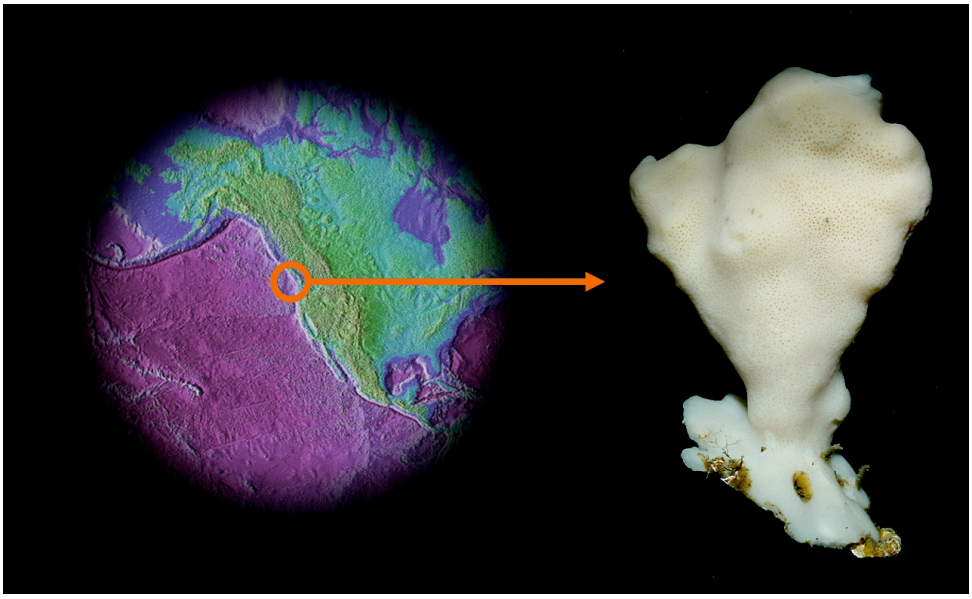

Figure 4.4: Photograph of a living specimen of the Eastern Pacific hexactinellid, *Aphrocallistes vastus*.

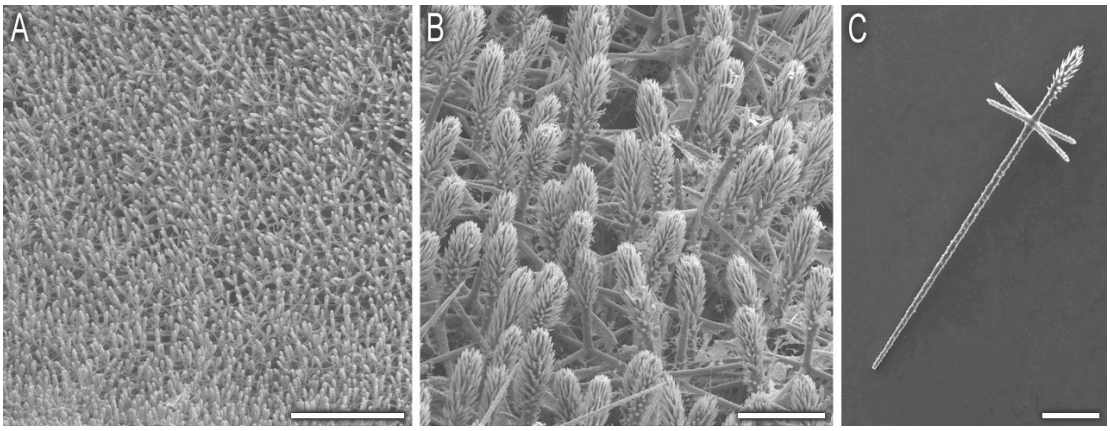

Figure 4.5: External armament of *Aphrocallistes vastus*. The external surface (A, B) of *A. vastus* is completely covered with protective pinnule spicules (C), each of which measures ca. 650μm in length. Scale bars: A: 1mm; B: 100μm; C: 100μm.

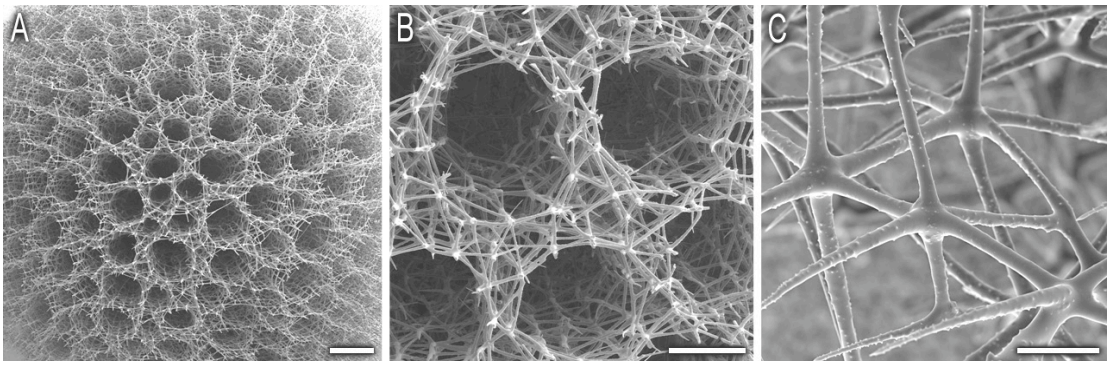

Figure 4.6: Primary skeletal system of *Aphrocallistes vastus*. Various progressively magnified views of the honeycomb-like skeletal network of *A. vastus* which is composed entirely of fused hexactines. Scale bars: A: 1mm; B: 500μm; C: 100μm.

Beneath this outer layer of protective spicules is the main skeletal lattice. The basis of this skeletal lattice consists of an intricate network of fused six rayed spicules (hexactines), each of which measures ca. 200μm in length.

These spicules are fused together at the end of each ray in such a manner that results in the synthesis of a rigid honeycomb-like architecture (Figure 4.6) and exhibits a remarkably degree of ordering when view in cross-section, with nearly all

of the constituent spicules fused at right angles with respect to one another (Figure 4.7).

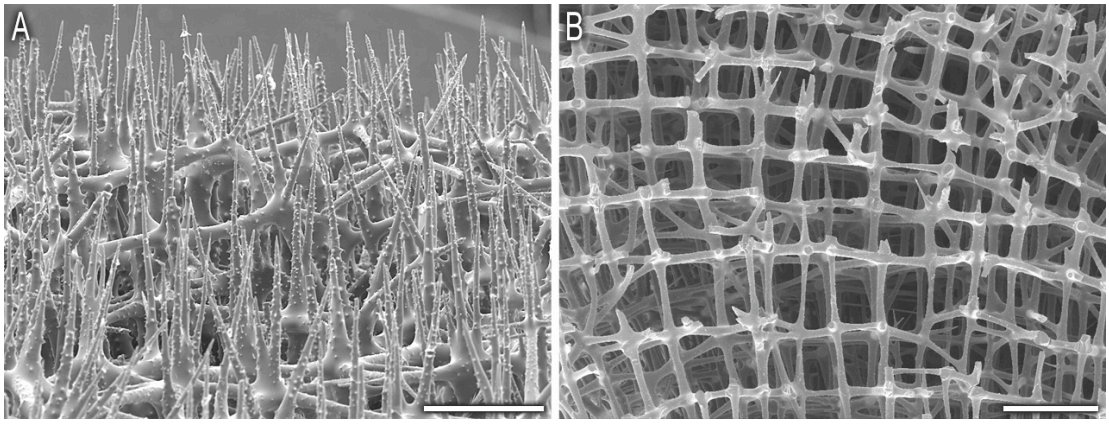

Figure 4.7: Exterior (A) and interior (B) views of the highly ordered network of fused hexactines in *Aphrocallistes vastus*. Scale bars: A: 250μm; B: 500μm.

The organic scaffold (consisting of the six-rayed axial filaments) is not continuous throughout the lattice although it may overlap at the points of fusion between two neighboring spicules (Figure 4.8). This observation suggests that the constituent spicules were largely synthesized in their entirety prior to incorporation into the lattice. While this may be the case, at the points of spicule fusion there is no indication of structural boundaries, indicating that the lattice formation is largely a continuous process and that the cementation of the spicules together is merely a continuation of the lateral growth of the constituent spicules. In *A. vastus* as is the case in many additional hexactinellid sponges of the order Hexactinosida, the incorporation and direct fusion of small spicules into a rigid skeletal lattice is a common and characteristic design strategy. Since the maximum length of all spicules

in these species does not exceed a few mm in length, a design strategy similar to that observed in the demosponge megascleres is sufficiently strong to survive the likely experienced loading regimes.

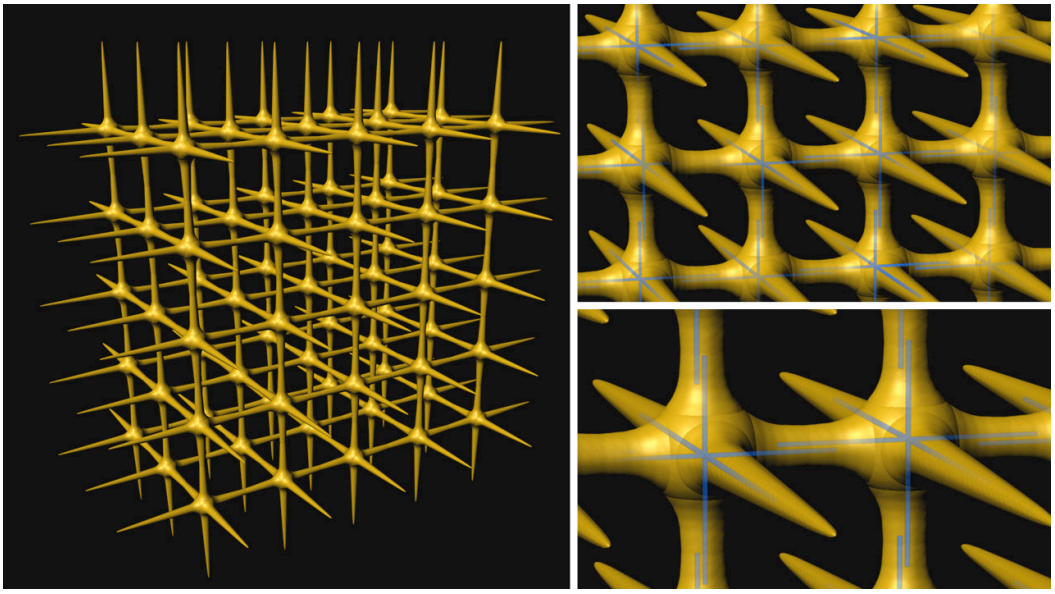

Figure 4.8: Three-dimensional structural rendering of the location of the organic scaffold (shown in blue) within the skeletal lattice of *Aphrocallistes vastus*. Data obtained from Schulze (1904) and optical microscopy studies.

4.2B Farrea occa

In contrast to the highly regular mode of spicule fusion observed in *A. vastus*, the skeletal system of *Farrea occa* (Figure 4.9) consists largely of spicules fused off-axis with respect to one another (Figure 4.10). While at the macroscopic level, this results in a significantly more disordered skeletal lattice, from a mechanics perspective it may be beneficial for the synthesis of a less rigid and morphologically plastic structure. The distinct differences in skeletal agglomeration modes observed in these two species may be directly related to the morphology of the final skeletal

lattice (Figure 4.11). In stark contrast to the skeletal systems of *A. vastus*, which adopt large, stiff, thick-walled vase-like morphologies, the skeleton of *F. occa* consists of a complex, relatively thin-walled interconnected gyroid-like structure (Figure 4.9).

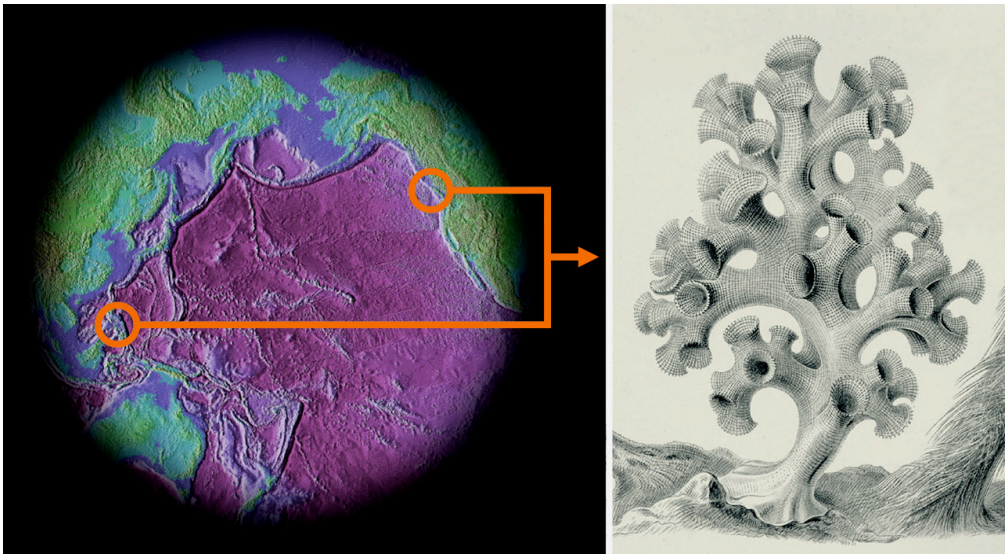

Figure 4.9: Illustration of a living specimen of the widely distributed hexactinellid, *Farrea occa* (adapted from Haeckel, 1904).

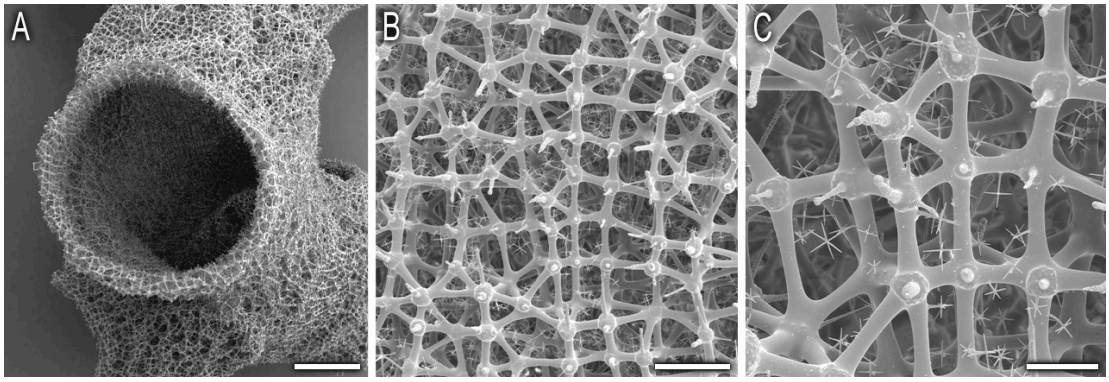

Figure 4.10: Primary skeletal system of *Farrea occa*. Various progressively magnified views of the gyroid-like skeletal network of *F. occa* which is composed almost entirely of hexactines that are fused off-axis. Scale bars: A: 2mm; B: 500µm; C: 200µm.

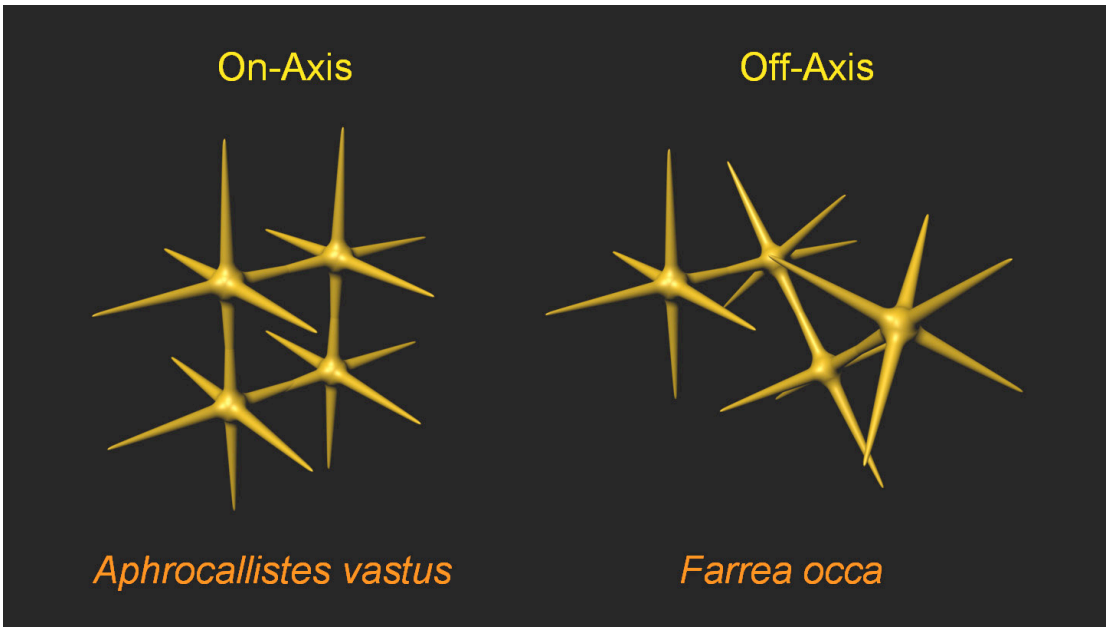

Figure 4.11: Graphical representations of on-axis vs. off-axis spicule fusion and their effect on local skeletal ordering.

4.2C Rhabdocalyptus dawsoni

From a structural and mechanics perspective, the most remarkable of the hexactinellid spicules are the significantly larger ones that form the basis of the skeletal system of many species such as *Rhabdocalyptus dawsoni* (Figure 4.12A). These spicules, which can frequently measure up to a centimeter or more in length (Figure 4.12B) are characterized by their distinctive laminated architecture which consists of a solid featureless central cylinder of silica which encases the axial filament and is surrounded by alternating layers of silica and organic forming a microlaminant. This design strategy is only encountered in spicules which either as a consequence of their orientation in the living sponge or their dimensions, encounter significantly larger stresses than their smaller non-laminated counterparts.

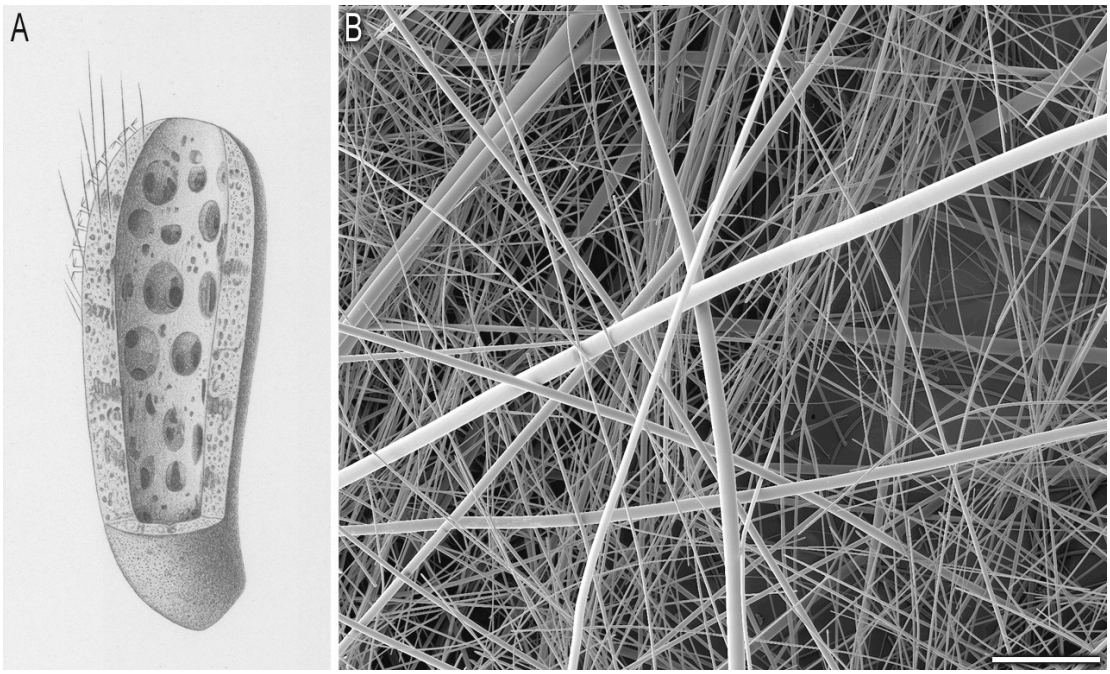

Figure 4.12: Skeletal system of *Rhabdocalyptus dawsoni*. Illustration of the North Eastern Pacific hexactinellid *Rhabdocalyptus dawsoni* (A) (adapted from Schluze, 1904) and its mineralized skeletal system consisting largely of laminated needle-like spicules (B). Scale bars: A: shown approximately life-size; B: 500μm.

When examined in cross-section, there is a distinct reduction in silica layer thickness from the spicule core to its periphery. The thinner outer layers significantly limit the depth of crack penetration into the spicule interior, effectively increasing the toughness of this composite structure.

The benefits to damage tolerance and flaw sensitivity imparted by the laminated structure can be predicted through established fracture mechanics models for two limiting cases, shown in Figure 4.13. In the first, the material is modeled as a series of weakly bonded brittle plates, each of thickness t and with flaws of length c, and a fracture toughness K_c. Provided the dominant crack (consisting, say, of several broken plates) is sufficiently blunted by the organic interlayer to completely mitigate

the associated stress intensity, re-nucleation can occur only when the stress in the intact layers reaches its intrinsic strength: $\sigma_o = K_c / 1.12\sqrt{\pi c}$. Since, in this limit, the stress in the intact layers is uniform, the fracture stress (in normalized form) becomes $\sigma_f \sqrt{t} / K_c = (1 - a/W)\sqrt{t/\pi c} / 1.12$. In the second case, the material is treated as a homogeneous monolithic body, also with fracture toughness K_c. The corresponding fracture stress is $\sigma_f \sqrt{t} / K_c = \sqrt{t/W} / 1.12\sqrt{\pi a/W}$. Comparisons of flaw sensitivities of the two structures are presented in Figure 4.13, for the case wherein t/W=0.01 (a laminate with 100 layers) and an intrinsic flaw size c/t=0.2. Clearly, the effects of the laminated structure on strength are significant. For instance, for a crack comprising 5 broken layers (a/t=5 and hence a/W=0.05), the retained strength of the weakly bonded laminate is about 5 times that of the monolithic body with the same crack. The behavior of the spicules is expected to lie between these two limits, depending on the extent to which the organic interlayers mitigate the near tip stresses.

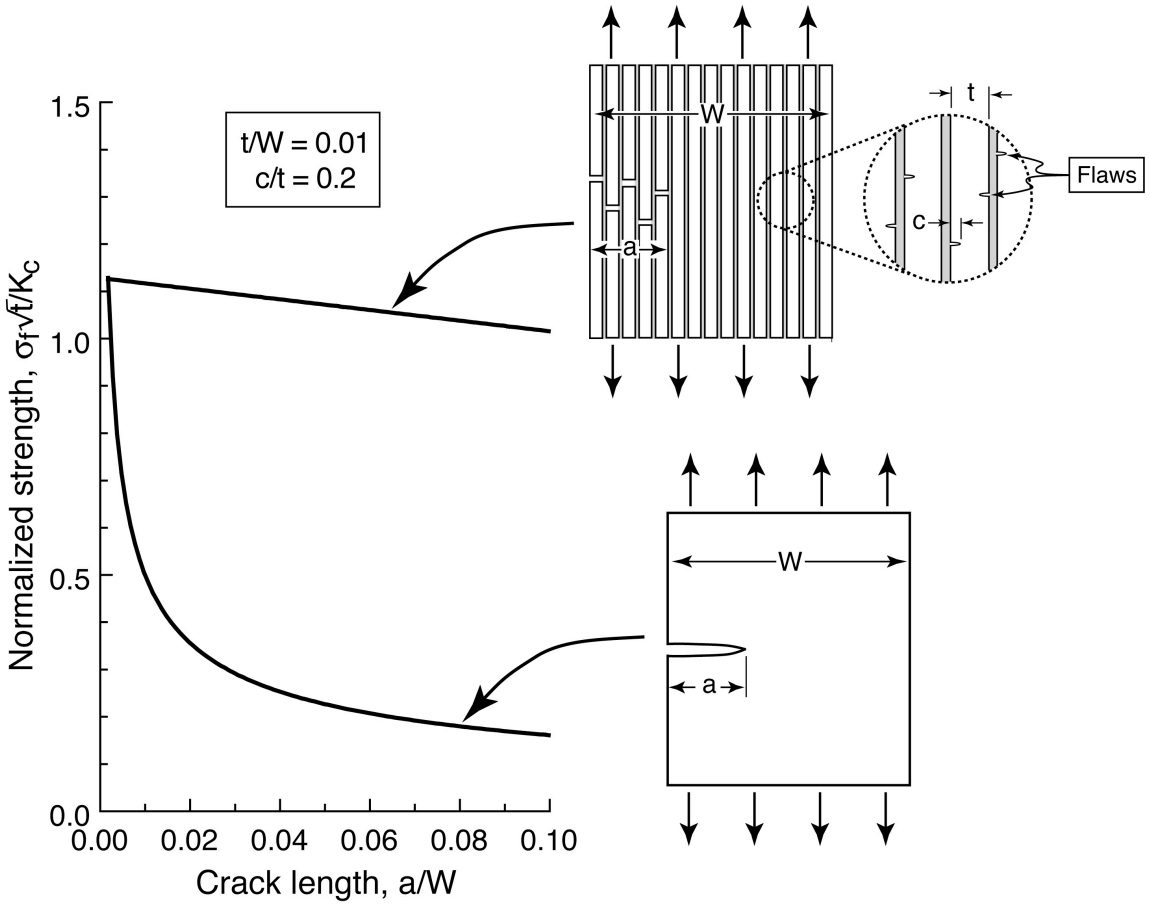

Figure 4.13: Normalized strength vs. crack length for laminated and monolithic materials.

4.2D Monorhaphis chuni

A modification to the basic laminated spicule design strategy described in *R. dawsoni* is observed in *Monorhaphis chuni* (Figure 4.14A). In this species, skeletal support and benthic anchoring is provided by a single monolithic anchoring spicule measuring up to 3m long and almost one centimeter thick (Chun, 1900), a portion of one such spicule is shown in Figure 4.15.

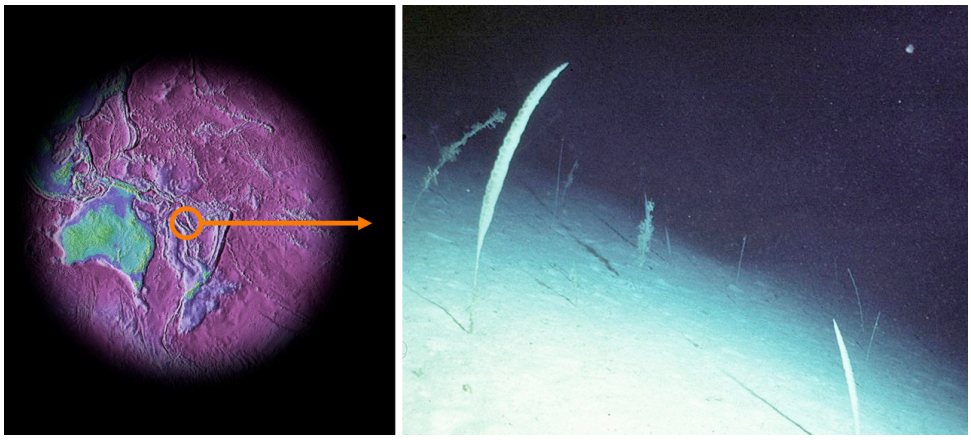

Figure 4.14: Photograph of a group of living specimens of the deep sea hexactinellid, *Monorhaphis chuni*. The large anchor spicule and the natural curvature of the sponges are clearly visible. Original photograph by Michel Roux, Reims University.

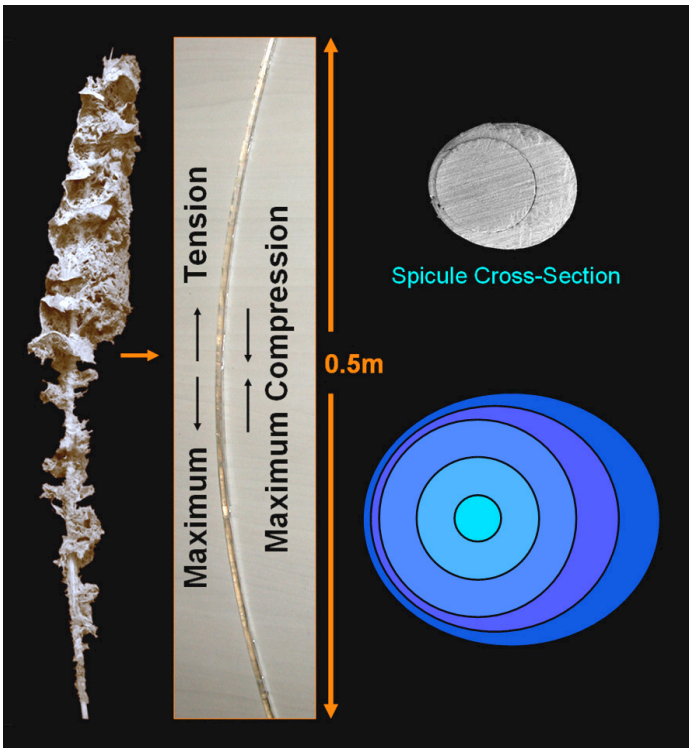

Figure 4.15: Design features of the giant anchor spicule of *Monorhaphis chuni* (sponge photo adapted from Schulze, 1904). Unidirectional spicule curvature results in asymmetrical strain accumulation. Cross-sections through the spicule (SEM image upper and graphical representation, lower) reveal the accompanying asymmetrical silica deposition.

Presumably as a consequence of its large size and the local environmental conditions (prevailing currents, etc.), the spicule develops a natural curvature. This creates spicule zones of maximum tension and compression and is accompanied in large spicules by a distinct asymmetry in silica layer thickness (Figure 4.15); the thinnest exterior layers under maximum tension help limit the depth of crack penetration, while the thickest layers prevent buckling in the zone of maximum compression (Figure 4.16).

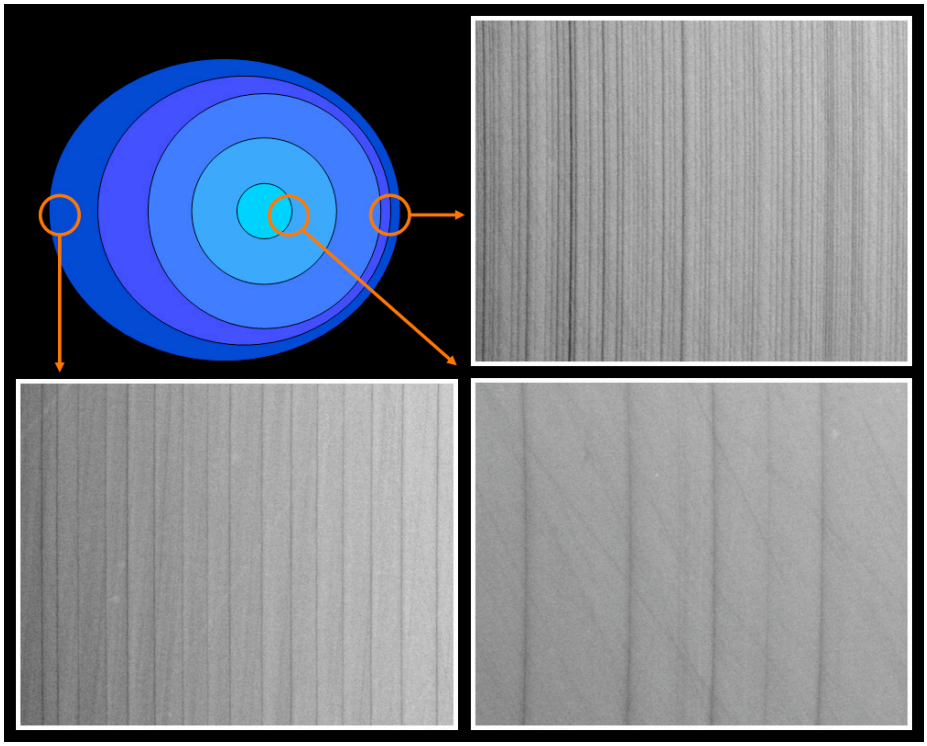

Figure 4.16: Asymmetric layer thickness in the giant anchor spicule of *Monorhaphis chuni*. Environmental scanning electron microscopy reveals that this spicule appears to be structurally optimized to deal with unidirectional bending regimes. The difference in silica layer thickness from one end of the spicule to the other (in the direction of loading) is nearly 6-fold (ca. 500nm per layer, upper right; ca. 3µm per layer, lower left). The thickest layers, immediately surrounding the central cylinder (lower right), measure ca. 10µm thick. Field diameter of each micrograph is ca. 50µm.

It is important to note that this significant asymmetry in silica deposition only occurs once the spicules reach a critical size, as smaller individuals exhibit a symmetrical design, which as is seen in the basalia of *E. aspergillum*, is structurally optimized to deal with multidirectional bending regimes. Layer asymmetry observed in *M. chuni* is a unique to this species and is most likely a stress-induced response to the predominantly unidirectional bending regimes of this monolithic structure, thus raising intriguing questions as to the sensory and silica deposition regulatory mechanisms that result in this unique design strategy. Despite its exceptional rarity and deep dwelling nature (frequently encountered at depth exceeding 2000m), the giant anchor spicule from *M. chuni* has proved to be an exceptionally useful model system for investigating a wide range of chemical, mechanical, and ultrastructural properties of laminated spicules, mainly due to its unusually large size (Woesz, et al., 2006). No other described species of sponge synthesize spicules that are even remotely comparable in dimensions to that encountered in this species. This attribute makes it an ideal research subject for mechanical and compositional studies of the biosilica, using techniques that are otherwise dimensionally limited in spatial resolution. For instance, using Raman chemical mapping on the spicules from this species, it was revealed for the first time that the organic interlayers are protein rich, based on their characteristic C-H stretch and amide vibrational spectral signatures (Figure 4.17).

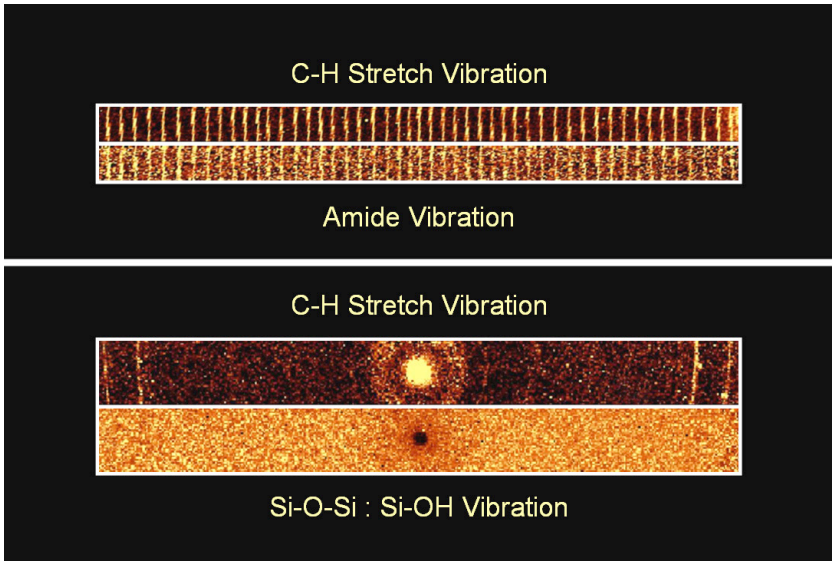

Figure 4.17: Raman chemical mapping of *Monorhaphis chuni* spicule cross-sections. C-H stretch and amide vibrations through the spicule cortex confirm that the organic interlayers are protein rich. C-H stretch vibrations around the axial filament, confirm the presence of extra-axial filament occluded organics within the biosilica and an accompanying decrease in the degree of silica condensation (adapted from Woesz, et al, 2006).

Additional information obtained from high load nanoindentation studies have revealed the remarkable energy dissipating properties of this laminated architecture. Nanoindentation results reveal that when compared to the monolithic material encountered in the central cylinder region immediately surrounding the axial filament, the laminated architecture effectively inhibits crack initiation from the corners of the indent (Figure 4.18) as all of the applied energy is dissipated locally with no global net effect on the spicule structural integrity. Cross-sections through a fractured spicule (Figure 4.19) clearly reveal the crack-stopping properties of the organic interlayers.

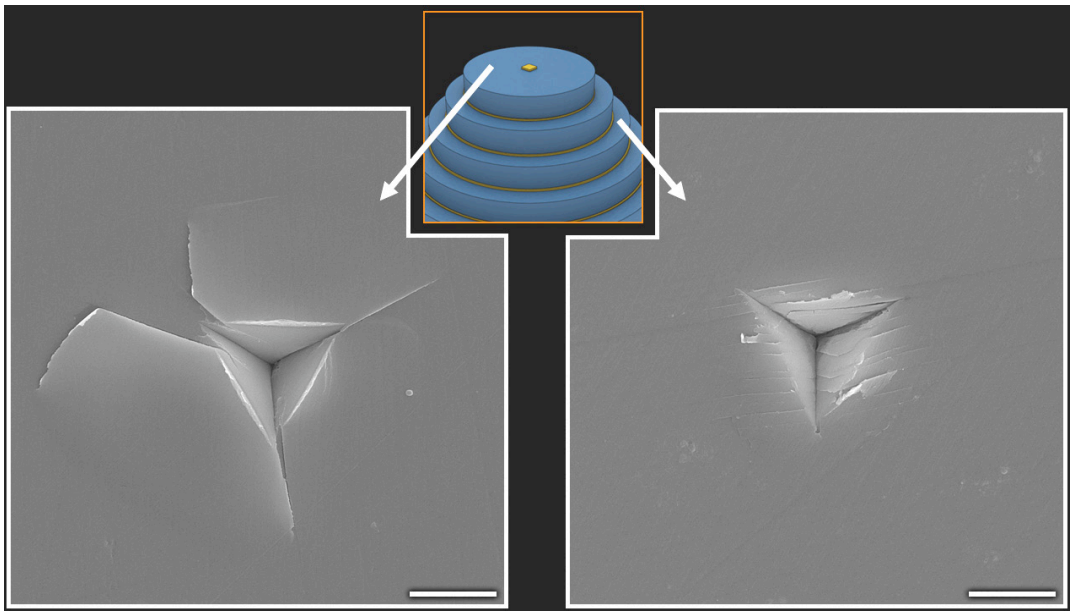

Figure 4.18: Crack-stopping properties of the laminated spicule architecture. 100mN nanoindents in the spicule cortex do not result in radial crack initiation (right), while those in the central cylinder do (left), despite the fact that the micromechanical properties of the mineral phases are identical in both regions. Scale bars: 5μm.

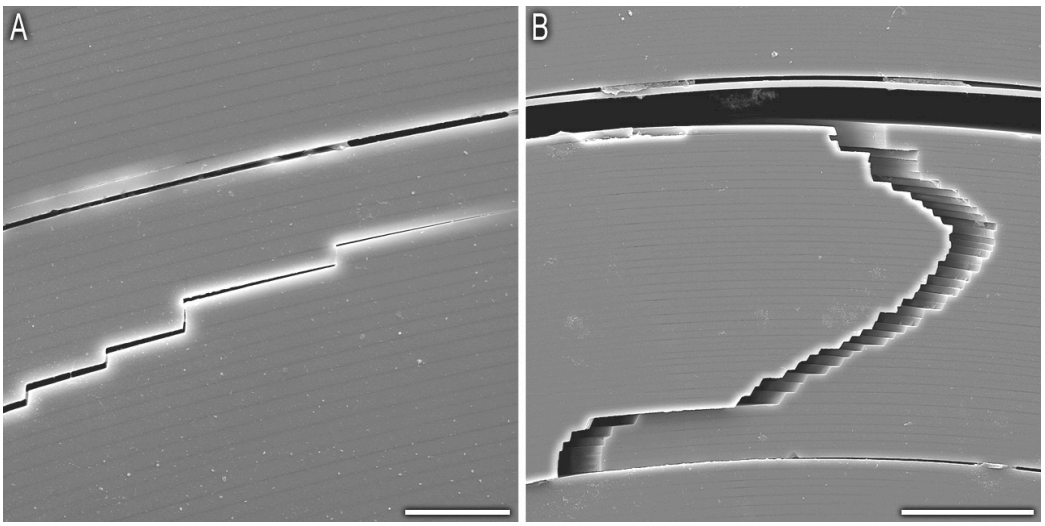

Figure 4.19: Fracture dynamics of laminated spicules: Cracks propagating through a damaged anchor spicule from *Monorhaphis chuni* exhibit a distinct step-mode, clearly illustrating the crack-deflecting properties of the organic interlayers. Scale bars: A: 20μm; B: 50μm.

4.3 Summary

As we have seen from these studies and those discussed in the previous chapters, the siliceous skeletal systems of sponges are structurally optimized to meet the needs of each species and it is hoped that additional research into the structure-function relationships of these materials can provide inspiration for the fabrication of the next generation of complex, robust, hierarchically ordered, fracture-resistant three-dimensional composites.

The following statements help summarize the general design strategies observed in the siliceous skeletal elements of the Porifera:

1) Spicules greater that a few millimeters in length exhibit a unique laminated architecture, which effectively retards crack propagation through these materials.

2) Layer number increases with spicule length and typically decreases in thickness outward from the core.

3) Mode of spicule consolidation, when present, follows the general design schemes present in the dominant constituent spicules (laminated spicules use a laminated cement, nonlaminated spicules use a nonlaminated cement)

4) Large spicules confronting unidirectional bending regimes exhibit a unique graded architecture for enhanced fracture resistance.

Chapter 5

Real-Time Detection of Spiculogenesis in Living Demosponges Using a Silica-Specific Fluorescent Tracer

This Chapter is adapted from:
Real-Time Detection of Spiculogenesis in Living Demosponges Using a Silica-Specific Fluorescent Tracer
Contributing researchers: James C. Weaver, Michael Bartl, Katsuhiko Shimizu, Yolanda Del Amo, Mark A. Brzezinski, Galen D. Stucky, and Daniel E. Morse

5.1 Introduction

As we have seen in the previous four chapters, much has been learned in recent years regarding the ultrastructural properties of a wide range of demosponge and hexactinellid spicules. While this may be the case, until recently, however, detailed analysis of the cellular and developmental mechanisms controlling spicule formation *in vivo* have relied to a large extent on transmission electron micrographs of frozen or fixed samples (Simpson, 1984; Uriz, et al., 2000); these consequently have failed to provide a detailed developmental trajectory for silica biogenesis.

Recently, using "primmorphs" (actively dividing sponge cell aggregations) grown under controlled conditions, Müller (1999) and his colleagues have succeeded in the initiation of morphogenesis, during which they observed the initial stages of megasclere biosynthesis in the Mediterranean littoral demosponge *Suberites domuncula*. As the sponges continue to develop and expand three-dimensionally, however, it becomes progressively more difficult to monitor real-time spicule formation due the opacity of the growing cellular masses. For this reason, new methods for investigating spicule biosynthesis in living sponges are needed to help truly understand the fundamentals of silica formation in living sponges and other species.

Although there are currently many immunohistochemical fluorescent probes available for monitoring numerous biomolecules and physiological processes, tracking the uptake, transport, and deposition of silicon in biological systems has been problematic. While several flourophores were known to be incorporated into

biogenic silica, their fluorescence is relatively weak when conjugated with silica or silicic acid and in many cases not readily discernable from non-silicate bound tracer. Recently, the fluorescent probe 2-(4-pyridyl)-5-((4-(2-dimethylaminoethylamino-carbamoyl) methoxy) phenyl) oxazole (PDMPO) was demonstrated to fluoresce intensely when bound to newly made silica *in vivo* and *in vitro,* (Shimizu, et al., 2001); this dye was used successfully to track silica deposition in diatoms (Shimizu, et al., 2001; Hazelaar, et al, 2005; cf. Figure 5.1). We report here the use of PDMPO as a powerful tool for monitoring microsclere spicule biosynthesis in real time in the Eastern Pacific temperate demosponge, *Tethya aurantia*.

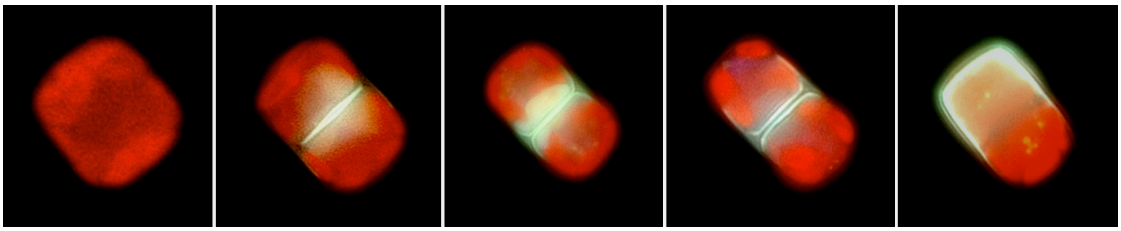

Figure 5.1: Fluorescent micrographs of *Thalassiosira weissflogii* grown in the presence of PDMPO. Diatom samples were collected at different times to illustrate the various stages of frustule biosynthesis. Newly deposited silica fluoresces bright green. Original micrographs by Katsuhiko Shimizu and Yolanda Del Amo.

The demosponge *T. aurantia* has proved to be a useful model system for analysis of the fundamental mechanisms involved in biosilicification (Shimizu, et al., 1998; Cha, et al., 1999, 2000; Zhou, et al., 1999; Shimizu and Morse, 2000; Morse, 1999, 2000; Weaver and Morse, 2003). *T. aurantia* synthesizes three main spicule types (one megasclere and two microscleres), which together comprise ca. 75% of the sponge's dry weight. The bulk of the spicule mass from this species (greater than

99%) is comprised of megascleres (structurally described as strongyloxea, or fusiform needles) measuring ca. 2mm in length and 30μm in diameter (Figure 5.2A). The two classes of microscleres (Figure 5.2B and C) comprise spherasters (measuring ca. 50μm in diameter) and smaller acanthasters (ca. 10μm in diameter). While numerically abundant, the microscleres contribute negligibly to the total skeletal mass and are predominantly restricted to the sponge cortex. As we report here, the newly synthesized microscleres become intensely fluorescent when labeled with PDMPO in explants of the living sponges.

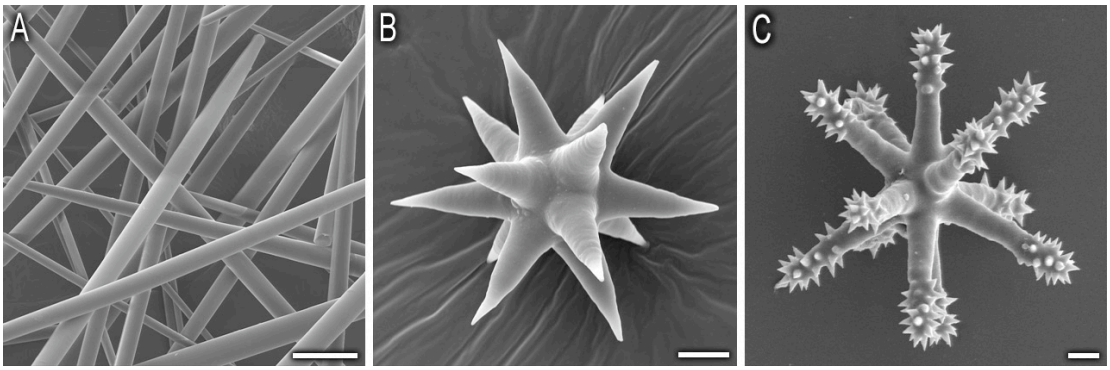

Figure 5.2: Scanning electron micrographs illustrating the three spicule types present in *Tethya aurantia*. (A) Strongyloxea megascleres, each measuring ca. 2mm in length and 30μm in diameter; (B) Spheraster microscleres, each measuring ca. 50μm in diameter; (C) Acanthaster microscleres, each measuring ca. 10μm in diameter. Scale bars: A: 100μm; B: 10μm; C; 1μm.

5.2 Results

After two weeks in culture, all explants had on average increased in mass by ca. 3x with a comparable increase in megasclere quantity as verified by light microscopic analysis. In all of the paired treatments, there were no obvious differences in growth and spicule biosynthetic rates between those in the presence or absence of PDMPO. While new synthesis of megascleres was clearly evident from the optical microscopic analyses of the isolated, cell-free spicules (i.e., roughly 3x increase in megasclere number had occurred), there was no detectable fluorescence attributable to incorporation of the fluorophore into the megascleres. Fluorescence microscopy did, however, reveal extensive fluorophore labeling of the newly synthesized microscleres, with synthesis of the acanthasters clearly outnumbering that of the spherasters (Figure 5.3).

Sodium hypochlorite treatments of the sponges and subsequent examination of the cleaned spicules (Figure 5.4) revealed that the strong fluorescence intensity of the microscleres remained long after extensive oxidation of the sponge's organic matter, indicating that the observed fluorescence was more than simply a surface binding phenomenon and that the fluorophore was actually occluded within the newly deposited silica.

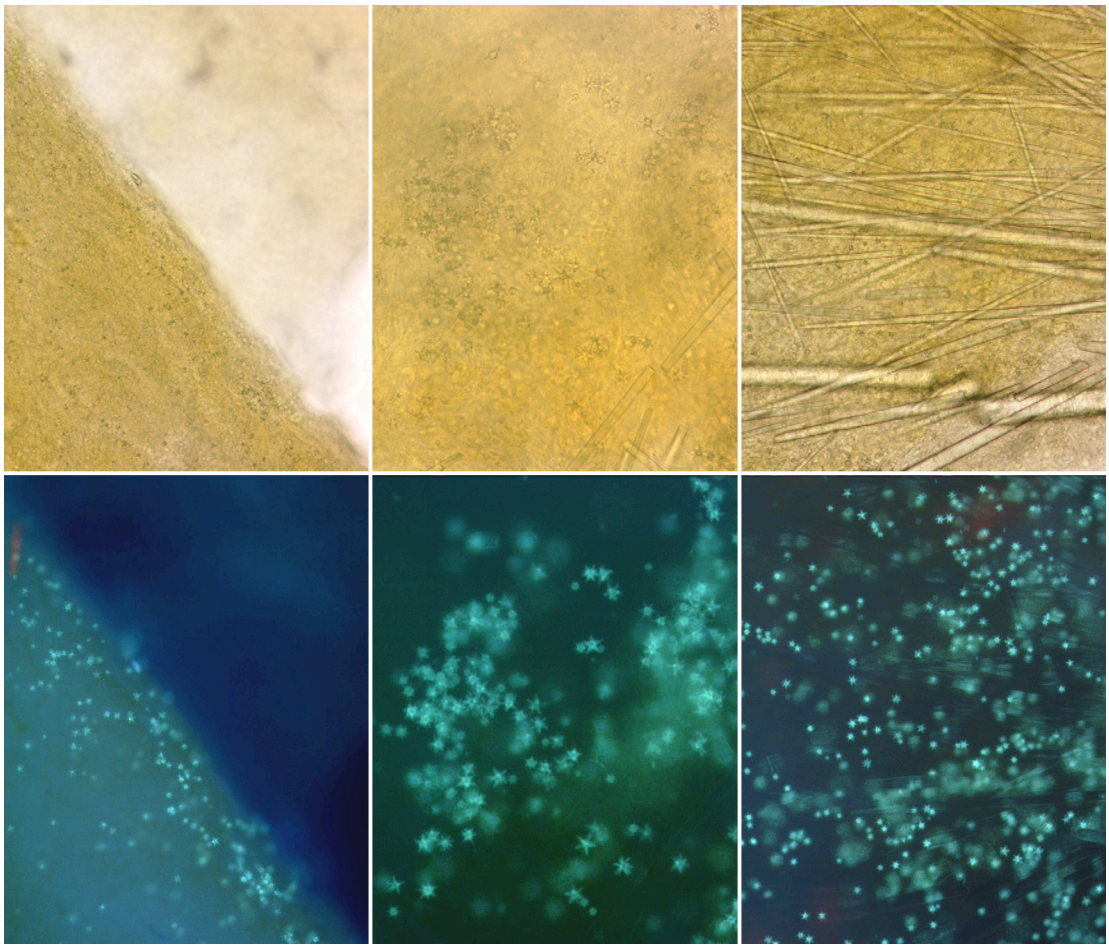

Figure 5.3: Brightfield (upper) and fluorescence (lower) optical micrographs of living explants grown in the presence of PDMPO clearly indicating the extent of acanthaster microsclere biosynthesis. The intense fluorescence of the newly synthesized spicules above background (these samples were photographed while still in the PDMPO-containing growth medium) allows for the accurate localization of the actively mineralizing microsclerocytes. The greenish background masses consist of fluorescently labeled acanthaster microscleres that are out of the focal plane.

Spectroscopic analyses of the fluorescent microscleres revealed a dominant emission peak at ca. 540nm (Figure 5.5), consistent with the bright green fluorescence of the spicules revealed by fluorescence microscopy.

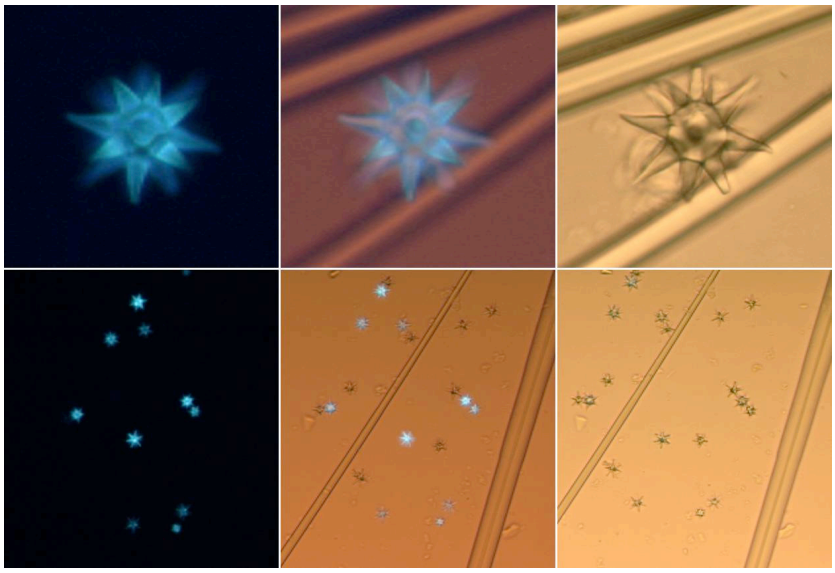

Figure 5.4: Optical micrographs transitioning from bright field to fluorescent illumination for spheraster (upper) and acanthaster (lower) microscleres isolated from living sponges reveals the high intensity of the fluorescence, even when viewed with partial transmitted light illumination. This technique provides an excellent method for rapidly identifying newly synthesized microscleres from those that had been synthesized prior to explantation. Variability in the degree of fluorescence labeling probably results from non-synchronized fluorophore introduction and microsclere biosynthesis. The blue color (observed green before photographed, cf. Figure 5.5) is an artifact of the camera software used during image capture.

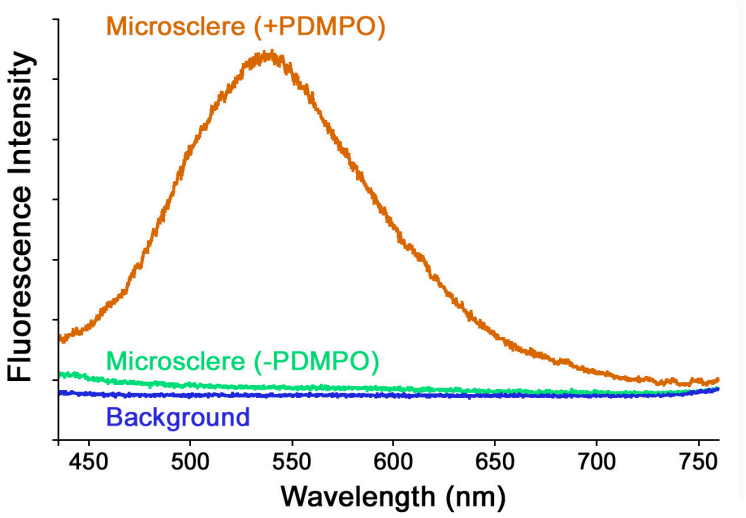

Figure 5.5: Fluorescence emission spectra of single PDMPO labeled and unlabeled acanthaster microscleres.

5.3 Discussion

In order to advance our understanding of the fundamental developmental, cellular, and molecular mechanisms governing the synthesis of biomineralized structures, new techniques are needed to monitor the synthesis of these structures in real time *in vivo*. As seen from previous studies, PDMPO provides an excellent fluorescent indicator for monitoring silicic acid metabolism in a wide range of biosilicifying taxa (Shimizu, et al., 2001; Schröder, et al., 2004; Hazelaar, et al., 2005). While initial studies proved its reliability in monitoring frustule biosynthesis in diatoms, this present work reveals that this fluorophore also can be used as a powerful tool for monitoring spicule formation in living sponges. Recently, PDMPO was used in effort to follow silicic acid metabolism in the Mediterranean demosponge *Suberites domuncula* (Schröder, et al., 2004) In these studies, however, the authors did not report fluorophore incorporation into the newly synthesized spicules. These observations can now be explained in view of the results reported here, since *S. domuncula* lacks microscleres as part of its mineralized skeletal system. The negative results with *S. domuncula* are therefore consistent with our observations, as we saw no PDMPO incorporation into the megascleres of *T. aurantia,* under conditions in which extensive labeling of the newly synthesized microsclere occurred.

The significance of these results is two-fold. First, they point to a new method for accurately localizing actively mineralizing microsclerocytes in order to monitor the details of the synthesis of these spicules in living sponges and to gain additional insight into the factors controlling their remarkable species-specific morphologies.

Secondly, they clearly indicate that the mega- and microsclerocytes (the cells producing the mega- and microscleres) are spatially segregated from one another and that the fluorophore may be differentially taken up (or excluded) by the two types of spicule- producing cells. This latter conclusion also raises the intriguing possibility that there may be major fundamental differences in the mechanisms by which spicule biosynthesis takes place in these two unique cell types (as originally suggested by Simpson, 1984).

Incubation with PDMPO may provide a valuable method for studying a broad range of growth and developmental phenomena in sponges. For example, many sponge species are well known for their ability to modify their skeletal systems when grown under different environmental conditions (Maldonado, et al., 1999). Using the techniques described here, it may be possible to investigate environmentally directed alteration of skeletal architecture in hopes of gaining additional insight into the physical factors and cellular mechanisms regulating site-specific spicule biosynthesis. Our results also have potentially broad taxonomic implications. Maldonado, et al. (1999) showed that changes in ambient concentrations of silicic acid could induce changes in spicule morphology in certain sponges, raising intriguing questions as to the reliability of spicule morphology as a diagnostic for species identification. By culturing such species in the presence of PDMPO, it would be possible to investigate these adaptive processes in real time in living sponges, allowing one to track the formation of specific spicule types. This technique also may be applied to analyses of spicule biosynthesis in larval sponges; such studies would be especially interesting

with the hexactinellid sponges that synthesize and hierarchically arrange some of the most elaborate and structurally complex spicules known (Leys, 2003; Aizenberg, et al, 2005).

In addition to the possibility of monitoring the details of silica deposition in specific species of interest, this method could also be applied to the study of oceanographic phenomenon. One example would be the analysis of diatom community population dynamics during blooms of normal and harmful microalgae. By incubating freshly collected diatoms in PDMPO for a short period of time, one could accurately determine which cells were actively dividing and which remained dormant, potentially yielding powerful insights into mechanisms of intraspecific competitive dominance for available nutrients.

The studies reported here illustrate the use of PDMPO as a tool for monitoring microsclere biosynthesis in *T. aurantia*. Further experiments with additional species of demosponges and hexactinellids will reveal whether the techniques described here have wide applicability in research aimed at understanding the fundamental mechanisms of microsclere formation within the many structurally diverse silicifying sponge taxa.

Chapter 6

Conclusions and Future Directions

Contributing researchers: James C. Weaver, David Kisailus, Mark Najarian, Mark S. Demarest, Clarissa R. Anderson, Mark A. Brzezinski, and Daniel E. Morse

Although the detailed interrelationships of the poriferan classes still remain unresolved (Cavalier-Smith, et al., 1996; Kruse, et al., 1998; Müller, 1998; Adams, et al., 1999), recent molecular evidence from 18s rDNA sequences suggests an early divergence of the Hexactinellida from the ancestral poriferan stock that gave rise to the Demospongiae and the Calcarea/eumetazoan lineages (Borchiellini, et al., 2001). This proposed early hexactinellid divergence is supported by the observation that the cellular anatomy of this group is so markedly different from the Calcarea and Demospongiae that some taxonomists believe this ancient lineage should be elevated to the rank of phylum (Bergquist, 1985; Borojevic, 1970). Hexactinellids exist predominately as multinucleate syncytia and although single cells, functionally comparable to amoebocytes and archeocytes of demosponges are present, they are closely associated with the syncytia and exhibit limited mobility. An additional feature of hexactinellids is that the choanocytes, which appear to be discontinuous from the syncytial networks, lack nuclei (Boury-Esnault and De Vos, 1988; Iijima, 1904; Mackie and Singla, 1983; Reiswig and Mackie, 1983; Schulze, 1880, 1899).

Recent studies investigating early larval development of the hexactinellid *Oopsacas minuta* reveal that their syncytial architecture is secondarily derived, arising from the 32 cell stage, after which micromere fusion results in the formation of a syncytial mass (Leys, et al., 2006). These results are significant in that they suggest that the ancestral metazoan group that gave rise to the Porifera was cellular and not syncytial, thus raising intriguing questions as to the selective pressures that may have favored the evolution of the unique hexactinellid body plan. One possible

answer to this question can be found by exploring the adaptive zone of the hexactinellids. While virtually all other sponge species occur on solid substrates, the hexactinellids are unique in that they have evolved the capacity to colonize soft sediments. One unifying feature of the sediment dwelling hexactinellids is the evolution of a holdfast apparatus, which typically consists of long basalia measuring 10s of cm in length (Figure 6.1). These long anchor spicules are essential for soft sediment colonization and hexactinellids lacking basalia are confined to more solid substrates.

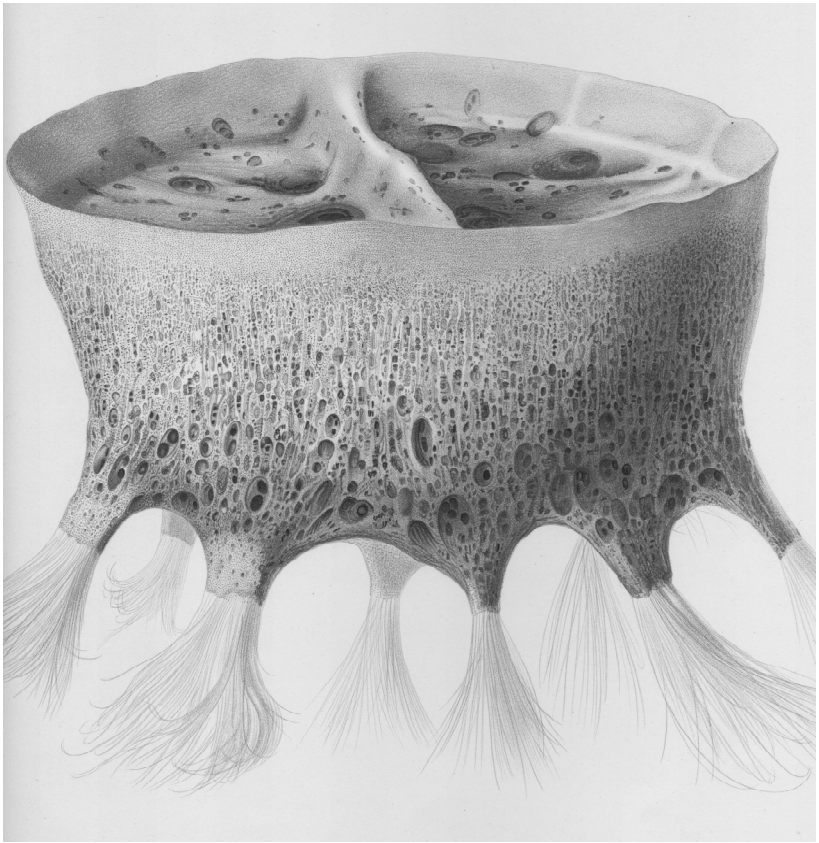

Figure 6.1: Hexactinellid anchor spicules for effective soft sediment colonization (adapted from Schulze, 1904).

Since as discussed in chapters 3 and 4, only a syncytial body plan (Figure 6.2) could facilitate the synthesis of spicules greater that a few mm in length, perhaps the syncytial architecture evolved in this group of early sponges in a habitats of reduced solid substrate availability, which characterizes the predominantly deep sea habitats in which the majority of hexactinellids now survive.

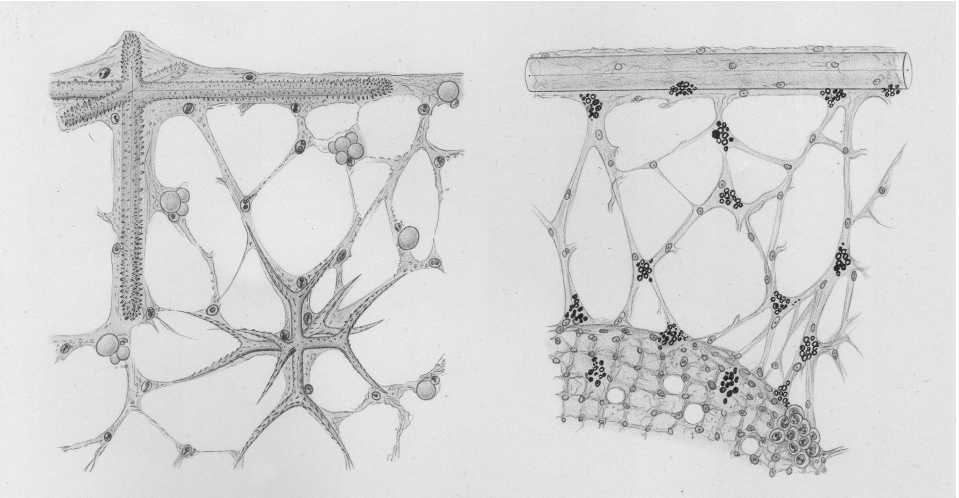

Figure 6.2: Illustration of the hexactinellid syncytial architecture and their associated spicules (adapted from Schulze, 1904).

While it is now clear that both groups of silicifying sponges, the demosponges and the hexactinellids most likely evolved from a common cellular ancestor, we have recently discovered a marked difference in spicule axial filament protein composition of hexactinellids compared to those obtained from demosponges. Preliminary SDS-PAGE analysis of axial filament proteins from the hexactinellid *Euplectella aspergillum* reveals that they are dominated by proteins of higher molecular weights than those isolated from demosponges. Although the amino acid composition of these

protein filaments is similar to those isolated from *Tethya aurantia*, suggesting the possibility that demosponge silicateins might be truncated versions of their hexactinellid counterparts, it is at this point equally likely that further sequence analysis and structural characterization of these proteins may reveal that the formation of silicified skeletal elements has evolved independently within these two groups and that the presence of axial filaments within these spicules may be convergently derived.

The notion that a geometry-determining proteinaceous axial scaffold evolved independently in the two classes of silicifying sponges may be supported by recent ultrastructural studies of another silicifying taxa, the silicoflagellates. The silicoflagellates are a small enigmatic group of photosynthetic protests of uncertain phylogenetic positioning, although they are likely close relatives of the pedinellids and actinomonads, members of the polyphyletic and heterogeneous "Chrysophyceae". A unique feature of the silicoflagellates is their siliceous skeletal system, which is composed of a series of fused rod-like elements (Figure 6.3). While classical taxonomy of the group was largely based on skeletal diversity, the studies of Van Valkenberg and Norris (1970) suggest that much of the observed variability in skeletal architecture of extant "species" is related to local environmental heterogeneity and does not have a genetic basis, thus raising important questions as to its utility as a basis for classification.

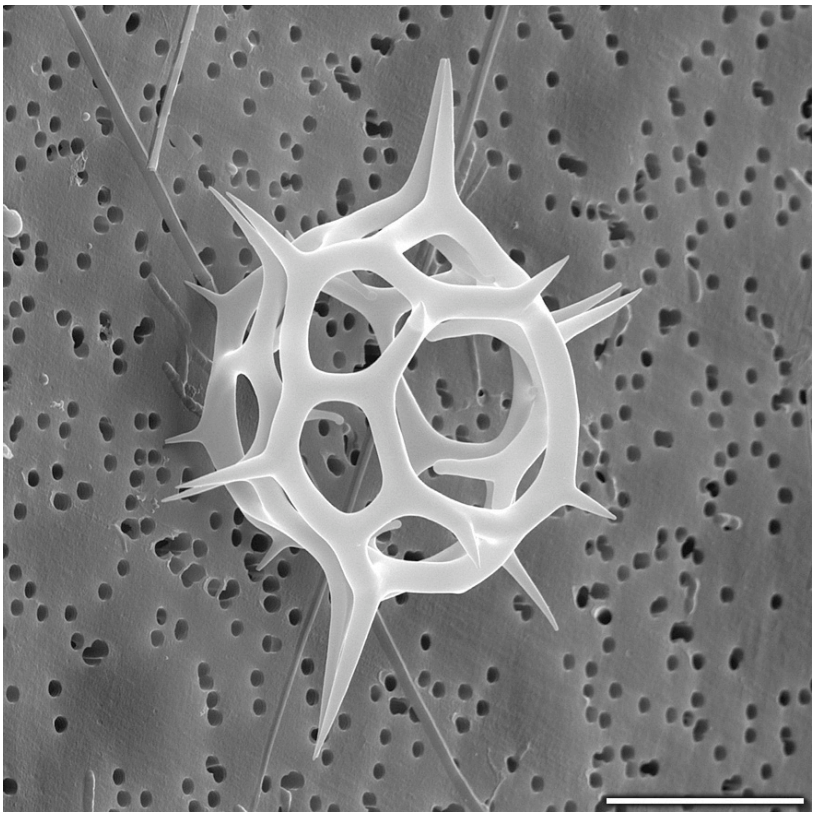

Figure 6.3: Scanning electron micrograph of an asexually reproducing specimen of the silicoflagellate *Dictyocha speculum* (specimen courtesy of Clarissa R. Anderson and Mark A. Brzezinski). Scale bar: 10μm.

Scanning electron microscopy studies of silicoflagellate skeletons collected from Antarctic sediment traps suggest that like the spicules from demosponges and hexactinellids, the skeletons of silicoflagellates consist of concentric lamellae of consolidated silica nanoparticles organized around an organic scaffold (Figure 6.4). This scaffold is distinctly branched and extends into all of the struts of the "skeletal crown", suggesting that it plays a critical role in establishing skeletal geometry in the silicoflagellates.

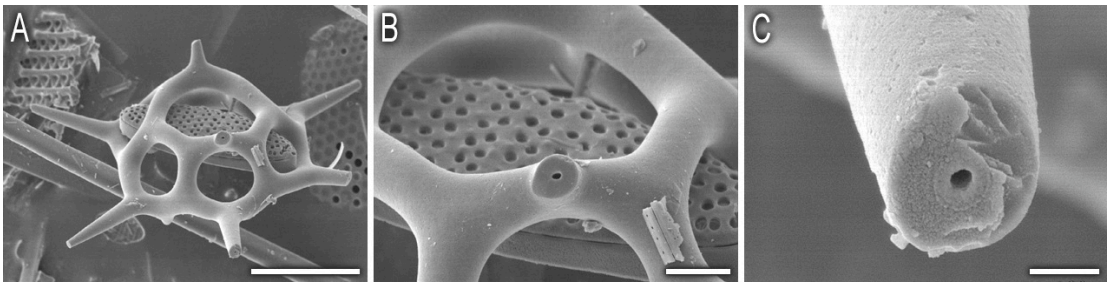

Figure 6.4: Scanning electron micrographs of a partially demineralized skeleton of *Dictyocha speculum*. These SEM images clearly reveal the location of the organic scaffold that apparently regulates the observed skeletal geometry in this group of unicellular algae (specimens courtesy of Mark S. Demarest and Mark A. Brzezinski). Scale bars: A: 10μm; B: 2μm; C: 500nm.

The fact that a completely unrelated group of photosynthetic flagellates shares similar skeletal design strategies with two groups of early metazoans strengthens the notion that this biomineralization motif evolved independently in multiple taxa. Additional studies investigating the biochemical nature of the organic scaffolds of both silicoflagellates and hexactinellids may reveal that they, like the silicateins of the demosponges, evolved from an ancestral group of hydrolytic enzymes, via unique and unrelated evolutionary divergences.

Despite the significant and obvious differences in demosponge and hexactinellid axial filament morphologies, there are some underlying design themes that can help explain their observed structural diversity. Previous x-ray diffraction (Croce, et al., 2004) and transmission electron microscopy studies (Garrone, 1969) have revealed that the subunits within the organic filaments from both classes exhibit highly regular ordering (Figures 6.5 and 6.6).

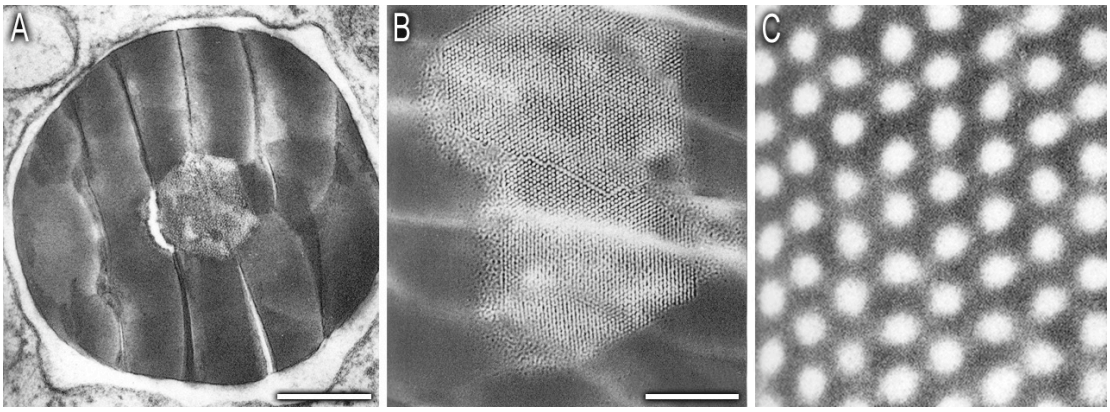

Figure 6.5: TEM images of progressively magnified demosponge spicule cross-sections. These images reveal that the axial filament constituent proteins associate with one another in a hexagonal array (adapted with permission from Garrone, et al., 1969). Scale bars: A: 250nm; B: 100nm.

The axial filaments and their characteristic packing morphologies thus have much in common with the design constraints seen in the formation of crystalline inorganic materials, where the mechanical, electrical, and optical properties are strongly dependent on the limited number of underlying structural unit variations that these crystals are built upon. Typically, the size, shape and charges of atoms/ions will predetermine their arrangement in a specific crystal structure. Furthermore, unit cell packing constraints can critically affect growth dynamics and can thus play a fundamental role in ultimately determining bulk crystal morphology

To help understand the potential relationship between axial filament protein composition and filament structure, we compared protein hydrodynamic radius ratios (Figure 6.7) of the major spicule-associated proteins from *T. aurantia* (Demospongiae) and *Euplectella aspergillum* (Hexactinellida). We found that the demosponge proteins exhibited a near monodisperse size distribution, while those

from the hexactinellid were distinctly bimodal. If we assume that each of the spicule-associated proteins are contained within the axial filaments of *E. aspergillum*, as has been suggested based on the original observations of Schulze (1904), we can then begin to establish a functional model to help explain spicule macroscopic symmetry. Based on predicted unit cell structures of inorganic crystal systems using ionic radii calculations, these results suggest that the axial filament proteins from demosponges most likely pack together in a hexagonal unit cell while those from hexactinellids are either cubic or simple tetragonal (Figures 4.1, 6.6).

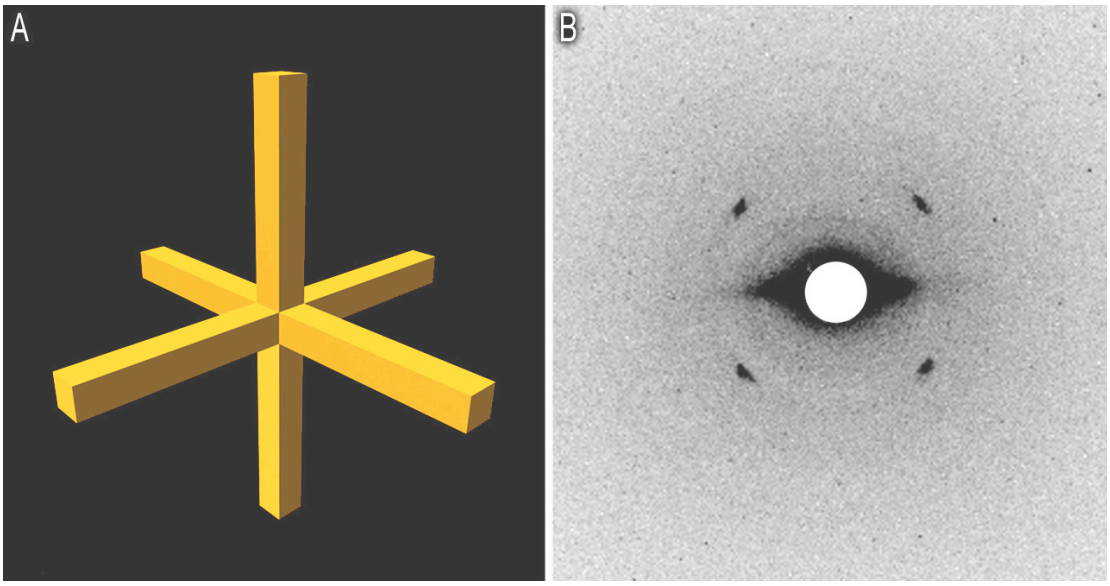

Figure 6.6: X-ray diffraction of the hexactinellid axial filaments (A). Small-angle x-ray diffraction pattern (B) obtained from the intact axial filaments of *E. aspergillum* reveals that the constituent proteins most likely associate with one another in a cubic or simple tetragonal unit cell. This result is consistent with the unique symmetry of hexactinellid axial filaments revealed previously from SEM studies and predictions based on molecular modeling (cf. Figures 3.3 and 6.8).

These predictions agree closely with observations obtained from TEM and XRD analyses of the native filaments, thus suggesting that the size distributions of the spicule associated proteins may be one of the major factors determining their final packing geometries. While hydrophobic, ionic and/or hydrogen-bonding interactions are likely to govern the pathways of hierarchical assembly of these protein subunits forming the axial filaments *in vivo* (Murr, et al., 2005), the minimization of surface free energy apparently is a major determinant of their final dense packing organization.

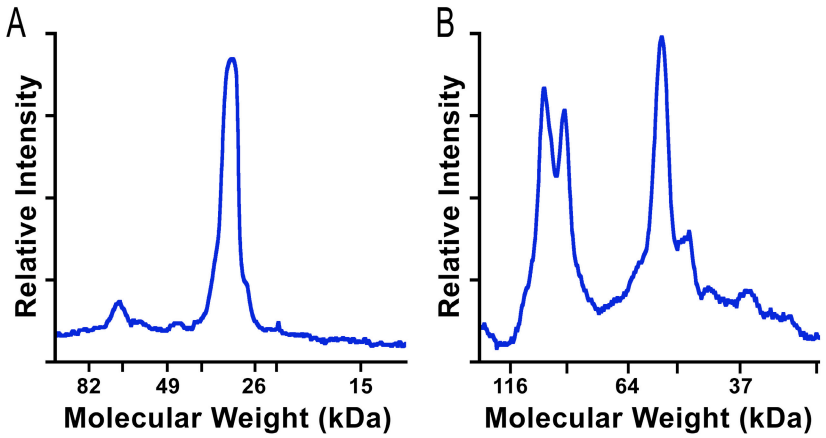

Figure 6.7: SDS-PAGE densitometry profiles of spicule-associated proteins from demosponges and hexactinellids. The major spicule-associated proteins of demosponges (A) exhibit a predominantly monodisperse size distribution, while those of hexactinellids (B) are distinctly bimodal. Using the predicted molecular weights based on SDS PAGE mobility, we can estimate molecular hydrodynamic radii of both the demosponge and hexactinellid spicule-associated proteins.

The resulting crystal-like packing of the protein subunits can be seen to govern the resulting supramolecular protein unit cell symmetry and the axial filament cross-sectional geometry (Figure 6.8). Subsequent accretion of protein subunits

preserving and extending the original close-packed structure would then be predicted to generate the tetrahedral morphologies observed in demosponges and the octahedral structures seen in hexactinellids (similar to those structures observed in related inorganic crystal systems; cf. Figure 6.8).

Not surprisingly, these branched structures have parallels to crystalline inorganic materials such as CdTe (tetrahedral) and chalcotrichite Cu_2O (octahedral). These observations help explain much of the observed structural diversity of siliceous sponge spicules and confirm the long established principle that simple thermodynamic considerations can frequently provide insight into the origins of symmetry in biological systems (Thompson, 1942; Ziherl and Kamien, 2000).

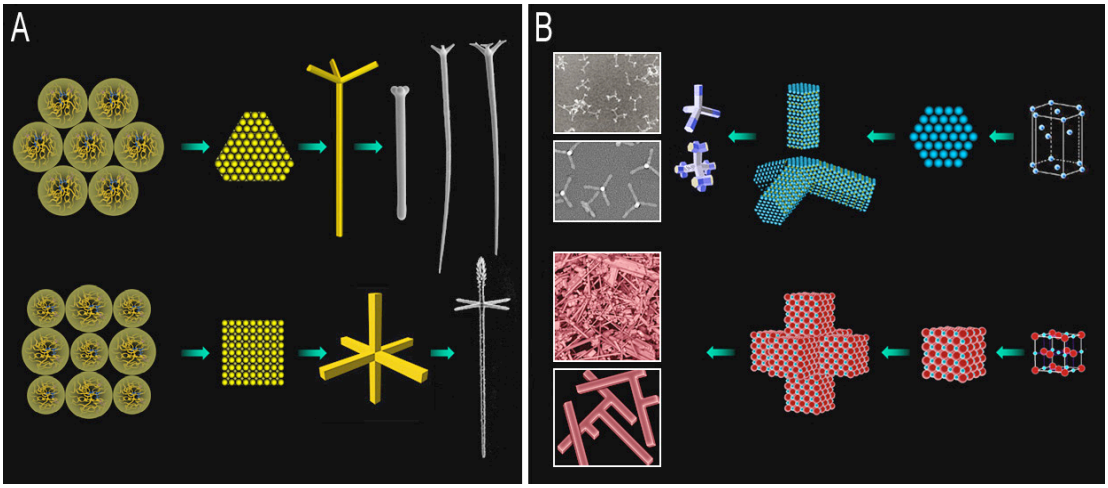

Figure 6.8: Illustration revealing the potential correlations between demosponge (upper) and hexactinellid (lower) spicule globular protein packing dynamics, filament symmetry, higher order branch geometries, and full-scale spicule morphology (A). Commonalities between symmetries observed in demosponge and hexactinellid spicule axial filaments and those of inorganic crystalline materials (CdTe, upper and chalcotrichite Cu_2O, lower) are clearly evident (B). Images adapted with permission from Manna, et al., 2003 and Milliron, et al., 2004.

Although much has been learned in recent years regarding the mechanisms of spicule formation in sponges and their remarkable ultrastructural and mechanical properties, there are still many unknowns concerning the molecular precursors of this synthesis, and the factors responsible for control of structure at the macro-, micro-, and nanoscale. New advances in high-resolution electron and atomic force microscopy, nuclear magnetic resonance spectroscopy, and the latest biotechnological innovations in protein structure determination, site-directed and combinatorial mutagenesis, and immunohistochemical localization should help in future investigations of the fabrication of some of nature's truly unique engineering marvels, the mineralized skeletal elements of the Porifera.

Chapter 7

Methods

Chapter 2:

2.1 Isolation of Spicules

Specimens of the marine sponge *T. aurantia* were collected at 17 m depths off Santa Barbara County, California (latitude 34°25.331′N, longitude 119°57.142′W) in July, 2000. Sponges were washed with seawater and treated with a 5.25% (v/v) sodium hypochlorite solution until all of the cellular material had been removed. The residual material was washed with Milli-Q (Millipore)-purified water five times and then soaked in concentrated HNO_3/H_2SO_4 (1:4) overnight. Acid-insoluble material (which consisted entirely of the cleaned silica spicules) was rinsed with Milli-Q water until the pH was $\geq$6, and then air-dried. Fig. 2.1 illustrates the cleaned spicules utilized for the following experiments.

2.2 Preparation of spicules for microscopy

Similar preparative techniques were used for both SEM and AFM analyses. After drying, the spicules were ground with a mortar and pestle until greater than 75% of the fragments were of the appropriate size for microscopic analyses. After fracture, the spicule fragments were rinsed with Milli-Q water, the suspension allowed to settle, and the fine particulates remaining in the suspension were decanted and discarded. The duration of time for gravity settling and the number of washings performed varied as a function of grinding intensity and the desired size of the final fragments to be examined. To avoid potential imaging artifacts resulting from the use of mounting adhesives, none were used for the following studies. The spicule

fragments were resuspended in 95% ethanol and small volumes were pipetted onto 12 mm round glass cover-slips (Fisherbrand, Pittsburgh, PA), the samples were air-dried, and examined microscopically. Adhesion to the glass cover-slips was facilitated entirely by electrostatic and/or other adhesive forces between the spicule fragments and the glass substrates. As specified, some samples were etched by treatment with sodium hypochlorite (5.25% v/v) for 6 weeks, washed five times with Milli-Q water and three times with 95% ethanol, and mounted for examination as described above.

2.3 Electron microscopy

The dried spicules (mounted on 12mm round glass cover-slips) were sputter-coated with gold/palladium and observed with a JEOL JSM 6300F cold-cathode field-emission scanning electron microscope.

2.4 Atomic force microscopy

All imaging was performed with a Dimension 3100 SPM (Digital Instruments, Santa Barbara, CA) equipped with commercially available silicon cantilevers (nominal tip radius of 10nm) measuring 125μm in length. The cantilever oscillation frequency was tuned to the resonant frequency of the cantilever (280–350kHz) and all imaging was performed in air at ambient conditions. The 512 x 512 pixel images were captured with a scan size between 0.6 and 10μm at a scan rate of 0.5–2 lines per second. Images were acquired simultaneously from the height, amplitude, and phase

signals. All imaging was done in tapping mode to minimize sample damage and to reduce the probability of dislodging the spicule fragments during scanning. Images were further processed by flattening using Nanoscope Software (Digital Instruments) to remove background slope.

2.5 Treatments with HF and heat

Freshly cleaved spicule cross-sections were analyzed for heat-induced structural changes to the deposited silica. (1) Spicule cross-sections were etched with 1 M HF for 1 min [an excellent technique for rapid visualization of the annular silica organization (Schwab and Shore, 1971b), washed five times with Milli-Q water and three times with 95% ethanol, and air-dried. The samples then were heated (in air) to 300 and 600 °C for 1h and any heat-induced structural changes were analyzed by SEM. (2) As a control, additional spicule cross-sections were first heated to 300 and 600 °C for 1 hour and then treated with 1 M HF for 1 min, washed and dried as described above. Any effect that the prior heating had on the samples' reactivity to HF treatment was analyzed by SEM. Samples were mounted for examination as described above. The heated samples (and a non-heat-treated control) also were analyzed by NMR spectroscopy.

2.6 NMR analyses

Solid-state ^{29}Si NMR spectra were acquired in a temperature-controlled room (20–23°C) on a Chemagnetics CMX-500 spectrometer using an 11.7T wide bore

magnet. A double resonance magic-angle-spinning (MAS) probehead with no ^{29}Si background signal was used with 7.5 mm Pencil MAS rotors containing 400–500mg of powdered sample. The ^{29}Si MAS NMR spectra were acquired with samples spinning at a rate of 6kHz using an 8.6μs 90° pulse and a continuous ^{1}H-decoupling field strength of ν_{dec}=12.5kHz. A spectral width of 16kHz was used during signal acquisition, with a filter width of 10.4kHz; 256 time domain points were acquired for each transient. Gaussian filtering of 100Hz (which is small compared to the ^{29}Si NMR peak widths) was applied during data processing. The ^{29}Si chemical shift scale was externally calibrated to the known chemical shifts of tetrakis(trimethylsilyl)silane [-9.8ppm for the CH_3–Si– groups referenced to the chemical shift standard tetramethylsilane (TMS)]. Three samples were investigated by ^{29}Si MAS NMR: a non-heated control sample (A), one heated to 300°C (B), and one heated to 600°C (C) (see *Treatments with HF and Heat* section for details). Recycle times between successive signal acquisitions were 10min for samples A and B and 260min for sample (C). The recycle times were chosen to prevent saturation of any parts of the spectrum during prolonged signal averaging. These differences show that the ^{29}Si T_1 relaxation times for sample (C) are approximately an order of magnitude larger than for samples (A) and (B). T_1 relaxation times are measures of the rates at which the longitudinal component of the nuclear magnetization is restored to thermal equilibrium. More transients were acquired for sample (B) than for sample (A) to improve the signal-to-noise ratio and thereby elucidate the less resolved features at larger chemical shifts in the ^{29}Si spectrum of (B).

A two dimensional $^{29}Si\{^{1}H\}$ heteronuclear correlation NMR spectrum (Janicke et al., 1998; Schmidt-Rohr and Spiess, 1994) was acquired for the non-heated sample (A) under MAS conditions at a spinning rate of 6kHz. A ^{1}H spin-diffusion delay (Goldman and Shen, 1966) of 75ms was included in the pulse sequence to allow resonance signals from spatially proximate moieties to be correlated up to distances of ca. 20nm (Schmidt-Rohr and Spiess, 1994). The contact time of 4 ms for the *rf* field-driven cross-polarization from ^{1}H to ^{29}Si was optimized by maximizing the ^{29}Si NMR signal intensity for the Q^3 silica species. Using time-proportional phase increments enabled an in-phase spectrum to be acquired. A continuous ^{1}H-decoupling field strength of ν_{dec}=25kHz was applied during detection of the ^{29}Si NMR transients with a spectral width of 25kHz and a filter width of 16kHz. Each ^{29}Si NMR transient consisted of 256 time domain points, and 256 transients were acquired for each increment in the ^{1}H NMR time-domain with a recycle delay of 4s. Fifty-nine ^{1}H NMR transients were detected indirectly with a spectral width of 10kHz; a Gaussian filter of 100Hz was applied to the ^{29}Si NMR time-domain and a sine-bell filter to the ^{1}H NMR time-domain before 2D Fourier transformation. The ^{29}Si and the ^{1}H chemical shift scales were externally calibrated to the known chemical shifts of tetrakis(trimethylsilyl)silane.

Chapter 3:

3.1 Experimental species

Skeletons of the hexactinellid sponge *Euplectella aspergillum* (of Philippine origin) were examined via SEM, dry in their natural state or following etching with hydrofluoric acid (HF).

3.2 Studies of the native skeleton

1cm x 1cm square sections from various regions of the skeletal lattice were excised with a razor blade and mounted on aluminum disks using either conductive carbon tabs, silver paint, or conductive epoxy, depending on the preferred orientation of the sample being examined.

3.3 Embedding and Polishing

5mm x 1cm portions of the skeletal lattice were embedded parallel to the long axis of the sponge in M-Bond AE-15 (M-Line, Raleigh N.C.) epoxy, sliced into 3mm thick sections using a diamond cutting wheel, and polished using diamond lapping films down to 0.1μm grit size under a constant flow of fresh water. Following polishing, the samples were secured to aluminum pin mounts using conductive carbon tape.

3.4 Scanning Electron Microscopy (SEM)

Following mounting, all samples were sputter-coated with gold and examined with a Tescan Vega TS 5130MM (Brno, Czech Republic) scanning electron microscope. The unique magnetic lens configurations of this microscope permit unusually large field diameters and ultra-high depth of field imaging. Previous attempts to examine the *E. aspergillum* skeletal lattice using traditional SEMs proved unsuccessful, as the inability to examine specimens at low magnifications (less than 50x) prevented the clear depiction of large-scale structural features. Due to the transparency of the skeletal system, optical microscopy in many instances was not a viable alternative.

3.5 Atomic Force Microscopy (AFM)

Embedded samples, describe above, were imaged with a MultiMode AFM system equipped with a Nanoscope 3a controller (Veeco Metrology, Santa Barbara, CA). Images were taken in tapping mode in air with a TAP300 cantilever (Veeco Probes, Santa Barbara, CA) with a nominal spring constant of ca. 40N/m and nominal resonance frequency of ca. 300kHz. To determine the thickness of the spicule organic interlayers, two different types of samples were examined. In one case, samples were imaged in their native state; in the other, samples were etched for 30s in 500mM NH_4F : 250mM HF to reveal the locations of the organic interlayers. Line scan profiles through 10 images of each sample type were used to calculate interlayer thickness.

3.6 Three-dimensional structural rendering

Based on the electron micrographs, the skeletal system was modeled using the three-dimensional structural rendering program, Maya 6.0 (Alias; Toronto, Canada).

Chapter 4:

4.1 Experimental species:

Aphrocallistes vastus and Rhabdocalyptus dawsoni

Both species were collected by SCUBA at Foley Head, Hotham Sound/Jervis Inlet, British Columbia at ca. 25m depth.

Euplectella aspergillum and Farrea occa

Both species were of Philippine origin and all specimens were received dry.

Monorhaphis chuni

Specimens used in this study were collected from two locations:

1) New Caledonia, near Lifou (Loyalty Island) at a depth of 1905m during the CALSUB campaign of the IRD 1989.
2) Norfolk Ridge at a depth of 1200m during the HALIPRO campaign in 1996.

4.2 Scanning electron microscopy

Excised portions of the mineralized skeleton of each sponge species were mounted on aluminum disks using either conductive carbon tabs, silver paint, or conductive epoxy, depending on the preferred orientation of the sample being examined. Following mounting, all samples were sputter-coated with gold and examined with a Tescan Vega TS 5130MM (Brno, Czech Republic) scanning electron microscope.

4.3 Mechanical testing

For mechanical testing, nanoindentation was performed using a Triboscan nanoindenter system (Hysitron, Minneapolis, MN, USA) and cube-corner tips. Indentations were applied over a loading span ranging from 1 to 1000mN, using two transducers: (1) a 30mN transducer indentation for indentation at relatively low loads (1-30mN), and (2) a high load transducer permitting applied loads up to 1N. High loads were mainly selected to ensure damage in the thin-layer region of the spicule, whereas lower loads were chosen in order to perform indents smaller than individual layer thickness in the thick layer region and in the central core. For all indents, the peak load was held constant for 10 seconds before unloading. Control indentations were made on a fused quartz control slide under similar experimental conditions. After indentation, the samples were sputter-coated with gold and examined with a Tescan Vega TS 5130MM (Brno, Czech Republic) scanning electron microscope.

The images presented in Figure 4.18, obtained from 100mN nanoindents, are representative of the results obtained.

Chapter 5:

5.1 Sponge collection and maintenance

Specimens of the marine sponge *Tethya aurantia* were collected at 17 m depths off Santa Barbara County, California (latitude 34°25.331'N, longitude 119°57.142'W) in February, 2002. Sponges were maintained in fresh, thermostatically controlled flowing seawater at ca 15°C for two weeks prior to experimental utilization.

5.2 Sponge growth experiments

Because of the spatial segregation of spicules in *T. aurantia*, [strongyloxea (Figure 5.2A) dominating the sponge interior and spherasters and acanthasters (Figure 5.2B, C) most abundant in the sponge cortex], explants were isolated from both regions to investigate the synthesis of both megascleres and microscleres in regenerating cellular masses.

144 8mm^3 (ca. 2mm per side) cuboidal explants (72 from the cortex and 72 from the sponge's interior), collected from two different specimens, were used for this study. The explants from both sponges (from each specific region) were combined and randomly distributed for the experiments discussed below.

The freshly isolated explants were rinsed for 6h in fresh flowing (non-recirculating) 5µm-filtered UV-treated seawater before placement in the growth chambers. The sponges were grown in 6-well sandblasted polystyrene tissue culture plates (Falcon) submerged in a 190mm x 100mm KIMAX (Kimble) crystallization dish. 18 spatially isolated explants (9 internal and 9 cortical) were placed in each tissue culture plate (3 explants per well). The explants were grown in 1L of 0.22µm-filtered UV-treated sea water enriched with 30µM dissolved Fe and 30µM silicic acid (Krasko, et al., 2002)). Feeding and maintenance followed previously published protocols (Maldonado and Uriz, 1999; Maldonado, et al., 1999). 50% of the cultures were grown in the presence of 1µM PDMPO (Molecular Probes). The sponges were grown in the dark for two weeks with weekly water changes with subsequent nutrient and fluorophore replenishment. After 2 weeks, the sponge growth rates in the samples with and without PDMPO were determined to ascertain whether exposure to the fluorophore had any effect on sponge cell growth or division rates.

5.3 Estimation of explant growth

Growth measurements were performed by two methods: (1) by measurement of changes in sponge wet mass; and (2) by light microscopic estimation of megasclere spicule abundance following isolation (Krasko, et al., 2002). While either method alone is probably insufficient to accurately determine true growth rates, the approximate agreement of the two methods was interpreted to reflect a reasonable estimation of the magnitude of growth.

5.4 Microscopy

After 2 weeks of growth, the sponges were examined (live) using an Olympus BX-60 fluorescence microscope equipped with a real-time enhancement digital video camera (Optronics LE-Digital) equipped with a wide-band filter cube (Olympus U-MWU filter). Excitation was provided by a UV source (220-285nm); transmission >420nm revealed incorporation of the fluorophore. Following live examination, the explants were treated with a 5.25% solution of sodium hypochlorite (to remove all of the sponge cellular material), washed 5 times with Milli-Q (Millipore-purified) water and the remaining silica spicules reexamined with the same microscope set-up described above.

For SEM analyses, the cleaned spicules were isolated as described above, air dried, mounted on conductive carbon tape (Ted Pella), sputter-coated with gold and examined with either a Tescan Vega TS 5130MM or a JEOL JSM-6300F scanning electron microscope.

5.5 Spectral characterization of spicule-PDMPO complexes

Cleaned, dry samples of spicules (PDMPO-labeled and unlabeled) were mounted on quartz microscope slides (Chem-Glass) and observed during excitation with the 365nm line of a continuous wave argon ion (Ar+) laser (Spectra-Physics 2065). Emission spectra were acquired from single spicules by diverting the emitted light from the microscope objective lens (50x) through a fiber-optic wave-guide to a

spectrometer equipped with a liquid nitrogen cooled CCD detector. A 400nm highpass filter was used to eliminate scattered background light from the laser.

Chapter 6:

6.1 Experimental species

Specimens of the silicoflagellate *Dictyocha speculum* were collected from two locations:

1) Live specimens, collected from the Santa Barbara Channel, were provided by Clarissa R. Anderson and Mark A. Brzezinski.

2) Partially demineralized skeletons, collected from Antarctic sediment traps, were provided by Mark S. Demarest and Mark A. Brzezinski.

6.2 Scanning electron microscopy

Skeletons of *D. speculum* were mounted on aluminum disks using conductive carbon tabs, sputter-coated with gold and examined with a Tescan Vega TS 5130MM (Brno, Czech Republic) scanning electron microscope.

6.3 Small-angle x-ray diffraction studies of E. aspergillum spicules

Anchor spicules (basalia) from *E. aspergillum* were partially demineralized with HF to reduce the diameter from approximately 50μm to 10μm in order to reduce x-ray absorption by the silica surrounding the axial filaments while maintaining adequate filament stiffness to effectively align them for examination. The partially demineralized spicules were washed 5 times with Milli-Q water to remove the dissolved silica and residual HF. The remaining spicules were aligned longitudinally and wrapped in a cylinder of x-ray transparent Kapton® film (E.I. du Pont de Nemours and Company, High Performance Materials, Circleville, OH). The sample was then mounted in a small angle x-ray diffractometer (custom built, intermediate 2-circle small angle diffractometer; x-ray source: 18kW Rigaku rotating anode (Cu anode, wavelength = 1.54Å), monochromator: bent graphite, detector: 18cm diameter Mar image plate detector; Optics: 4 sets of Huber slits) and oriented such that the beam direction was perpendicular to the axis of the spicule.

6.4 Gel Electrophoresis of spicule-associated proteins

Spicules from either *T. aurantia* or *E. aspergillum* were ground with a mortar and pestle to a fine powder under liquid nitrogen. The resulting material was sonicated in 8M guanidine hydrochloride and 2% β-mercaptoethanol for 30 minutes. The remaining insoluble material was separated by centrifugation and the soluble proteins of the supernatant were precipitated with TCA and sodium deoxycholate.

The resulting pellet was washed three times with 70% ethanol, allowed to air dry, and analyzed by SDS-PAGE.

While it has yet to be fully determined whether or not this technique is able to effectively extract all of the hexactinellid spicule-associated proteins, it nevertheless provides an alternative method for biosilica protein isolation without the use of HF (Kröger, et al., 2002). For reference, the yield and composition of extractable demosponge spicule-associated proteins (in this case, those from *T. aurantia*) using this guanidine hydrochloride/β-mercaptoethanol method yields nearly identical results to those obtained from the use of HF. These observations suggest that equally reliable results are reasonable to expect for the hexactinellids.

Chapter 8

References

Adams, C.L., McInerney, J.O., Kelly, M., 1999. Indications of relationships between poriferan classes using full-length 18s rRNA gene sequences. Mem. Queensl. Mus. 44, 33-43.

Aizenberg, J., Sundar, V.C., Yablon, A.D., Weaver, J.C., Chen, G., 2004. Biological glass fibers: Correlation between optical and structural properties. Proc. Natl. Acad. Sci. USA. 101, 3358-3363.

Aizenberg, J., Weaver, J.C., Thanawala, M.S., Sundar, V.C., Morse, D.E., Fratzl, P., 2005. Skeleton of *Euplectella sp*.: Structural hierarchy from the nanoscale to the macroscale. Science 309, 275-278.

Beaulieu, S.E., 2001a. Colonization of habitat islands in the deep sea: Recruitment to glass sponge stalks. Deep-Sea Res. Pt. I. 48, 1121-1137.

Beaulieu, S.E., 2001b. Life on glass houses: Sponge stalk communities in the deep sea. Mar. Biol. 138, 803-817.

Bergquist, P.R., 1978. Sponges. University of California Press, Berkeley and Los Angeles.

Bergquist, P.R. 1985. Poriferan Relationships. In: The origins and relationships of lower invertebrates (S. Conway Morris, J. D. George, R. Gibson, and H. M. Pratt, eds.) 14-27. Clarendon Press, Oxford.

Bhattacharyya, P., Volcani, B.E., 1983. Isolation of silicate ionophore(s) from the apochlorotic diatom *Nitzschia alba*. Biochem. Biophys. Res. Commun. 114, 365-372.

Borchiellini, C., Manuel, M., Alivon, E., Boury-Esnault, N., Vacelet, J., Le Parco, Y. 2001. Sponge paraphyly and the origin of Metazoa. J. Evol. Biol. 14: 171-179.

Borojevic, R. 1970. Différentiationcellulaire dans l'embryogénèse et la morphogénèse chez les Spongiaires. In: Fry W.G., editor. The biology of the porifera. London: Academic Press. 467-490.

Boury-Esnault and L. De Vos. 1988. *Caulophacus cyanae n. sp.,* une éponge hexactinellide des sources hydrothermales. Biogéographie du genre Caulophacus Schulze, 1887. Oceanol. Acta. 8: 51-60.

Brasier, M., Green, O., Shields, G., 1997. Ediacarian sponge spicule clusters from southwestern Mongolia and the origin of the Cambrian fauna. Geology. 25, 303-306.

Brott, L.L., Naik, R.R., Pikas, D.J., Kirkpatrick, S.M., Tomlin, D.W., Whitlock, P.W., Clarson, S.J., Stone, M.O., 2001. Ultrafast holographic nanopatterning of biocatalytically formed silica. Nature. 413, 291-293.

Bütschli, O., 1901. Einige Beobachtungen über Kiesel- und Kalknadeln von Spongien. Z. Wiss. Zool. 69, 235-286.

Carnelli, A. L., Madella, M., Theurillat, J.P., 2001. Biogenic silica production in selected alpine plant species and plant communities. Ann. Bot-London. 87, 425-434.

Carbonelli, S., A. Zampella, A. Randazzo, C. Debitus, and L. Gomez-Paloma. 1999. Sphinxolides E-G and Reidispongiolide C: Four new cytotoxic macrolides from the New Caledonian lithistida sponges *N. superstes and R. coerulea*. Tetrahedron. 55, 14665-14674.

Carter, P., Wells, J.A., 1988. Dissecting the catalytic triad of a serine protease. Nature. 332, 564-568.

Cattaneo-Vietti R., Bavestrello, G., Cerrano, C., Sara, M., Benatti, U., Giovine, M., Gaino, E. 1996. Optical fibres in an Antarctic sponge. Nature. 383, 397-398.

Cavalier-Smith, T., Allsopp, M.T.E.P., Chao, E.E., Boury-Esnault, N., Vacelet, J., 1996. Sponge phylogeny, animal monophyly, and the origin of the nervous system: 18s rRNA evidence. Can. J. Zool. 74, 2031-2045.

Cha, J.N., Shimizu K., Zhou Y., Christiansen S.C., Chmelka, B.F., Stucky G.D., and Morse, D.E. 1999. Silicatein filaments and subunits from a marine sponge direct the polymerization of silica and silicones in vitro. Proc. Natl. Acad. Sci. USA. 96, 361-365.

Cha, J.N., Stucky, G.D., Morse, D.E., Demming, T.J., 2000. Biomimetic synthesis of ordered silica structures mediated by block polypeptides. Nature. 403, 289-292.

Cha, J.N., 2001. Lessons from nature: Novel routes to biomimetic synthesis of silica based materials. Ph.D. Dissertation. UCSB.

Chai, H., Lawn, B.R., 2002. Cracking in brittle laminates from concentrated loads. Acta Mater. 50, 2613-2625.

Chisholm, S.W., Azam, F., Eppley, R.W. 1978. Silicic acid incorporation in marine diatoms on light:dark cycles: use as an assay for phased cell division. Limnol. Oceanogr. 23: 518-529.

Chun, C., 1900. Aus den Tiefen des Weltmeeres, *Gustav Fischer*, Jena, Germany.

Clegg, W.J., Kendall, K., Alford, N.M., Button, T.W., Birchall, J.D., 1990. Nature. 347, 455-457.

Crawford, S.A., Higgins, M.J., Mulvaney, P., Wetherbee, R., 2001. Nanostructure of the diatom frustule as revealed by atomic force and scanning electron microscopy. J. Phycol. 37, 543-554.

Croce, G., Frache, A., Milanesio, M., Marchese, L., Causa, M., Viterbo, D., Barbaglia, A., Bolis, V., Bavestrello, G., Cerrano, C., Benatti, U., Pozzolini, M., Giovine, M., Amenitsch, H., 2004. Structural characterization of siliceous spicules from marine sponges. Biophys. J. 86, 526-534.

Deming, T.J., 1997. Facile synthesis of block copolypeptides of defined architecture. Nature. 390, 386-389.

Deshpande, V.S., Ashby, M.F., Fleck, N.A., 2001. Foam topology bending versus stretching dominated architectures. Acta Mater. 49, 1035-1040.

Egerton-Warburton, L.M., Huntington, S.T., Mulvaney, P., Griffin, B.J., Wetherbee, R., 1998. A new technique for preparing biominerals for atomic-force microscopy. Protoplasma. 204, 34-37.

Engelhardt, G., and D. Michel, D., 1987. High-resolution solid-state NMR of silicates and zeolites., Wiley, Chichester.

Evans, D.F., Par, J., Coker, E.N., 1990. Nuclear-Magnetic-Resonance studies of silicon (IV) complexes in aqueous solution. I. Tris-catecholato complexes. Polyhedron. 9, 813-823.

Garrone, R., 1969. Collagène, spongine et squelette minèral chez l'èponge *Haliclona rosea* (O.S.) (Dèmosponge, Haplosclèride). J. Microsc. 8, 581-598.

Garrone, R., Simpson, T.L., Pottu-Boumendil, J. 1981. Ultrastructure and deposition of silica in sponges, in: Simpson, T.L., Volcani, B.E. (Eds.), Silicon and siliceous structures in biological systems. Springer-Verlag, New York, 495-525.

Gehling, J.G., Rigby, J.K., 1996. Long expected sponges from the neoproterozoic ediacara fauna of South Australia. J. Paleontol. 2, 185-195.
Gray, J.E. 1872. Annals and Magazine of Natural History, ser. 4, vol. IX, 442-461.

Haeckel, E.H.P.A., 1904. Kunstformen Der Natur, Bibliographisches Institut, Leipzig und Wien.

Harrison, C.C., Loton, N., 1995. Novel routes to designer silicas – studies of the deposition of $(M(+))(2)[Si(C_6H_4O_2)_3]\cdot XH_2O$ – Importance of M(+) identity of the kinetics of oligomerization and the structural characterization of the silicas produced. J. Chem. Soc. Faraday Trans. 91, 4287-4297.

Harrison, C.C., 1996. Evidence for intramineral macromolecules containing protein from plant silicas. Phytochemistry. 41, 37-42.

Hartman, W.D., 1981. Form and distribution of silica in sponges, in Simpson, T.L., Volcani, B.E. (Eds.), Silicon and siliceous structures in biological systems. Springer-Verlag, New York, 453- 493.

Hazelaar S., Strate H.J. van der, Gieskes W.W.C., Vrieling, E.G., 2005. Monitoring rapid valve formation in the pennate diatom *Navicula salinarum* (Bacillariophyceae). J. Phycol. 41, 354-358.

Hecky, R.E., Mopper, K., Kilham, P., Degens. E.T., 1973. Amino-acid and sugar composition of diatom cell-walls. Mar. Biol. 19, 323-331.

Iijima, I., 1904. Studies on the Hexactinellida, contribution IV (Rossellidae). J. College Sci. 18: 1-303.

Iijima, I., 1926. The Hexactinellida of the Siboga expedition. Leiden, Brill

Iler, R.K., 1979. The chemistry of silica; Solubility, polymerization, colloidal and surface properties, and biochemistry. John Wiley and Sons, New York.

Janussen, D., Tabachnick, K.R., Tendal, O.S., 2004. Deep-sea Hexactinellida (Porifera) of the Weddell Sea. Deep-Sea Res. Pt. II. 51, 1857-1882.

Jones, W.C., 1979. The microstructure and genesis of sponge biominerals. In: C. Levi and N. Boury-Esnault (eds.). Biologie des Spongiaires. Colloq. Internat. C.N.R.S., Paris., 291, 425-477.

Kelly, M., 2000. Description of a new lithistid sponge from northeastern New Zealand, and consideration of the phylogenetic affinities of families Corallistidae and Neopeltidae. Zoosystema. 22 (2): 265-283.

Kelly-Borges, M., Robinson, E.V., Gunasekera, S., Gunasekera, M., Pomponi, S.A., 1994. Species differentiation in the marine sponge genus *Discodermia* (Demospongiae, Lithistida): the utility of secondary metabolites as species-specific markers. Biochemical Systematics and Ecology. 22: 353-365.

Kinrade, S.D., Del Nin, J.W., Schach, A.S., Sloan, T.A., Wilson, K.L., Knight, C.T.G., 1999a. Stable five- and six-coordinated silicate anions in aqueous solution. Science. 385, 1542-1545.

Kinrade, S.D., Maa, K.J., Schach, A.S., Sloan, T.A., Knight, C.T.G., 1999b. Silicon-29 NMR evidence of alkoxy substituted aqueous silicate anions. J. Chem. Soc., Dalton Trans. 3149-3150.

Kinrade, S.D., Gillson, A-M.E., Knight, C.T.G., 2002. Silicon-29 NMR evidence of a transient hexavalent silicon complex in the diatom *Navicula pelliculosa*. Journal of the Chemical Society-Dalton Transactions. 3, 307-309.

Kisailus, D., Choi, J.H., Weaver, J.C., Yang, W.J., Morse, D.E., 2005a. Enzymatic synthesis and nanostructural control of gallium oxide at low temperature. Adv. Mater. 17, 314-318.

Kisailus, D., Najarian, M., Weaver, J.C., Morse, D.E., 2005b. Functionalized gold nanoparticles mimic catalytic activity of a polysiloxane-synthesizing enzyme. Adv. Mater. 17, 1234-1239.

Kisailus, D., Truong, Q., Amemiya, Y., Weaver, J.C., Morse, D. E., 2006. Self-assembled bifunctional surface mimics an enzymatic and templating protein for the synthesis of a metal oxide semiconductor. Proc. Natl. Acad. Sci. USA. 103 (15), 5652-5657.

Krasko, A., Lorenz, B., Batel, R., Schröder, H.C., Müller I.M., Müller, W.E.G., 2000. Expression of silicatein and collagen genes in the marine sponge *Suberites domuncula* is controlled by silicate and myotrophin. Eur. J. Biochem. 267, 1-11.

Krasko, A., Schröder, H.C., Batel, R., Grebenjuk, V.A., Steffen, R., Müller, I.M., Müller, W.E.G., 2002. Iron induces proliferation and morphogenesis in primmorphs from the marine sponge *Suberites domuncula*. DNA Cell Biol. 21, 67-80.

Kröger, N., Deutzmann, R., Sumper, M., 1999. Polycationic peptides from diatom biosilica that direct silica nanosphere formation. Science. 286, 1129-1132.

Kröger, N., Deutzmann, R., Bergsdorf, C., Sumper, M., 2000. Species-specific polyamines from diatoms control silica morphology. Proc. Natl. Acad. Sci. USA. 97, 14133-14138.

Kröger N., Lorenz, S., Brunner, E., Sumper, M., 2002. Self-assembly of highly phosphorylated silaffins and their function in biosilica morphogenesis. Science. 298, 584-586.

Kruse, M., Leys, S.P., Müller, I.M., Müller, W.E.G., 1998. Phylogenetic position of the hexactinellida within the phylum porifera based on the amino acid sequence of the protein kinase C from *Rhabdocalyptus dawsoni*. J. Mol. Evol. 46, 721-728.

Levi, C., Barton, J.L., Guillemet, C., Lebras, E., Lehuede, P., 1989. A remarkably strong natural glassy rod - the anchoring spicule of the *Monorhaphis* sponge. J. Mater. Sci. Lett. 8, 337-339.

Levi, C. 1991. Lithistid sponges from the Norfolk Rise. Recent and Mesozoic Genera. In: Fossil and Recent Sponges. Springer-Verlag, Berlin.

LEVITUS 1994: http://ingrid.ldgo.columbia.edu/SOURCES/.LEVITUS94

Leys, S.P., Lauzon, N.R.J., 1998. Hexactinellid sponge ecology: growth rates and seasonality in deep water sponges. J. Exp. Mar. Biol. Ecol. 230, 111-129.

Leys, S.P., 2003. Comparative study of spiculogenesis in demosponge and hexactinellid larvae. Microsc. Res. Techniq. 62, 300-311.

Leys, S.P., Cheung, E., Boury-Esnault, N., 2006. Embryogenesis in the glass sponge *Oopsacas minuta*: Formation of syncytia by fusion of blastomeres. Integrative and Comparative Biology. 46 (2), 104-117.

Lichtenegger, H., Reiterer, A., Stanzl-Tschegg, S.E., Fratzl, P., 1999. Variation of cellulose Microfibril angles in softwoods and hardwoods – a possible strategy of mechanical optimization. J. Struct. Biol. 128, 257-269.

Lobel, K.D., West, J.K., Hench, L.L., 1996. Computational model for protein-mediated biomineralization of the diatom frustule. Marine Bio. 126, 353-360.

Mackie, G.O., Singla, C.L., 1983. Studies on hexactinellid sponges. I. Histology of *Rhabdocalyptus dawsoni* (Lambe, 1873). Phil. Trans. R. Soc. Lond. 301, 365-400.

Maldonado, M., Yound, C.M., 1996. Bathymetric patterns of sponge distribution on the Bahamian slope. Deep Sea Research I. 43 (6), 897-915.

Maldonado, M., Carmona, M.G., Uriz, M.J., Cruzado, A., 1999. Decline in Mesozoic reef-building sponges explained by silicon limitation. Nature. 401, 785-788.

Maldonado, M., Uriz, M.J., 1999. An experimental approach to the ecological significance of microhabitat-scale movement in an encrusting sponge. Mar. Ecol.-Prog. Ser. 185, 239-255.

Maldonado, M., Carmona, M.C., Van Soest, R.W.M., Pomponi, S.A., 2001. First record of the genera Crambe and Discorhabdella fro the eastern Pacific, with description of three new species. Journal of Natural History. 35, 1261-1276.

Manna, L., Milliron, D.J., Meisel, A., Scher, E.C., Alivisatos, A.P., 2003. Controlled growth of tetrapod-branched inorganic nanocrystals. Nat. Mater. 2, 382-385.

McInerney, J. O., Adams, C.L., Kelly, M., 1999. Phylogenetic resolution potential of 18s and 28s rRNA genes within the lithistid Astrophorida. In*:* Hooper, J. N. A. (ed.). Proceedings of the 5th International Sponge Symposium. Memiors of the Queensland Museum. 44, 343-352.

Milliron, D.J., Hughes, S.M., Cui, Y., Manna, L., Li, J.B., Wang, L.W., Alivisatos, A.P., 2004. Colloidal nanocrystal heterostructures with linear and branched topology. Nature. 430 (6996), 190-195.

Minchin, E.A., 1909. Sponge-spicules. A summary of present knowledge. Ergeb. Fortschr Zool. 2, 171-274.

Mizutani, T., Nagase, H., Fujiwara, N., Ogoshi, H., 1998. Silicic acid polymerization catalyzed by amines and polyamines. Bull. Chem. Soc. Jpn. 71, 2017-2022.

Morse, D.E., 1999. Silicon biotechnology: Harnessing biological silica production to construct new materials. Trends Biotechnol. 17, 230-232.

Morse, D.E., 2000. Silicon biotechnology: Proteins, genes and molecular mechanisms controlling biosilica nanofabrication offer new routes to polysiloxane synthesis. *In* Organosilicon Chemistry IV: From Molecules to Materials. N. Auner and J. Weis, editors. Wiley-VCH, New York, 5-16.

Morse, D.E. 2001. Biotechnology reveals new routes to synthesis and structural control of silica and polysilsesquioxanes. *In* The chemistry of organic silicon compounds, Vol 3. Z. Rappoport and Y. Apeloig, editors. John Wiley and Sons, New York, 805-819.

Müller, W.E.G., 1998. Molecular Phylogeny of Eumetazoa: Genes in sponges (Porifera) give evidence for monoplyly of animals. Progr. Molec. Subcell. Biol. 19, 89-132.

Müller, W.E.G., Wiens, M., Batel, R., Steffen, R., Schröder, H.C., Borojevic, R. Custodio, M.R., 1999. Establishment of a primary cell culture from a sponge: Primmorphs from *Suberites domuncula*. Mar. Ecol.-Prog. Ser. 178, 205-219.

Müller, W.E.G., Müller, I.M., 2003. The hypothetical ancestral animal the Urmetazoa: Telomerase activity in sponges (Porifera). J. Serb. Chem. Soc. 68, 257-268.

Müller, W.E.G., Rothenberger, M., Boreiko, A., Tremel, W., Reiber, A., Schröder, H., 2005. Formation of siliceous spicules in the marine demosponge Suberites domuncula. Cell Tissue Res. 321, 285-297.

Murr, M.M., Morse, D.E., 2005. Fractal intermediates in the self-assembly of silicatein filaments. Proc. Natl. Acad. Sci. USA. 102, 11657-11662.

Noll, F., Sumper, M., Hampp, N., 2002. Nanostructure of diatom silica surfaces and of biomimetic analogues. Nano Lett. 2, 91-95.

Parkinson, J. Gordon, R., 1999. Beyond micromachining: the potential of diatoms. Trends Biotechnol. 17, 190-196.

Perkins, D., 2002. Mineralogy, 2nd edition. Prentice Hall, New York.

Perry, C.C., Yun, L.J., 1992. Preparation of silicas from silicon complexes – role of cellulose in polymerization and aggregation control. J. Chem. Soc., Faraday Trans. 88, 2915-2921.

Pozzolini, M., Sturla, L., Cerrano, C., Bavestrello, G., Camardella, L., Parodi, A.M., Raheli, F., Benatti, U., Müller, W.E.G., Giovine, M., 2004. Molecular cloning of silicatein gene from marine sponge *Petrosia ficiformis* (Porifera, Demospongiae) and development of primmorphs as a model for biosilicification studies. Mar. Biotechnol. 6, 594-603.

Qureshi, A., Colin, P.L., Faulkner, D.J., 2000. Microsclerodermins F-I, Antitumor and Antifungal Cyclic Peptides from the lithistid sponge *Microscleroderma sp.* Tetrahedron. 56, 3579-3685.

Reiswig, H.M. 1971. Axial symmetry of sponge spicules and its phylogenetic significance. Can. Biol. Mar. 12, 505-514.

Reiswig, H.M., Mackie, G.O., 1983. Studies on Hexactinellid sponges. III. The taxonomic status of Hexactinellida within the porifera. Phil. Trans. R. Soc. Lond. 301, 419-428.

Roth, K.M., Zhou, Y., Yang, W.J., Morse, D.E., 2005. Bifunctional small molecules are biomimetic catalysts for silica synthesis at neutral pH. J. Am. Chem. Soc. 127, 325-330.

Rützler, K., Smith, K.P., 1993. The genus Terpios (Suberitidae) and new species in the "Lobiceps" complex, in: Uriz, M.J., Rützler, K. (Eds.), Recent advances in ecology and systematics of sponges. Scientia Marina, Barcelona, Spain, 381-393.

Saito, T., Uchida, I., Takeda, M., 2002. Skeletal growth of the deep-sea hexactinelid sponge Euplectella oweni, and host selection by the symbiotic shrimp Spongicola japonica (Crustacea: Decapoda: Spongicolidae). J. Zool. Lond. 258, 521-529.

Sandhage, K.H., Dickerson, M.B., Huseman, P.M., Caranna, M.A., Clifton, J.D., Bull, T.A., Heibel, T.J. Overton, W.R., Schoenwaelder. M.E.A., 2002. Novel, bioclastic route to self-assembled, 3D, chemically tailored meso/nanostructures: Shape-preserving reactive conversion of biosilica (diatom) microshells. Adv. Mater. 14, 429-433.

Sarikaya M., Fong H., Sunderland N., Flinn B.D., Mayer G., Mescher A., Gaino E., 2001. Biomimetic model of a sponge-spicular optical fiber - mechanical properties and structure. J. Mater. Res. 16, 1420-1428.

Schmid, A.M., Schulz, D., 1979. Wall morphogenesis in diatoms—deposition of silica by cytoplasmic vesicles. Protoplasma. 100 (3–4), 267–288.

Schmidt, E. W., Obraztsova, A.Y., Davidson, S.K., Faulkner, D.J, Haygood, M.G. 2000. Identification of the antifungal peptide-containing symbiont of the marine sponge *Theonella swinhoei* as a novel delta-proteobacterium, "*Candidatus Entotheonella palauensis*" Marine Biology. 136: 969-977.

Schmidt, W.J., 1926. Uber das wesen der lamellierung und das gegenseitige verhalten von organischer und anorgnischer substanz bei den keiselschwammnadeln. Zool. Zb. Anat. Ont. Tiere. 48, 311-364.

Schmidt-Rohr, K., Spiess, H.W., 1994. Multidimensional solid-state NMR and polymers. Academic Press, London.

Schonberg, C.H.L., 2001. New mechanisms in deposponge spicule formation. J. Mar. Biol. Assoc. UK. 81, 345-346.

Schröder, H.C., Perovic-Ottstadt, S., Rothenberger, M., Wiens, M., Schwertner, H., Batel, R., Korzhev, M., Müller, I. M., Müller, W.E.G., 2004. Silica transport in the demosponge Suberites domuncula: Fluorescence emission analysis using the PDMPO probe and cloning of a potential transporter. Biochem. J. 381, 665-673.

Schröder, H.C., Boreiko, A., Korzhev, M., Tahir, M.N., Tremel, W., Eckert, C., Ushijima, H., Müller, I.M., Müller, W.E., 2006. Co-expression and functional interaction of silicatein with galectin: Matrix-guided formation of siliceous spicules in the marine demosponge *Suberites domuncula*. J. Bio. Chem. 281 (17): 12001-12009.

Schulze, F.E., 1880. On the structure and arrangement of the soft parts in *Euplectella aspergillum*. Trans. R. Soc Edinburgh. 29, 661-673.

Schulze, F.E., 1887. Report on the Hexactinellida collected by H. M. S. Challenger during the years 1873-1876 . Volume XXI.

Schulze, F.E., 1899. Zur Histologie der Hexactinelliden. Sitz. Ber. K. Pr. Akad. Wiss. Berlin. 14, 198-209.

Schulze, F.E., 1904. Hexactinellida, in scientific results of the German deep-sea expedition with the steamboat, "Valdivia" 1898-1899, edited by C. Chun. Verlag Gustav Fischer, Jena, Germany.

Schultze, M., 1860. Die Hyalonemen. Ein Beitrag zur Naturgeschichte der Spongien. A. Marcus, Bonn, Germany.

Schulze, P. 1925. Zur morphologischen feinbau der keiselschwammnadeln. Zeit. Morph. Okol. Tiere. 4: 615-625

Schwab, D.W., Shore, R.E., 1971a. Fine structure and composition of a siliceous sponge spicule. Biol. Bull. 140, 125-136.

Schwab, D.W., Shore, R.E., 1971b. Mechanism of internal stratification of siliceous sponge spicules. Nature. 232, 501-502.

Schwenzer, B., Roth, K.M., Gomm, J.R., Murr, M., Morse, D.E., 2006. Kinetically controlled vapor-diffusion synthesis of novel nanostructured metal hydroxide and phosphate films using no organic reagents. J. Mater. Chem. 16, 401-407.

Seshadri, M., Bennison, S.J., Jagota, A., Saigal, S., 2002. Mechanical response of cracked laminated plates. Acta Mater. 50, 4477-4490.

Shimizu, K., Cha, J.N., Stucky, G.D., Morse, D.E., 1998. Silicatein α: cathepsin L-like protein in sponge biosilica. Proc. Natl. Acad. Sci. USA. 95, 6234-6238.

Shimizu, K. Morse, D.E., 2000. Biological and biomimetic synthesis of silica and other polysiloxanes, in Baeuerlein, E. (Ed.), Biomineralization: From Biology to Biotechnology and Medical Application. Wiley-VCH, New York, 207-220.

Shimizu, K., Del Amo, Y., Brzezinski, M.A., Stucky, G.D., Morse, D.E., 2001. A novel fluorescent silica tracer for biological silicification studies. Chem. Biol. 8, 1051-1060.

Shore, R.E., 1972. Axial filament of siliceous sponge spicules, its organic components and synthesis. Biol. Bull. 143, 125-136.

Simpson, T.L., Vaccaro, C.A., 1974. An ultrastructural study of silica deposition in the freshwater sponge *Spongilla lacustris*. J. Ultrastruc. Res. 47, 296-309.

Simpson. T.L., Volcani, B.E., 1981. Silicon and siliceous structures in biological systyems. Springer-Verlag, New York.

Simpson, T. L. 1984. The cell biology of sponges. Springer-Verlag, New York.

Simpson, T.L., Langenbruch, P.F., Scaleraliaci, L., 1985. Silica spicules and axial filaments of the marine sponge *Stelletta grubii* (Porifera, Demospongiae). Zoomorphology. 105, 375-382.

Sullivan, C.W., 1986. Silicification in diatoms. In: Silicon biochemistry. John Wiley and Sons, New York.

Sumerel, J.L., Morse, D.E., 2003. Biotechnological advances in biosilicification, in Müller, W.E. (Ed.), Prog. Molec. Subcellular Biol. 33: "Silicon biomineralization: Biology - Biochemistry - Molecular Biology – Biotechnology." Springer-Verlag, Berlin, 225-247.

Sumerel, J.L., Yang, W.J., Kisailus, D., Weaver, J.C., Choi, J.H., Morse, D.E., 2003. Biocatalytically templated synthesis of titanium dioxide. Chem. Mat. 15 (25), 4804-4809.

Sumper, M., 2002. A phase separation model for the nanopatterning of diatom biosilica. Science. 295 (5564), 2430-2433.

Sundar, V.C., Yablon, A.D., Grazul, J.L., Ilan, M., Aizenberg, J., 2003. Fibre-optical features of a glass sponge - some superior technological secrets have come to light from a deep-sea organism. Nature. 424, 899-900.

Theunissen, J.D. 1994. A method for isolating and preparing silica bodies in grasses for scanning electron microscopy. Biotech. Histochem. 69, 291-294.

Thopmson, D. T., 1942. On growth and form, the complete revised edition. Cambridge University Press, Cambridge, England.

Travis, D., Francois, C., Bonar, L., Glimcher, M., 1967. Comparative studies of the organic matrices of invertebrate mineralized tissues. J. Ultrastruc. Res. 18, 519-550.

Uriz, M.J., Turon, X., Becerro. M.A., 2000. Silica deposition in Demosponges: spiculogenesis in *Crambe crambe*. Cell Tiss. Res. 301, 299-309.

Van Valkenburg, S. D., Norris, R. E., 1970. The growth and morphology of the silicoflagellate *Dictyocha speculum* Ehrenberg in culture. J. Phycol. 6, 48–54.

Volcani, B.E., 1981. In: Simpson, T.L., Volcani, B.E. (Eds.), Silicon and siliceous structures in biological systems. Springer-Verlag, New York, 157-201.

Vrieling, E.G., Beelen, T.P.M., Santen, R.A. van, Gieskes, W.W.C., 1999. Diatom silicon biomineralization as an inspirational source of new approaches to silica production. J. Biotechnol. 70, 39-51.

Wetherbee,R., Crawford, S.A., Mulvaney, P., 2000. The nanostructure and development of diatom biosilica. In: E. Baeuerlein, Editor, Biomineralization: from Biology to Biotechnology and Medical Application, Wiley-VCH, Weinheim, 189-206.

Weaver, J.C., Morse, D.E., 2003. Molecular biology of demosponge axial filaments and their roles in biosilicification. Microsc. Res. Techniq. 62, 356-367.

Weaver, J.C., Pietrasanta, L.I., Hedin, N., Chmelka, B.F., Hansma, P.K., Morse, D.E., 2003. Nanostructural features of demosponge biosilica. J. Struct. Biol. 144, 271-281.

Weissenfels, N., Landschoff, H.W., 1977. Bau und Funktion des Sußwasserschwamms *Ephydatia fluvatilis* L. (Porifera). IV. Die Entwicklung der Monaxialen SiO_2 Nadeln in Sandwich-Kulturen. Zool. Jb. Anat. Bd. 98, 355-371.

Wilkinson, C.R. Garrone, R., 1980. Ultrastructure of spicules and microsclerocytes in the marine sponge *Neofibularia irata n. sp*. J. Morphol. 166, 51-64.

Woesz, A., Weaver, J.C., Kazanci, M., Dauphin, Y., Aizenberg, J., Morse, D.E., Fratzl, P., 2006. Micromechanical properties of biological silica in skeletons of deep sea sponges. Journal of Materials Research. 21 (8), 2068-2078.

Zampella, A., Valeria D'Auria, C., Minale, L., 1997. Callipeltosides B and C, two novel cytotoxic glycoside macrolides from the marine lithistida sponge Callipelta sp. Tetrahedron. 53, 3243-3248.

Zaremba, C.M., 1998. Structure and Reaction Studies of Biological organic and inorganic composite materials: Abalone shells, diatoms, and a unique birch bark. Ph.D. Dissertation. UCSB.

Zhou, Y., Shimizu K, Cha, J.N., Stucky, G.D., Morse, D. E., 1999. Efficient catalysis of polysiloxane synthesis by silicatein alpha requires specific hydroxy and imidazole functionalities. Angew. Chem. Int. Ed. 38, 780-782.

Ziherl, P., Kamien, R.D., 2000. Soap Froths and Crystal Structures. Phys. Rev. Lett. 85, 3528-3531.